Characterization of the Role of Insulin, IGF-1 and their Receptor Signaling in Proliferation and Survival of Non-Small Cell Lung Cancer Cells

Dissertation

zur Erlangung des Doktorgrades (Dr. rer. nat.)

der Mathematisch-Naturwissenschaftlichen Fakultät

der Rheinischen Friedrich-Wilhelms-Universität Bonn

vorgelegt von

Carolin Maria Frisch

aus Koblenz

Bonn 2015

Angefertigt mit Genehmigung der Mathematisch-Naturwissenschaftlichen Fakultät der
Rheinischen Friedrich-Wilhelms-Universität Bonn

Erster Gutachter: Prof. Dr. Kurt Racké

Zweiter Gutachter: Prof. Dr. Ulrich Jaehde

Tag der mündlichen Prüfung: 29.01.2016

Erscheinungsjahr 2016

Für meine Familie

Table of Contents

List of Abbrevations

A

ADP	Adenosine diphosphate
Akt	see PKB
approx.	Approximately
Ask1	Apoptosis signal-regulating kinases 1
ATP	Adenosine triphosphate

B

BAD	Bcl-2-associated death promoter
bHLH	Basic helix-loop-helix
BSA	Bovine serum albumin

C

° C	Degree celsius
CDH2	N-cadherin
CDK	Cyclin-dependent kinases
cDNA	Complementary DNA
Ci	Curie
Co-IP	Co-immunoprecipitation
conc.	Concentration
COX	Cyclooxygenase
CP	Crossing point
Ct	Threshold cycle
ctr.	Control

D

Da	Dalton
DM	Diabetes mellitus

DMSO	Dimethyl sulfoxide
DNA	Deoxyribonucleic acid
dNTP	Desoxynucleosidtriphosphate
dpm	Disintegrations per minute

E

EAPII	ETS1-associated protein II
EC_{50}	50 % Effective concentration
ECL	Enhanced chemiluminescence
EDTA	Ethylenediaminetetraacetic
e.g.	Exempli gratia (for example)
EGF	Epidermal growth factor
EMA	European Medicines Agency
EMT	Epithelial mesenchymal transition
ERK	Extracellular signal-regulated kinase
ET-1	Endothelin
et al.	Et alii (and others)
Ex11	Exon 11

F

FCS	Fetale calf serum
FDA	Food and Drug Administration
FGF	Fibroblast growth factor
Fig.	Figure
FKHR	Forkhead transcription factor
FN1	Fibronectin

G

g	Gram
g	Gravitational acceleration (9,81 m/s^2)
GAPDH	Glyceraldehyde-3-phosphate dehydrogenase

GDP	Guanosine diphosphate
Grb2	Growth-factor-receptor-bound protein 2
GTP	Guanosine triphosphate

H

^{3}H	Tritium (hydrogen isotope)
h	Hour
HbA_{1C}	Glycated haemoglobin A_{1C}
HBE	Human bronchial epithelial
HCC	Hepatocellular carcinoma cells
HCl	Hydrogen chloride
HR	Heterodimeric receptor (s)
HR-A	Heterodimeric receptor (s) (with IR-A component)
HRP	Horseradish peroxidase

I

IDE	Insulin-degradating enzymes
i.e.	Id est (that is)
IGF-1	Insulin-like growth factor-1
IGF-1R	Insulin-like growth factor-1 receptor (s)
IGFBP	Insulin-like growth factor binding proteins
IGFL	IGF-like
IL	Interleukin
INSL	Insulin-like
IR	Insulin receptor (s)
IR-A	Insulin receptor isoform A
IR-B	Insulin receptor isoform B
IRS	Insulin receptor substrate

J

JNK1	Jun N-terminale kinases

K

k	Kilo
KCl	Potassium chloride
K_D	Equilibrium dissociation constant
KD	Knockdown
kDa	Kilo-Dalton
KH_2PO_4	Potassium dihydrogen phosphate

L

l	Liter
LCLC	Large cell lung carcinoma
LSD-1	Lysine specific demethylase 1

M

µ	Mikro (10^{-6})
m	Milli (10^{-3})
M	Molar
MAPK	Mitogen-activated protein kinase
MAPKK	MAPK kinase
MAPKKK	MAPK kinase kinase
Mdm2	Mouse double minute homolog
MEC	Mucoepidermoid carcinoma
MEK	MAPK/ERK-activating kinases
$MgCl_2$ x 6 H_2O	Magnesium chloride hexahydrate
min	Minute
mio	Million
MMAD	Median aerodynamic diameter
MMP	Matrix metalloproteinases

MOPS	4-Morpholinepropanesulfonic acid
mRNA	Messenger RNA

N

n	Number of replicates (within one experiment)
n	Nano (10^{-9})
N	Number of independent experiments
NaF	Sodium fluoride
NaOH	Sodium hydroxide
Na_3VO_4	Sodium orthovanadate
NSCLC	Non-small cell lung cancer

P

p	Significance level
p	Phosphorylated
p	Pico (10^{-12})
PBS	Phosphate buffered saline
PCR	Polymerase chain reaction
PDE	Phosphodiesterase
PH	Pleckstrin homology
pH	Measure of the acidity or basicity of an aqueous solution
PI	Protease inhibitors
PI3K	Phosphatidylinositol-3 kinase
PIP_3	Phosphatidylinositol-3,4,5-triphosphate
PKB	Proteinkinase B
PMSF	Phenylmethanesulfonyl fluoride
PVDF	Polyvinylidene fluoride

Q

Qol	Quality of life

R

Raf	Rapidly accelerated fibrosarcoma
Ras	Rat sarcoma
RNA	Ribonucleic acid
RT	Reverse transkriptase
RTK	Receptor tyrosine kinase (s)
RT-PCR	Real time quantitative PCR

S

s	Second
s.c.	Subcutaneous
SCC	Squamous cell carcinoma
SCLC	Small cell lung cancer
SDS	Sodium dodecyl sulfate
SDS-PAGE	SDS-Polyacrylamide gel electrophoresis
SEM	Standard error of the mean
shRNA	Short hairpin ribonucleic acid
siRNA	Silencer ribonucleic acid
SOS	Son of sevenless

T

T1DM	Type 1 diabetes mellitus
T2DM	Type 2 diabetes mellitus
TBS	Tris buffered saline
TBST	Tris buffered saline + Tween
TCA	Trichloroacetic acid
TGF-β	Transforming growth factor β
Thr	Threonine

TI	Technosphere® insulin
TNF	Tumor necrosis factor
Tris (-HCl)	Tris-(hydroxymethyl)-aminomethan (-hydrochloride)
Tyr	Tyrosine

U

U	Unit
U/min	Rotations per minute
USA	United States of America

V

viz.	Videlicet (namely)

W

WB	Western blot
WHO	World Health Organization

Z

ZEB	Zinc finger E-box binding

I Introduction

1 Diabetes and Cancer

Diabetes mellitus (DM) and cancer are amongst the most frequent chronic diseases worldwide with a rapidly increasing number of people affected (Steward & Wild, 2014; Vigneri et al., 2009).

To date cancer has evolved to be the leading cause of death in the United States (Jemal et al., 2010), whereas it follows cardiovascular diseases as second most common cause of death in Europe (WHO, 2012).

Since recent years DM has been suspected to provoke tumorigenesis and notably, epidemiological studies underline a positive correlation between both diseases (see chapter 1.3).

However, it is not known to which extent DM possibly contributes to cancer cell development and promotion of malignancies (Chen Li & Kong, 2014). Furthermore, there is no proof yet that DM is causally correlated to cancer diseases in general.

Against this background, it becomes evident that insulin-related cancer research is highly necessary to further illuminate implications of DM in tumor promotion.

1.1 Diabetes Mellitus

Next to the minor groups of *impaired glucose tolerance* and *gestational diabetes* (WHO, 2015), the metabolic disorder DM can be classified into the two most common groups *type 1 diabetes mellitus (T1DM)* and *type 2 diabetes mellitus (T2DM)* (National Diabetes Data Group, 1979).

T1DM is marked by an absolute deficiency of insulin resulting in increased glucose levels in the blood and urine. In the majority of T1DM patients, autoimmune destruction of

insulin-producing beta cells in the pancreas is the underlying cause for the chronic disease.
A lifelong insulin substitution therapy remains compulsory to avoid lethal consequences of hyperglycaemia (Bastaki, 2005).

In contrast, development of T2DM is a long-term process. The main risk factor for its manifestation is a sedentary lifestyle characterized by hyper-caloric diet and lack of physical activity for an extended period (Tuomilehto et al., 2001). As causal consequence, this results in a vicious circle of *obesity, inflammation, hyperinsulinemia* and *insulin-resistance* (McArdle et al., 2013; van Greevenbroek et al., 2013). These developments highly favor manifestation of T2DM.
Without any interventions, the pancreas further increases the insulin production attempting to compensate the present relative insulin deficiency. This however empowers the vicious circle of hyperinsulinemia and leads to an exacerbation of T2DM.
If patients are not willing to change their unhealthy lifestyle, a medical treatment with oral-antidiabetics will be required in order to prevent long-term effects of elevated blood glucose levels by offsetting the *relative* insulin deficiency (DeFronzo, 1999).
A depletion of the pancreas can be a consequence of long-term overload accompanied by a marked reduced insulin production. At this point, an insulin substitution therapy becomes indispensable for T2DM patients.

1.1.1 Worldwide Prevalence of Diabetes Mellitus

The International Diabetes Federation reported a total number of 371 mio diabetics worldwide in 2012 (Abdullah et al., 2014). The majority (90-95 %) suffered from T2DM (American Diabetes Association, 2008). According to forecasts, the prevalence of T2DM will grow significantly in the future (Wild et al., 2004) indicating that the metabolic disorder takes features of a pandemic disease. The increasing sedentary lifestyle within our society can be attributed to be the major reason for its expansion. In addition, dramatically enhanced numbers of children and young people affected (Fagot-Campagna,

2000) as well as steadily ascending life expectances pose further challenges in DM management.

Especially in Southeast Asia, T2DM has become a large public health problem. Fast-growing population rates, urbanization and rapid economic development along with changes in living conditions and nutrition within a short period of time are reasons for this observation (Cheema et al., 2014).

Thus, the classical image of T2DM as a disease that concerns elder people of the western population exclusively ("senile DM") is undergoing a radical transformation.

In consequence, a successful diabetes management based on precise knowledge about molecular implications of T2DM becomes more important in current and future times.

1.2 Cancer

1.2.1 Characteristic Features of Tumor Cells

Cancer is the general name for a group of diseases marked by presence of *malignant* tumor cells. In contrast to their normal differentiated counterparts, cancer cells are characterized by abnormal uncontrolled growth, the ability to invade to adjacent tissues and to spread via blood vessels or the lymphatic system through the body establishing new tumors (metastases) (Koda-Kimble et al., 2009). Those features can be attributed to an efficient use of several growth factors, the capability to stimulate the formation of new blood vessels (angiogenese) and avoidance of apoptosis (Fig. 1). However, during their development, malignant tumors obtain a differing set of functional capabilities by using varying mechanistic strategies (Hanahan et al., 2000).

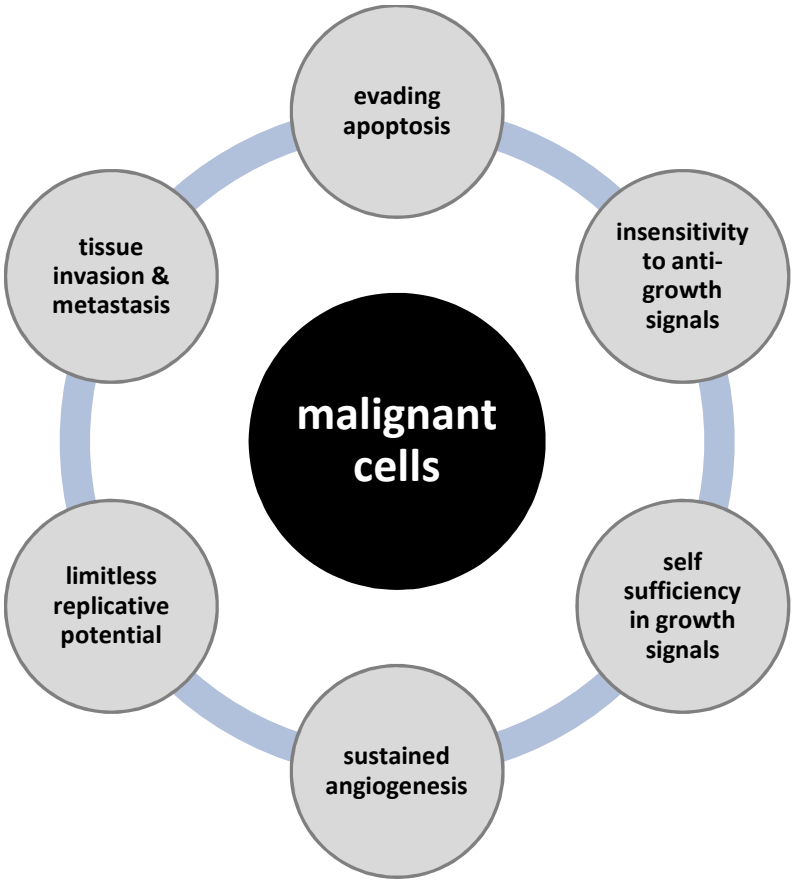

Figure 1: Specific Features of Malignant Tumor Cells.

During their development from normal to malignant cells, cells acquire various capabilities in order to become independent from their cell environment and to empower growth and survival. Source: own illustration following (Hanahan et al., 2000).

Reasons for the process of carcinogenesis are heterogenous. Endogenous reasons comprise genetic dispositions. Physical, chemical and biological carcinogens are counted among exogenous reasons. Those include environmental factors, viruses or bacteria, medical drugs and an unhealthy lifestyle, e.g. cigarette smoke, long-term stress, poor-diet, obesity, lack of physical activity or abuse of alcohol.

Exposure to carcinogens can cause mutations resulting in activation of oncogenes and/ or inactivation of tumor suppressor genes.

1.2.2 Lung Cancer

Lung cancer remains the leading cause of death within cancerous diseases worldwide (1.59 mio deaths per year) (Jemal et al., 2010; Steward & Wild, 2014). Consumption of cigarettes, cigars or pipes displays the predominant reason for its development; in 75-80 %, smoking is considered to be the accountable chemical carcinogen leading to lung cancer (Koda-Kimble et al., 2009).

There are more than ten different types of primary pleuropulmonary malignancies. However, adenocarcinoma, squamous cell, large cell and small cell carcinoma represent the four major types accounting for 95 % of all lung cancers (Koda-Kimble et al., 2009).

Due to their similarities in prognosis and response to therapy, adeno-, squamous and large cell carcinoma, each named in conformity with their morphology, can be classified as non-small cell lung cancer (NSCLC). However, each type reveals specific characteristics in cell growth, spread and aggressiveness ("Non-Small Cell Lung Cancer Treatment (PDQ®)," 2014).

Relapse and mortality rates are high, albeit NSCLC and small cell lung carcinoma (SCLC) are responsive to first-line chemotherapy (Schiller, 2001).

The overall five year survival for lung cancer is approx. 16 % (American Cancer Society, 2014).

1.3 Association between Diabetes Mellitus and Cancer

Results of the Cancer Prevention Study conducted by the American Cancer Society clearly indicate an association between cancer and excess body weight; 14 % of cancer deaths in men and 20 % in woman can be attributed to obesity (Calle et al., 2003).

Beyond, various epidemiological studies reveal an explicit involvement of T2DM in tumorigenesis (Li & Kong, 2014). In the population of diabetic patients an increased incidence of several cancer entities, including liver (El-Serag et al., 2006), pancreas (Everhart & Wright, 1995), breast (Wolf et al., 2005), colorectal (Larsson et al., 2005), endometrial (Friberg et al., 2007), bladder (Larsson et al., 2006), kidney (Bao et al., 2013) and Non-Hodgkin's lymphoma (Frasca et al., 2008; Sciacca et al., 2013) and elevated rates

of cancer mortality have been reported (Barone et al., 2014). However, considered from a pathophysiological point of view, precise molecular mechanisms providing an explanation for this link are still not proved.

As insulin is a potent anabolic hormone (see chapter 2), long-term hyperinsulinemia, caused by raised circulating endogenous insulin levels or substitution therapy, is esteemed to be one key factor for the association between T2DM and cancer (Weinstein et al., 2014).

2 Role of the Insulin and IGF-1 Family in Cancer Progression

2.1 Insulin and IGF-1

Insulin and IGF-1 are cognate peptides which show large similarities in their molecular structures indicating that both derived from a common ancestor gene (Varewijck & Janssen, 2012). Although their physiological roles are specific, certain features are overlapping due to binding to closely related receptor tyrosine kinases (RTK) (see chapter 2.2) (Versteyhe et al., 2013).

The peptide hormone insulin is secreted in pancreatic β-cells in response to elevated blood glucose levels. Its main function is glucose-uptake in skeletal muscles and fatty tissue (Löffler et al., 2007).

Besides, insulin has several additional effects of which stimulation of protein biosynthesis takes an outstanding role. As prominent anabolic hormone, insulin has the potential to empower the growth of pre-existing neoplasms (Corpet et al., 1997; Heuson et al., 1972).

However, a number of unsolved questions remain. It is still unclear whether activation of insulin receptors (IR) or IGF-1 receptors (IGF-1R) leads to mitogenic effects. Moreover, the concentration range and the period of (elevated) insulin levels provoking an enhanced cell proliferation are not generally determined.

Based on the aforementioned context of increasing rates of diabetics going along with an enhanced use of exogenous insulin administration, it is of growing importance to analyze insulin's impacts on tumor promotion in more detail.

Since IGF-1, also called somatomedin C, is the major growth promoting factor in vivo, it plays a crucial role in malignancies. It upregulates cell growth, survival and differentiation (Siddle et al., 2001). Cancer cells can regulate their growth and survival via increase of IGF-1 production (Wang & Wong, 1998).

Attributed to increased insulin levels in the portal circulation, the growth hormone receptor signaling is induced resulting in an enhanced hepatic IGF-1 production (Baxter et al., 1980). Hyperinsulinemia can consequently influence the IGF-1 production.

This mechanism represents one approach explaining the correlation between tumor development and T2DM.

2.2 Insulin and IGF-1 Receptors

Like their ligands, the IR and the IGF-1R are highly homologous. Their ligand-binding and their tyrosine kinase domains reveal approx. 65 % and 80 % homology (Frasca et al., 2008; Heidegger et al., 2012). Those relevant structural and functional similarities are responsible for cross-reaction binding of the ligands insulin and IGF-1 to the respective non-cognate receptor (De Meyts & Whittaker, 2002).

IR and IGF-1R are tetrameric integral membrane proteins which belong to subtype 2 of RTK (Yarden & Ullrich, 1988). Both are synthezised via translation as single chain pro-receptors (precursors), each consisting of a linear α-β-chain sequence. After dimerization of two precursors in the endoplasmatic reticulum and subsequent post-translational processing in the Golgi apparatus, the receptor becomes functional. In its final conformation, the α-subunit is positioned in the extracellular space, whereas the β-subunit spans the cell membrane.

The molecular weight of the α-subunits is 135 kDa for both, IR and IGF-1R. The β-subunits are 95 kDa weigh in IR and 97 kDa in IGF-1R (Löffler et al., 2007; Surmacz, 2000). Via covalent disulfide bridges, monomers are held together (Fig. 2) (Olefsky, 1990).

The first step of insulin/IGF-1 receptor signaling is initiated by ligand-binding to the extracellular α-subunits of the respective receptor. A conformational change of the receptor follows which in turn leads to activation of the intracellular tyrosin kinase. This mediates ATP-dependent autophosphorylation of the β-subunit. Docking proteins, particularly insulin receptor substrates (IRS), subsequently bind to phosphorylated tyrosin residues and become phosphorylated themselves. Activated effectors constitute a binding target for downstream signaling proteins that belong to various different intracellular pathways.

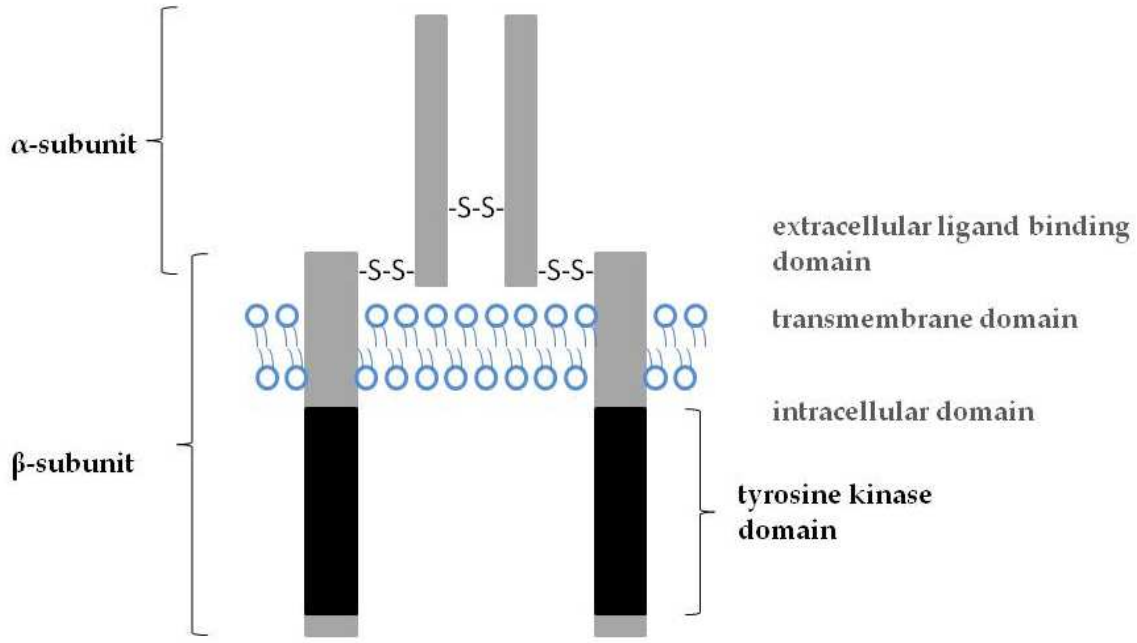

Figure 2: Structure of the Insulin/IGF-1 Receptor.

The receptor tyrosine kinases IR and IGF-1R consist of two identical subunits and reveal the structure $\alpha_2 \beta_2$. Disulfide bridges link receptor chains to each other. The α-chains form the ligand-binding site of the receptor. After ligand-binding, the tyrosin kinase domain, located in the β-chains, becomes autophosphorylated (IR: Tyr1146/1150/1151; IGF-1R: Tyr1131/1135/1136). This phosphorylation results in an activation of downstream signaling pathways. Source: own illustration.

The human IR is encoded by a single gene of which alternative splicing of exon 11 leads to two receptor isoforms, IR-A and IR-B. Exon 11 includes 36 additional nucleotides encoding 12 amino acids of the IR α-subunit at the carboxyl terminus. Transcript IR-A (Ex11-) excludes, whereas IR-B (Ex11+) contains exon 11 (Frasca et al. 1999).

Presence or absence of exon 11 influences receptor-ligand interaction. Thus, IGF-2 binds IR-A but not IR-B with the same affinity as IGF-1R (Kido et al., 2001). In addition, IGF-1 reveals a 10-fold higher affinity towards IR-A as compared to IR-B (Yamaguchi et al., 1993).

IR-B is known to be the predominant isoform expressed in liver, fat and muscle tissues, whereas IR-A is found to be overexpressed in placenta, fetal and cancer tissues (Denley et al., 2004; Frasca et al., 2008).

IR possess a key function in the regulation of glucose homeostasis. Besides, recent studies give evidence that IR expression plays a crucial role in malignancies (Frasca et al., 2008) . Importantly, Kim et al. (2012) further revealed for the first time the impact of IR in survival of NSCLC cells.

Especially the insulin receptor splicing isoform A is considered to be involved in mitogenesis and found to be overexpressed in many malignancies (see above) (Frasca et al., 1999).

However, precise molecular mechanisms of insulin and IR implications in tumor promotion in general are poorly understood yet.

It is well studied that the IGF-1R is linked to prominent mitogenic signaling pathways (see chapter 2.2.1). After activation by IGF-1 or insulin in higher concentrations, tumor transformation, cell proliferation and survival are mediated (Khandwala et al., 2000). For this reason, members of the IGF family, particularly IGF-1 and IGF-1R, represent a prominent target for cancerogenous mutations. Upregulated expression levels of IGF-1 and IGF-1R are frequently found in advanced-stage tumors (Nakagawa et al., 2012), however, mechanisms of aberrant overexpression remain evasive (Guo et al., 2013). Regarding NSCLC cells, several studies associated IGF-1R expression to poor prognosis (Merrick et al., 2007; Nakagawa et al., 2012; Pollak, 2008), whereas others reported no significant correlation between survival and IGF-1R expression (Cappuzzo et al., 2010; Ludovini et al., 2009).

Next to expression of mere homodimeric IR and IGF-1R, heterodimeric hybrid receptors (HR), formed of each one IR and IGF-1R α-β-dimer (Fig. 3) can be detected in mammalian tissues that coexpress IR and IGF-1R (De Meyts & Whittaker, 2002; Johansson & Arnqvist, 2006). Heterodimerization of pro-receptors occurs with a similar probability like homodimerization. In consequence, amounts of HR are proportional to the mole fraction of IR and IGF-1R in the respective tissue (Benyoucef et al., 2007). It follows that overexpression of IR and IGF-1R in malignant cells also leads to overexpression of HR (Frasca et al., 2008).

It was detected that HR bind IGF-1 with high but insulin with low affinity (Bailyes et al., 1997). However, it is still unclear which role heterodimeric IR/IGF-1R take in vivo in general and in malignant tissues in particular.

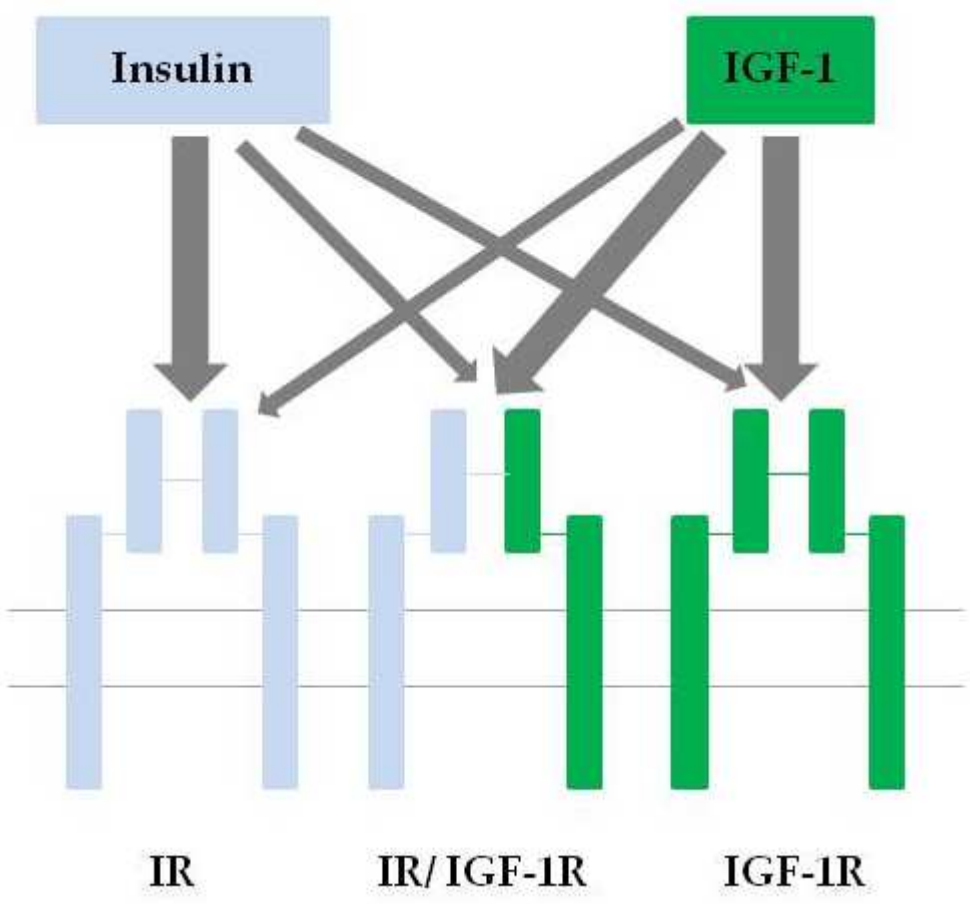

Figure 3: IR, IGF-1R and Heterodimeric IR/IGF-1R.

Rough outline of homodimeric IR (left), IGF-1R (right) and heterodimeric IR/IGF-1R (middle). Thickness of arrows implies ligand affinity to respective receptors: insulin and IGF-1 bind their cognate receptors with the highest affinity, physiological concentrations of IGF-1 but not insulin activate HR. Source: own illustration.

2.2.1 Mitogenic Signaling Pathways

The insulin/IGF superfamily is highly complex. It includes different ligands, notably insulin, IGF-1 and IGF-2 and a variety of receptors (see chapter 2.2). This large number of molecules being involved in IR signaling results in approx. 1,000 combinatorial possibilities in the first steps of the insulin/IGF-1 signaling pathway (Taniguchi et al., 2006).

Furthermore, insulin-like growth factor binding proteins (IGFBP) belong to the insulin/IGF superfamily. By modulating IGF distribution and disturbing the access of IGF to its receptor, IGFBP further complicate the signaling network (Baxter, 2014).

The recently identified IGF-like (IGFL) gene family and insulin like proteins (INSL) represent new ligands and receptors of the insulin/IGF superfamily (Lobito et al., 2011; Lu et al., 2005); their explicit functions are not clearly understood yet.

Cancer cells acquire the capabilities of unlimited cell growth accompanied by independence of proliferative signals and avoidance of apoptosis. Further properties like invasion, angiogenesis and metastatic spread complete their malignant behavior (Fig. 1).

In order to develop these features, malignant cells exploit Phosphatidylinositol-3 kinase (PI3K)/Akt and Extracellular-signal-regulated kinases (ERK)/mitogen activated protein kinase (MAPK) pathways by excessive upregulation. Thus, both pathways constitute key nodes in IR-induced mitogenic signaling (Taniguchi et al., 2006).

2.2.1.1 Akt Signaling

The serine/threonin kinase Akt, also referred to as Proteinkinase B (PKB), is a downstream effector of PI3K (Burgering & Coffer, 1995) and takes a critical regulatory role in insulin metabolism and cancer progression (Manning & Cantley, 2007).

Akt kinases exist in three isoforms, *Akt 1* (PKB α), *Akt 2* (PKB β) and *Akt 3* (PKB γ), each encoded by a particular gene (Murthy et al., 2000). The isoforms slightly vary in their explicit functions and are expressed to a specific extent in different tissues. The predominant type in mammals in general is Akt 1. It triggers protein synthesis and cellular survival. Akt 2 is mainly required to induce the glucose transport; hence, it is a mediator of basic insulin functions. High expression rates are found in all "classical" insulin-responsive tissues. The role of Akt 3 which is mostly detected in brain and testes is less clear (Bhaskar & Hay, 2007).

After IR/IGF-1R activation upon ligand-binding, IRS docking proteins are recruited to the receptor. In consequence of IRS phosphorylation, the regulatory subunit p85 and the catalytic subunit p110 of PI3K are activated, leading to generation of phosphatidylinositol-3,4,5-triphosphate (PIP3). Proteins with pleckstrin homology (PH), including Akt, are subsequently translocated to the plasma membrane and bound to the

second messenger PIP3 (Fig. 4). After phosphorylation of Akt at threonin 308 and serine 473 (Bhaskar & Hay, 2007), various signaling cascades are initiated.

Next to its metabolic function of glucose uptake, downstream PKB/Akt signaling has essential impacts on tumor promotion, including mediation of cell proliferation, survival and anti-apoptotic effects (Fig. 4) (Fresno Vara et al., 2004).

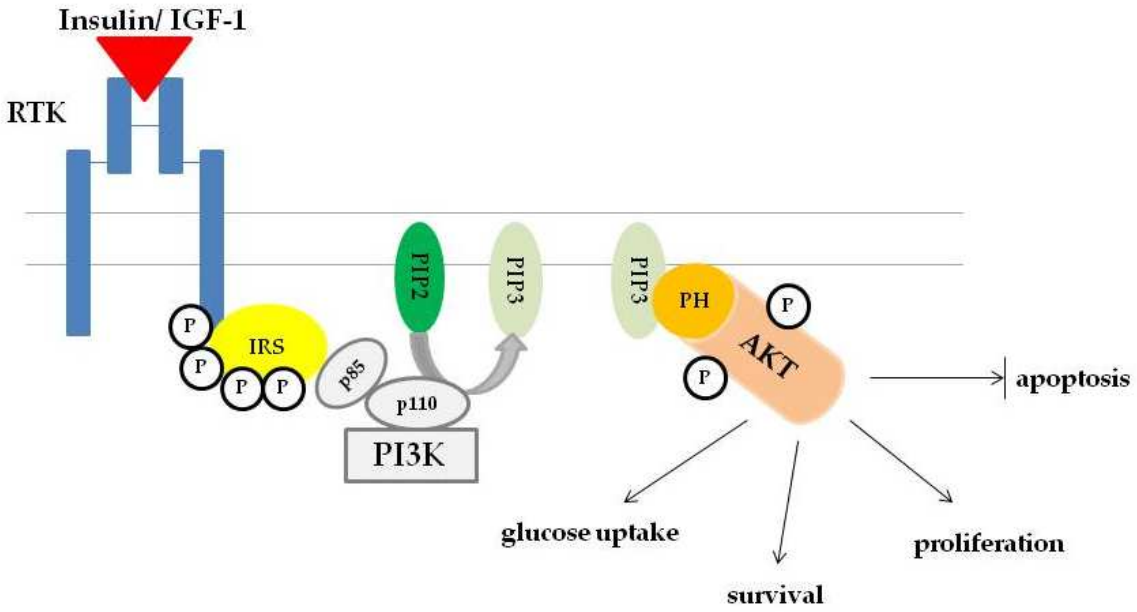

Figure 4: Akt Signaling.

Activation of the RTK leads to receptor autophosphorylation of the tyrosin residues resulting in binding of docking proteins IRS. The catalytic subunit of PI3K is activated by IRS phosphorylation and mediates production of the second messenger PIP3. PIP3 in turn recruits signaling proteins with PH domains, particularly Akt, to the membrane. Akt activation triggers numerous downstream signaling pathways which contribute to different cellular processes (i.e. enhancement of survival, proliferation, glucose uptake and suppression of apoptosis). Source: own illustration based on Bhaskar and Hay 2007; Fresno Vara et al. 2004.

It hence appears obvious that PI3K/Akt signaling is frequently deregulated in many cancer tissues (De Luca et al., 2012; Fresno Vara et al., 2004; Skeen et al., 2006).

In terms of *over-activated* PKB/Akt, cells are enabled to trigger proliferation more effectively. A reinforced response towards growth factors is a general mechanism leading to cell growth autonomy (Manning & Cantley, 2007).

Besides, anti-proliferative signals mediated by the tumor suppressor gene p53 are undermined due to Akt-caused induction of the pro-oncogene Mdm2 (Testa & Bellacosa, 2001).

Suppression of apoptosis by PKB/Akt is steered by the general mechanism (Robey & Hay, 2006) of inhibition of pro-apoptotic proteins, i.e. Ask1, FKHR (Kim et al., 2001) and BAD (Lawlor & Alessi, 2001). However, Akt can directly prevent apoptosis by an inhibitory phosphorylation of initiator caspase 9 (Lawlor & Alessi, 2001).

2.2.1.2 ERK/MAPK Signaling

MAPK pathways include a three-tier kinase module, containing a *MAP kinase kinase kinase* (MAPKKK), a *MAP kinase kinase* (MAPKK) and a *MAP kinase* (MAPK) (Ferrell, 1996). Phosphorylated MAPKKKs activate MAPKKs via phosphorylation of two serine residues. By this, seronine/threonine residues of MAPKs are phosphorylated (Fig. 5).

Figure 5: Schematic Overview of the Three-tier Kinase MAPK Module.

Activation of MAPK proceeds as signal-relay cascade: Upon stimulus-induced activation of MAPKKKs, MAPKKs are phosphorylated which in turn phosphorylate MAPKs. Source: own illustration.

On the basis of different activating factors, to date, six different MAPKs are characterized in mammals (Dhillon et al., 2007; Roux & Blenis, 2004):

ERK1/2, *ERK3/4* (Marquis et al., 2014), *ERK 5* (Davis, 2000; Kyriakis & Avruch, 2001),*ERK7/8* (Cargnello & Roux, 2011), *p38-kinases isozymes* (p38-α,-β,- ɣ,-δ) and *Jun N-terminale kinases* (JNK1, JNK2, JNK3) (Schaeffer & Weber, 1999).

ERK1 and ERK2 share 83 % amino acid homology and reveal equal functions in intracellular signaling (Chen et al., 2001). The ERK1/2 cascade, also named *Ras/Raf/MEK/ERK MAPK pathway*, is stimulated by growth factors and presents the

classical mitogen kinase pathway that plays a crucial role in malignancies. In this Ras-dependent signaling, serine/threonine Raf kinases (Raf-1, Raf-2, Raf-3) take on the function as MAPKKKs (Qi & Elion, 2005). The MAPKKs are represented by MAPK/ERK-activating kinases 1 and 2 (MEK1/MEK2), whereas ERK1/2 are the final MAPKs.

After binding of growth factors, i.e. insulin or IGF-1 to their appropriate RTK, receptor autophosphorylation follows. The phospho-tyrosine residues serve as docking sites for the growth-factor-receptor-bound protein 2 (Grb2). Grb2 acts as adaptor protein between the RTK and the guanine-nucleotide exchange factor son of sevenless (SOS) protein (Watanabe et al., 2000). Via exchange of GDP into GTP, the proto-oncogene Ras becomes active and binds Raf kinases. Activated Raf phosphorylates MEK which in turn phosphorylates ERK (Meier et al., 2005). Upon ERK activation numerous cytoplasmic and nuclear targets can be phosphorylated resulting in proliferation and survival as well as migration and angiogenesis (Dhillon et al., 2007; Yoon & Seger, 2006) (Fig. 6).

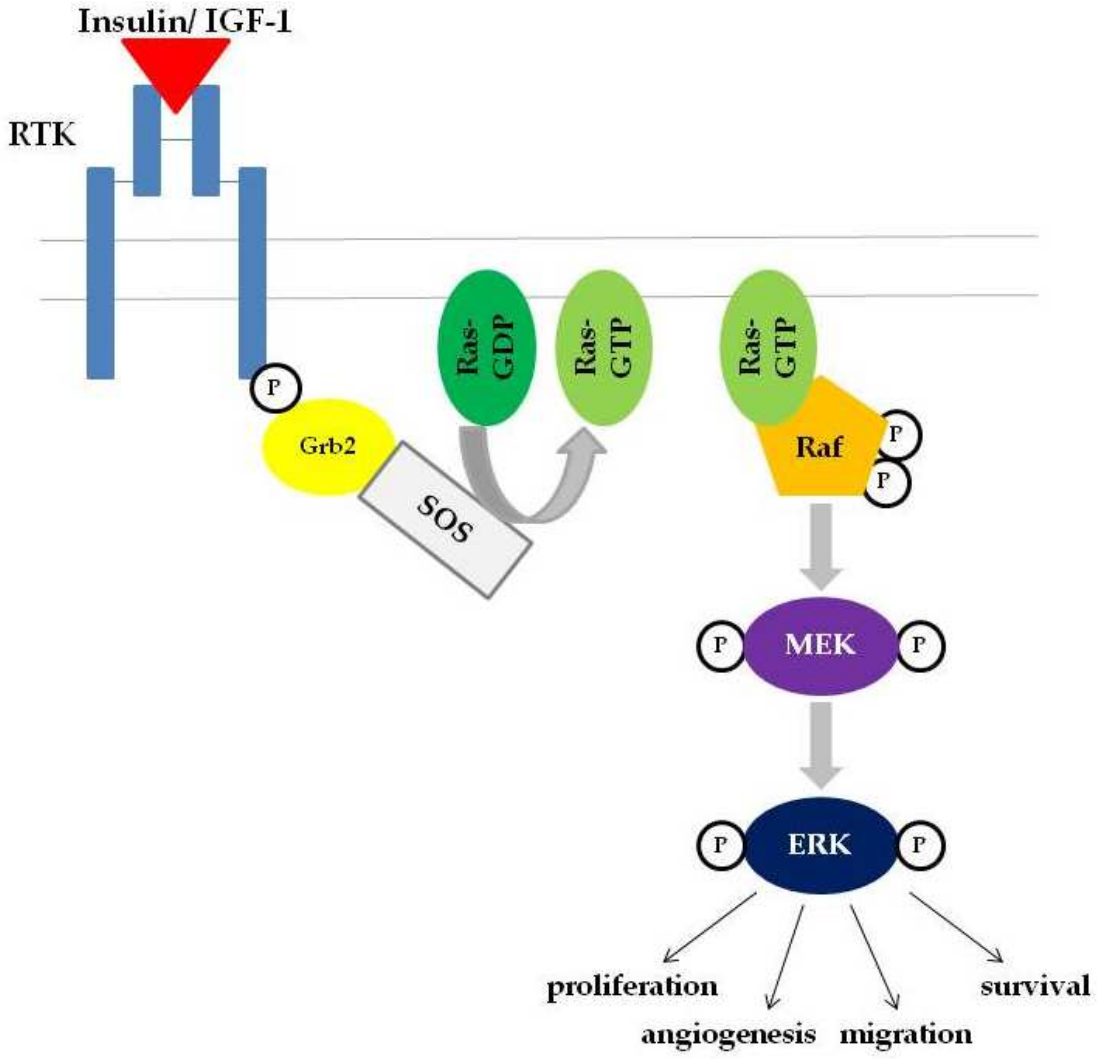

Figure 6: Schematic Overview of ERK/MAPK Signaling.

Activation of RTK results in recruitment and phosphorylation of Grb2. Ras proteins are transformed into their active GTP-form by the guanine-nucleotide exchange factor SOS. After binding of Ras-GTP to Raf, Raf becomes phosphorylated. In a signal-relay-process, following kinases are phosphorylated resulting in MAPK-dependent mitogenic effects. Source: own illustration following (Roberts & Der, 2007).

The Ras-dependent Ras/Raf/MEK/ERK MAPK signaling pathway is abnormally activated in the majority of cancers. Mutations occur in upstream RTK or in components of the MAPK module (Mccubrey et al., 2007). ERK1/2 activation is associated to an aggressive tumor behavior and poor survival (Roberts & Der, 2007).

3 Role of TGF-β in Tumor-Promotive Processes

3.1 Epithelial Mesenchymal Transition and Cancer Progression

Epithelial and mesenchymal cells are two main cell types in mammals and reveal specific differences in their morphology and functions.

Epithelial tissue is composed of highly sorted cell monolayers that form a barrier in order to protect from pathogens and to participate in secretion (Xu et al., 2009).

Epithelial cells have apical-basal polarity and are characterized by cohesive interactions, adherence to each other through tight junctions and a lack of mobility of individual cells (Larue & Bellacosa, 2005).

In contrast, mesenchymal tissue consists of loosely associated cells without polarity which allows cell mobility. As a result, mesenchymal cells display a high capacity for migration and invasion (Larue & Bellacosa, 2005).

Epithelial mesenchymal transition (EMT) is a process of conversion of epithelial cells to mesenchymal cells (Xiao & He, 2010) with respective changes of cell capabilities.

During EMT, epithelial cells lose their polarity and their cell-cell adhesion by disintegration of tight junctions (Kalluri & Neilson, 2003). The transitory process is accompanied by a switch of epithelial cell marker expression (e.g. E-cadherin) to expression of mesenchymal cell markers (e.g. N-cadherin and fibronectin) (Rosanò et al., 2006; Xiao & He, 2010). In consequence, the phenotype of (former) epithelial cells becomes smooth-muscle like and cells obtain mesenchymal functions (Fig. 7).

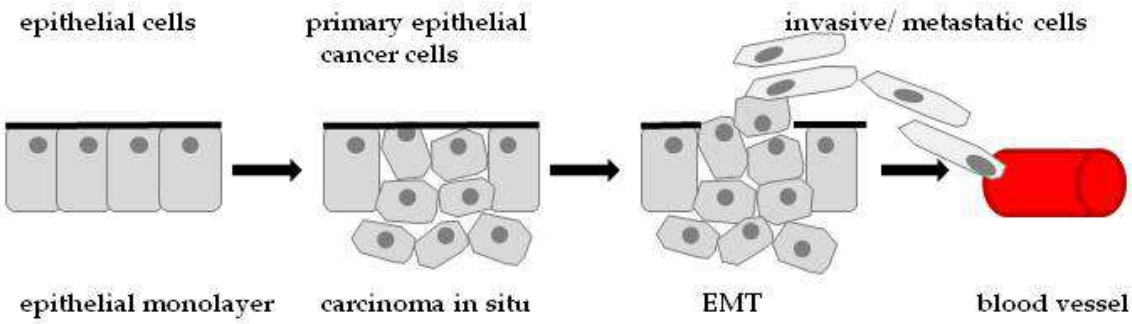

Figure 7: Schematic Overview of the EMT Process in Cancer Cells.

EMT contributes to tumor promotion through initiation of invasion of malignant cells into the blood stream. Epithelial cells form a monolayer surrounded by a basement membrane. During the invasive carcinoma stage, epithelial cells lose their polarity and begin to detach from the basement membrane. The phenotype of (former) epithelial cells becomes smooth-muscle like. Cell-cell interactions are entirely dissolved facilitating cell migration and invasion into other tissues. Source: own illustration following (Kalluri & Weinberg, 2009).

EMT is highly involved in cancer progression by initiating metastasis and invasion into other tissues (Hugo et al., 2007; Lee et al., 2006). Notably, there are important differences between physiological and pathophysiological EMT, mostly referring to the complexity of the transitory process. While normal EMT comprises multiple comprehensive mechanisms, EMT during tumor development appears to be based on activation of single cellular or molecular EMT-inducing events.

Activation of several mitogenic signaling pathways (Boyer et al., 1997), such as Smad (Moustakas & Heldin, 2007), Akt (Grille et al., 2003) or ERK (Jechlinger et al., 2002) are known to trigger the EMT program. Besides, IGF-2 represents a prominent inducer of EMT (Larue & Bellacosa, 2005).

However, the full spectrum of agents initiating the invasion-metastasis-cascade in carcinoma cells still remains unclear (Kalluri & Neilson, 2003).

The cytokine transforming growth factor β (TGF-β) is one major inducer of EMT during embryonic development and cancer progression (Lamouille et al., 2014; Miettinen et al., 1994).

Adding TGF-β to epithelial cells in vitro is an appropriate way to induce EMT (Xu et al., 2009). In response to TGF-β-binding to its cognate receptor, phosphorylation of Smad2 and Smad3 is initiated. Subsequently, a trimeric Smad complex containing phoshpho-Smad2/3 and recruited Smad 4 is formed and translocated into the nucleus. Association and cooperation with DNA-binding transcriptional factors, such as Snail, ZEB and bHLH family members (Jechlinger et al., 2002; Thiery, 2002) follows, resulting in repression of epithelial marker gene expression and initiation of mesenchymal gene expression (Fuxe et al., 2010; Kalluri & Weinberg, 2009).

3.2 TGF-β Interactions with the IGF-1 Family in Cancer Progression

TGF-β reveals bidirectional functions in cancer promotion. The growth factor supports EMT induction but also acts as tumor suppressor by inhibition of cell proliferation (Muraoka-Cook et al., 2005).

A molecular mechanism yielding antiproliferative effects of TGF-β can be assigned to inhibition of Cyclin-dependent kinases (CDKs) which control cell cycle progression. Activation of CDKs leads to enhanced gene transcription of various cell cycle regulators, particularly oncogenes. However, TGF-β is capable of mediating cell cycle arrest due to induction of CDK-inhibitor expression (Lebrun, 2012).

Furthermore, TGF-β directly represses the expression of several growth promoting factors, like the oncogene c-MYC (Chen et al., 2002; Lasorella et al., 2000).

Insulin and IGF-1 are not known to initiate the EMT program but favor cell proliferation (see chapter 2.1).

Hence, it becomes evident that TGF-β could take an oppositional role compared to IGF-1 and insulin in malignant cells.

4 Inhalable Insulin: a Novel Route of Insulin Substituiton Therapy

Insulin substitution therapy is required to lower blood glucose in patients with T1DM and later stage T2DM. Currently, subcutaneous (s.c.) injections via insulin pens or syringes constitute the most common method in insulin application (Magwire, 2011). However, prevention of daily injections would be a new milestone in the management of DM (Cefalu, 2004).

Since its initial discovery in 1922 by Banting and Best, it was aimed to develop and establish an alternative route of insulin administration, e.g. via oral, nasal, buccal or inhaled application (Yaturu, 2013).

Noninvasive insulin delivery systems are associated with an increased clinical acceptance and lower psychological barriers to insulin treatment compared to s.c. injections (Cefalu, 2001). The lung represents a suitable portal for peptide drug delivery. It provides a large surface area (≈ 40-150 m^2), high vascularization of approx. 500 mio alveoli and low thickness of the alveolar-capillary barrier (0.2 μM) resulting in a rapid absorption of the hormone (Santos Cavaiola & Edelman, 2014; Scheuch et al., 2006).

Marked pharmacological advantages of pulmonary drug administration are absence of the hepatic first-pass effect, only low expression rates of local proteases and a rapid onset of action (Siekmeier & Scheuch, 2008).

Various studies revealed that patients would prefer an inhalable to an injectable route (Cappelleri et al., 2002; Chancellor et al., 2008) which in turn emerges as parameter for an enhanced quality of life (Qol) and an improved compliance.

Next to the aforementioned benefits, however, pulmonary insulin administration poses several requirements for deposition of the appropriate amount of insulin for a therapeutic effectiveness (Labiris & Dolovich, 2003).

Technological challenges mainly refer to the particle size, shape, density and aerosol homology. At this, the median aerodynamic diameter (MMAD) plays a critical role.

Being too small (< 1 μm), particles are exhaled, being too large (> 3 μm), particles are most likely deposited in the oropharynx or swallowed without reaching the alveolar area (Agu et al., 2001).

After its investigation in 1971 (Wigley et al., 1971), inhaled insulin remained far away from being introduced into clinical therapy (Siekmeier & Scheuch, 2008). The major disadvantage of this route of administration has always been the comparably *low* bioavailability of insulin; even after two decades of research and development of improved aerosol and application features, only 20-25 % of insulin reach the systemic circulation (Cefalu, 2004; Niven, 1995). As a result, the amounts of the inhaled insulin concentration have to be increased drastically.

Varying bioavailability rates, attributed to individual patient-related factors, further complicate an appropriate adjustment of insulin. Genetically-determined and pathophysiologically-caused variations in the lung architecture influence delivery of constant insulin concentrations.

Additionally, it appears difficult for patients to proceed a steadily correct breathing maneuver marked by a precise deep and slow breathing procedure (Siekmeier & Scheuch, 2008).

4.1 Inhalable Insulin: Exubera® and Afrezza®

Exubera® (Pfizer Inc/ Nektar Therapeutics) is a dry powder formulation consisting of regular short-acting recombinant human insulin. It was approved for adult T1DM and T2DM patients by the US Food and Drug Administration (FDA) and the European Medicines Agency (EMA) and reached market launch in September 2006.

Clinical trials confirmed similar quality of HbA_{1C} adjustment as compared to s.c. insulin. The single-dosage of Exubera® amounted 1 mg (approx. 3 U insulin) or 3 mg per blister. After inhalation of the aerosol (MMAD < 5 μm), insulin was absorbed quickly resulting in an onset of action that was even faster than after s.c. administered human insulin (Siekmeier & Scheuch, 2008). In fact, Exubera® mimicked the natural pattern of postprandial insulin secretion like the rapid-acting insulin analogs (Rave et al., 2005)

insulin lispro, insulin aspartat and insulin glulisine. The duration of action was comparable to s.c. human insulin (Rave et al., 2005).

However, bioavailability rates of insulin via Exubera® inhaler were 10-16 % (Siekmeier & Scheuch, 2008).

Due to the significant impact of smoking on pulmonary drug absorption (Fountaine et al., 2008), smokers were excluded from inhaled insulin treatment.

Exubera® was withdrawn in October 2007. The main reason for its failure was the lack of market acceptance. Although the technology of aerosol distribution into the deep lung worked fine, patients did not accept the big inhaler with its cumbersome handling, not allowing a discret, simple and quick insulin inhalation (Heinemann, 2008).

Besides, fears for lung safety (see chapter 4.2) have been a further issue for the missing clinical success.

Since June 2014 a new inhaled insulin product, Afrezza® (MannKind Corporation), received its approval by the FDA.

Afrezza® is a dry powder Technosphere® insulin (TI), serving as novel drug delivery system. Technosphere® formulations consist of 3,6-bis[N-fumaryl-N-(n-butyl)amino]-2,5-diketopiperazine molecules that micro-encapsulate and stabilize peptides in small particles (MMAD: 2 μm) (Pfützner et al., 2002). This results in a higher percentage of drug absorbance compared to former inhaled insulin formulations. The bioavailability of TI amounts 21-25 % (Sarala et al., 2012). Afrezza® is an ultra-rapid-acting insulin. The onset of action is faster and the duration of action is shorter than rapid-acting insulin analogs (Klonoff, 2014). As already determined for Exubera®, Afrezza® is not recommended for children and patients who smoke or have recently stopped smoking.

The TI is applicated in an inhaler called DreamBoat or Gen2, which was designed to reduce device cost, decrease local side effects and improve efficiency (Nuffer et al., 2014). As compared to the Exubera® inhaler, the Gen2 inhaler may overcome the barrier of patients' acceptance due to its smaller and handier size.

4.2 Safety Concerns of Inhaled Insulin Therapy Regarding Lung Cancer Promotion

Different clinical trials with durations of each three or six months have demonstrated safety and effectiveness of pulmonary insulin administration (Quattrin et al., 2004; White & Campbell, 2001).

General adverse drug reactions of TI were analyzed in a two-year-study in 635 non-smoking adults with T2DM. An overall positive outcome was shown (Rosenstock et al., 2008).

As long-term safety has not been established yet (Sarala et al., 2012), there still exist concerns about the inhaled insulin delivery approach (Mandal, 2005). Exposure to unphysiologically high insulin levels in the oropharynx and lungs (Santos Cavaiola & Edelman, 2014) which probably lasts over decades, bear a risk to provoke local pathophysiological modification (Siekmeier & Scheuch, 2008). Especially tumor-promotive effects, such as increased cell proliferation, support of cell survival and changes in cell phenotype display potentially harmful outcomes of insulin signaling (see chapter 2) caused by long-term insulin exposure in the respiratory system (Bloomgarden, 2014; Mayer et al., 2012).

Particularly patient groups with an increased prevalence of cancer entities in the respiratory system, e.g. ex-smoker, people being exposed to smog or patients with chronic inflammatory diseases, could be highly affected by mitogenic features of the anabolic peptide.

There are no further studies addressing these pharmacological concerns. It thus appears indispensable to focus on a comprehensive investigation of insulin and IR involvement in tumor promotion.

II Aim of the Study

The lung represents a novel non-invasive route for insulin administration. However, concerns about long-term safety of this delivery approach remain, because insulin as anabolic hormon might be involved in tumor-promotive processes in the respiratory system.

These safety concerns have arisen with the approval of Exubera® and attracted renewed attention with recently approved Afrezza® in the United States.

Clarification of this matter is of interest for approving authorities, the Federal Institute for Drugs and Medical Devices, pharmaceutical companies and not least for patients.

The present study focused on the following issues:

I. *Does insulin display mitogenic features in different human NSCLC cell lines?*

Inhaled insulin is accompanied by constantly increased drug concentrations as compared to s.c. injections. Thus, precise knowledge of insulin action (in supraphysiological concentrations) in the lungs is required.

This general enquiry mainly refers to anabolic effects of insulin, i.e. its impact on proliferation and mitogenic signal transduction, namely Akt and ERK.

Differences and similarities between effects of insulin and IGF-1 were studied and correlated to insulin and IGF-1 receptor expression in the respective cell lines.

Besides, further interest was given to interactions between TGF-β and insulin and their impact on phenotypical changes in NSCLC cells due to EMT.

II. *Which role does the insulin receptor take in tumor cell promotion in NSCLC cells?*

The insulin receptor is only rarely expressed in the respiratory system and it is not known yet which effects might follow when high insulin concentrations are present in the lungs over a long period.

Neither insulin nor the IR have been in the focus of cancer research in the last decades, since both were in the background of IGF-1 and the IGF-1R. Thus,

knowledge about precise implications of the IR on cancer-supporting development is required.

This study presents IR and IGF-1R knockdown studies in NSCLC cell lines in order to illuminate the role of IR as compared to IGF-1R in cancer cell progression.

Taken together, the roles of insulin and the IR in different NSCLC cell lines were analyzed in more detail to draw conclusions on pharmacological safety aspects in the therapy with inhalable insulin and, more generally, to obtain deeper insight in the role of the insulin receptor in tumor progression.

III Materials and Methods

1 Materials

1.1 Equipment

Centrifuges	Centrifuge 5702, Eppendorf, Hamburg Centrifuge 5810, Eppendorf, Hamburg Heraeus® PICO 17 Centrifuge, Thermo Scientific, MA, USA Minispin® plus, Eppendorf, Hamburg
Cell counter and analyzer	Cedex XS, Roche, Mannheim
Digital camera	Canon EOS 500 D, Canon, Japan
Electrophoresis and blotting systems for Western blot analysis	XCell SureLock® electrophoresis system with XCell II™Blot Module, Invitrogen, Karlsruhe
Electrophoresis system for PCR analysis	Electrophoresis power supply unit Macrodrive 5 with electrophoresis chamber, LKB Bromma, Sweden
Gels for Western blotting (ready-to-use)	NuPAGE® 4-12 % bis-tris gels, Invitrogen, Karlsruhe
Incubator	HERAcell™ 150i, Thermo Scientific, MA, USA HERAcell™ 240i, Thermo Scientific, MA, USA
Laminar air flow bench	MSC-Advantage™, Thermo Scientific, MA, USA HERAsafe®, Heraeaus, Frankfurt a. M.
Microscopes	Leica DMIL, Leica, Wetzlar Zeiss Axiovert 40C, Carl Zeiss, Jena
Multimode plate reader	Enspire®, Perkin Elmer, MA, USA

Photometer	SmartSpec™ Plus, Bio-Rad, Munich
PVDF Membranes for Western blotting	PVDF Blotting Membrane Immobilion® P, Millipore, Eschborn
Power supply	PowerPac 300, Bio-Rad, Munich
Real-Time PCR instrument	StepOnePlus®, Applied Biosystems, Darmstadt Light Cycler 480®, Roche, Mannheim
Semi-micro cuvettes	Sarstedt, Nümbrecht

Software	Adobe Standard 8.0	Creation of PDF-documents
	Graph Pad Prism 5.00	Graphic representation of results and statistical analyzis
	MS Office 2003/ 2007: Excel, Word	Calculations, text processing
	Gimp 2	Photo editing
	ImageJ	Quantification of Western blot analyzis

Szintillation counter	LS 5000 TD, Beckman, CA, USA
Thermocycler	MyCycler™, Bio-Rad, Munich
Thermomixer	Thermomixer® compact, Eppendorf, Hamburg
X-ray films	Hyperfilm ECL, Amersham, Braunschweig
X-ray film developer and fixer	CP1000, AGFA, Cologne

1.2 Chemicals

Agarose NEEO	Roth, Karlruhe
Albumine from bovine serum (BSA)	Sigma-Aldrich, Munich
Aqua resist	VWR International, Darmstadt
Boric acid	Roth, Karlsruhe
Bromphenol blue	Sigma-Aldrich, Munich
Dimethyl sulfoxid (DMSO)	Merck, Darmstadt
Ethanol (≥ 99.5 %)	Roth, Karlsruhe
Ethidium bromide solution	Roth, Karlsruhe
Ethylenediaminetetraacetic acid disodium salt dihydrate (EDTA)	Sigma-Aldrich, Munich
Fetal calf serum (FCS)	Biochrom, Berlin
Ficoll® 400	Sigma-Aldrich, Munich
Gemcitabine	Cayman Chemical Company, WI, USA
Glycine	Roth, Karlsruhe
Hydrogen chloride (HCl), 32 %	Merck, Darmstadt
Leupeptin	Sigma-Aldrich, Munich
Lipofectamine® RNAiMAX	Invitrogen, Karlsruhe
Lumasafe plus scintillation cocktail	Lumac LSC, Netherlands
Magnesium Chloride Hexahydrate ($MgCl_2$ x 6 H_2O)	Merck, Darmstadt
2-Mercaptoethanol	Sigma-Aldrich, Munich
Methanol	Roth, Karlsruhe
MOPS® SDS Runnung Buffer (20 x)	Invitrogen, Karlsruhe

Nonfat dried milk powder	AppliChem, Darmstadt
Nonidet P-40	Roche, Mannheim
Penicillin/streptomycin solution (10000 U/ml, 10 mg/ml)	Sigma-Aldrich, Munich
Pepstatin A	Sigma-Aldrich, Munich
Phenylmethanesulfonyl fluoride (PMSF)	Sigma-Aldrich, Munich
Ponceau S	Sigma-Aldrich, Munich
Potassium chloride (KCl)	Merck, Darmstadt
Potassium dihydrogen phosphate (KH_2PO_4)	Merck, Darmstadt
2-Propanol	Roth, Karlsruhe
Puromycin	Santa Cruz, CA, USA
RNase away®	Thermo Scientific, MA, USA
Roti®-Load 1	Roth, Karlsruhe
Sepharose® CL-4B	Sigma-Aldrich, Munich
Sodium chloride (NaCl)	Roth, Karlsruhe
Sodium deoxycholate	Sigma-Aldrich, Munich
Sodium dodecyl sulfate (SDS)	Sigma-Aldrich, Munich
Sodium fluoride (NaF)	Merck, Darmstadt
Sodium hydroxide pellets (NaOH)	Merck, Darmstadt
Sodium orthovanadate (Na_3VO_4)	Sigma-Aldrich, Munich
[^{3}H]-Thymidine (1mCi/ml)	Perkin Elmer, MA, USA
Trichloroacetic acid (TCA)	Merck, Darmstadt
Tris-(hydroxymethyl)-aminomethane (tris)	Roth, Karlsruhe
Tris-(hydroxymethyl)-aminomethan-hydrochloride (tris-HCl)	Boehringer, Ingelheim

Triton® X-100	Pharmacia Biotech, Sweden
10 x Trypsin-EDTA solution	Sigma-Aldrich, Munich
Tryptan blue stain (0.4 %)	Sigma-Aldrich, Munich
Tween 20	Sigma-Aldrich, Munich
X-tremeGENE® siRNA Transfection Reagent	Roche, Mannheim

1.3 Cell Culture

1.3.1 Cell Lines

All human bronchial epithelial (HBE) cell lines were purchased from American Type Culture Collection (ATCC, VA, USA):

Cell line	*ATCC Catalog No.*	*Histology*	*Additional information*
NCI-H292	CRL-1848	Mucoepidermoid pulmonary carcinoma	Derived from a 32 year old female of black ethnicity
NCI-H226	CRL-5826	Metastatic squamous cell carcinoma	Derived from a male
NCI-H460	HTB-177	Large cell lung carcinoma	Derived from a male

1.3.2 Culture Media

Culture medium	*Manufacturer*	*Application*
RPMI 1640 medium with L-glutamine	Gibco, CA, USA	Basic culture medium for epithelial cells
Opti-MEM® reduced serum medium	Invitrogen, Karlsruhe	Medium for cationic transfection

1.4 Test Compounds

Test compound	*Manufacturer*	*Concentration range*
Insulin	Sigma-Aldrich, Munich	10 nM- 1 μM
Insulin-like growth factor-1 (IGF-1)	Sigma-Aldrich, Munich	1 nM- 10 nM
Transforming growth factor-β (TGF-β)	Sigma-Aldrich, Munich	2 nM- 5 nM
Interleukin 6 (IL6)	Provitro, Berlin	100 nM
Interleukin 20 (IL20)	Provitro, Berlin	100 nM
Interleukin 24 (IL24)	Provitro, Berlin	100 nM
Tumor necrosis factor α (TNFα)	Provitro, Berlin	100 nM

1.5 Kits

DC™ Protein Assay	Bio-Rad, Munich
BM Chemiluminescence Blotting Substrate (POD)	Roche, Mannheim
Caspase-Glo® 3/7 Assay	Promega, WI, USA
dNTP-Mix	Fermantas, St.Leon-Rot
Nucleospin® RNA	Macherey-Nagel, Düren
Omniscript® RT Kit	Qiagen, Hilden
Power SYBR® Green PCR Master Mix	Applied Biosystems, Darmstadt

1.6 Enzymes

DNase (RNase free DNase Set)	Qiagen, Hilden
Omniscript™ Reverse Transcriptase	Qiagen, Hilden
rDNase	Macherey-Nagel, Düren
Taq DNA Polymerase	Invitrogen, Karlsruhe

1.7 Molecular Size Standards

DNA Ladder Ready-Load 100 bp	Invitrogen, Karlsruhe
PageRuler™ Prestained Protein Ladder	Bio-Rad, Munich

1.8 Nucleic Acids

1.8.1 Nucleic Acids for Reverse Transcription

dNTP-Mix	Fermentas, St.Leon-Roth
Oligonucleotide (dT) 18	MWG, Ebersberg

1.8.2 siRNAs

siRNAs were purchased from Applied Biosystems, TX, USA (Silencer® Select siRNA s7212, s7478, s7479) and Thermo Scientific, MA, USA (ON-TARGETplus Non-targeting siRNA).

Target Gene	*siRNA*	*Sequence (sense and antisense strands)*
IGF-1 receptor	s7212	CCGAAGAUUUCACAGUCAAtt
		UUGACUGUGAAAUCUUCGGct
Insulin receptor	s7478	GAACGAUGUUGGACUCAUAtt
		UAUGAGUCCAACAUCGUUCga
Insulin receptor	s7479	CUACGUGACAGACUAUUUAtt
		UAAAUAGUCUGUCACGUAGaa
ON-TARGETplus Non-targeting siRNA	1	-

1.8.3 shRNAs

shRNAs were purchased from Sigma-Aldrich, Munich.

Target Gene	*shRNA*	*Sequence (sense and antisense strands)*
IGF-1 receptor	sh-NM875a	GCTGATGTGTACGTTCCTGAT ATCAGGAACGTACACATCAGC
IGF-1 receptor	sh-NM875b	GCCTTTCACATTGTACCGCAT ATGCGGTACAATGTGAAAGGC
Insulin receptor	sh-NM208a	GCTCTGTTACTTGGCCACTAT ATAGTGGCCAAGTAACAGAGC
Insulin receptor	sh-NM208b	CCACCATTCGAGTCTGAAGA ATCTTCAGACTCGAATGGTGG
Non-mammalian shRNA control		-

1.9 Primers

Primer	*Accession number*	*Sequence (upstream and downstream primer)*
Endothelin	NM_001955	GTTAAAAGGGCACTTGGGCTGAAGG
		TGGGTCACATAACGCTCTCTGGAGG
Fibronectin	NM_212482	CGATCACTGGCTTCCAAGTTGATGC
		CATGAAGATTGGGGTGTGGAAGGGT
GAPDH	NM_002046	TCCTGTTCGACAGTCAGCCGCAT
		TGAAGACGCCAGTGGACTCCACG
IL6	NM_000600	CCCCCAGGAGAAGATTCCAAAGATGTAG
		GTGGTTGGGTCAGGGGTGGTTATTG
IL20	NM_018724	GCCTCTAGTCTTGCCTTCAGCCTTCTCTC
		GCAGCAGCATCACTTTCCTCCTATTCTGT
IL24	NM_001185156	GTTGTGCTCCCTTGCCTGGGTTTT
		CTCATTTTCTTGACTGGGTTGCAGTTGTG
IR (*splice variant sensitive)*	NM_001079817	GGAGAGGCAGGCGGAAGACAGTG
		CTGGTCGAGGAAGTGTTGGGGAAAG
IR	NM_000208	CAAGAGATGATTCAGATGGCGGCA
		GAGCAGGTTGACAATCTCCAGGAAGGT
IGF-1R	NM_000875	CCTCAACGCCAATAAGTTCGTCCAC
		GATGCTGCTGATGATCTCCAGGAAGG
N-cadherin	NM_001792	CATTCACTGCTCAGGACCCAGATCG
		GGAGTCACACTGGCAAACCTTCACG
TNF	NM_000594	GGCTCCAGGCGGTGCTTGTTC
		GGGCTCTTGATGGCAGAGAGGAGGT

1.10 Antibodies

1.10.1 Primary Antibodies for Western Blotting

Antibody	*Manufacturer*	*Molecular Weight*	*Species*	*Dilution*	*Exposure Time*
α-Tubulin	Cedarlane, Canada	55 kDa	mouse	1:1000	1 sec
phospho Akt (Ser473)	Cell Signaling, UK	60 kDa	rabbit	1:1000	1 sec
Akt	Cell Signaling, UK	60 kDa	rabbit	1:1000	1 sec
phospho p44/42 MAPK (ERK1/2) (Thr202/Tyr204)	Cell Signaling, UK	44/42 kDa	rabbit	1:1000	1 min
ERK 2 MAPK	Santa Cruz, CA, USA	42 kDa	rabbit	1:1000	1 sec
pIGF-1Rβ (Tyr1135/1136) / pIRβ (Tyr1150/1151)	Cell Signaling, UK	95 kDa	rabbit	1:1000	1 min
IGF-1Rβ	Santa Cruz, CA, USA	97 kDa	rabbit	1:500	1 sec
IRβ	Calbiochem, CA, USA	95 kDa	mouse	1:400	1 min

1.10.2 Secondary Antibodies for Western Blotting

Antibody	*Manufacturer*	*Species*	*Dilution*
anti-mouse	Santa Cruz, CA, USA	goat	1:8000
anti-rabbit	Santa Cruz, CA, USA	goat	1:2500

1.10.3 Primary Antibodies for Immunoprecipitation

Antibody	*Manufacturer*	*Molecular Weight*	*Species*	*Dilution*
IGF-1Rβ	Santa Cruz, CA, USA	97 kDa	rabbit	1:20
IRβ	Santa Cruz, CA, USA	95 kDa	rabbit	1:20

2 Methods

2.1 Cell Culture of Human Non-Small Cell Lung Cancer Cell Lines

2.1.1 Cell Culture and Trypsinization

The adherent cell lines NCI-H292, NCI-H226 and NCI-H460 were cultured in RPMI 1640 growth medium and incubated in a humidified incubator at 37° C in 5 % carbon dioxide.
After reaching confluence, cells were split by trypsinization:
Cells were washed twice with 15 ml sterile PBS (37° C), exposed to 5 ml sterile trypsin/EDTA solution (37° C) for 90 sec and placed for 5 min in the incubator.
Last residues of the peptidases-mixture were removed by dissolving cells in 10 ml growth medium. The cell solution was transferred to a sterile tube and centrifuged at 1000 U/min for 5 min. The supernatant was discarded and the received pellet was resuspended in 2 ml culture medium. 80 µl of this suspension were mixed with 20 µl of a 0.15 % tryptan-blue solution. Subsequently, cells were counted. Blue-stained cells (non-vital cells) were excluded from counting.
In order to seed the appropriate amount of cells, the calculated volume of cell suspension was pipetted into new culture flasks.
Culture medium was changed twice per week for H292 and H226 and three times per week for H460 cells.
Experiments were conducted with cells in low passages (below P10).

growth medium/ culture medium	RPMI 1640 medium penicillin [100 units/ml] streptomycin [100 µg/ml] FCS [10 %]
PBS [pH 7.4]	KCl [2.7 mM] KH_2PO_4 [1.5 mM] NaCl [0.14 M] Na_2HPO_4 [8.1 mM]
trypsin/EDTA solution	0.5 ml 10 x trypsin-EDTA solution 4.5 ml 1 x PBS buffer
tryptan-blue solution [0.15 %]	tryptan blue stain [0.4 %] 1 x PBS buffer

2.1.2 Cryo-Preservation of Cells

Cells were trypsinized and centrifuged as described above. The received cell pellet was dissolved in 2-4 ml growth medium. Each 450 µl of this solution were pipetted into a cryogenic vial. Freezing medium was added to a final volume of 900 µl (10 % DMSO). The vials had been stored at -80° C for 24 h, before they were transferred to liquid nitrogen (-196° C).

freezing medium	growth medium DMSO [20 %]

2.1.3 Thawing of Cryo-Preserved Cells

The frozen cryogenic vial with the required cells was taken out of the liquid nitrogen and quickly placed into the water bath (37° C) for approx. 2 min. The cell suspension was

transferred into a culture flask which previously was equilibrated with growth medium in a humidified incubator at 37° C for at least 30 min.
24 h after this thawing process, last residues of DMSO were removed by changing the growth medium.

2.2 Proliferation Assay: [^{3}H]-Thymidine Incorporation

In the field of proliferation assays, [^{3}H]-thymidine incorporation is one of the most sensitive methods at present. In order to draw conclusions on the cell proliferation rate, incorporation of the radioactively labelled building block thymidine into newly synthesized DNA is measured and quantified (Naito et al., 1987).

HBE cells were seeded in 12-well plates with a density of 1 x 10^5 cells per well and incubated for 24 h in growth medium. Afterwards, cells were cultured for another 24 h in starving medium to eliminate growth influences caused by FCS on cell proliferation. After the wash-out period, test compounds insulin, IGF-1 and/ or TGF-β in various concentrations or water (vehicle) as control were added for 29 h. During the last 24 h of incubation, cells were provided with [^{3}H]-thymidine (37 MBq/ml). The incubation period was followed by cell preparation and detection of radioactivity incorporated into DNA (Freitag et al., 1996; Matthiesen et al., 2006). Therefore, cells were washed twice with PBS (4° C), denaturated with TCA for 10 min, washed again with PBS (4° C) and treated with NaOH at 37° C for 1 h to extract DNA from cell lysates. After neutralization of the alkaline cell solution with tris-HCl, the scintillation cocktail was added to each sample and disintegrations per minute (dpm) were recorded by liquid scintillation spectrometry.

NaOH [0.1 N]	NaOH pellets [0.1 N] aqua bidest
starving medium	RPMI 1640 penicillin [100 units/ml] streptomycin [100 µg/ml]
TCA [5 %]	5 g TCA crystals ad 100 ml aqua bidest
tris-HCl [pH 7.4]	tris-HCl [1 M] HCl aqua bidest

2.3 Analysis of mRNA Expression Levels

According to different approaches of mRNA expression level analysis (basal mRNA expression, mRNA expression levels after treatment with test compounds or after knockdown), protocols differed with regard to cell culture procedure before RNA extraction was conducted.

Particular variations of the standard protocol (see chapter 2.3.1), mainly including substance incubation, transfection or viral transduction, can be found in the respective method part.

2.3.1 RNA Extraction

3 x 10^5 H292, H226 or 2 x 10^5 H460 cells were seeded in 6-well plates in a volume of 2 ml growth medium per well. After 48 h, the medium was aspirated and 350 µl lysis buffer (containing 1 % of 2-mercaptoethanol) were added to each well.

The following total RNA extraction, including DNase digestion to completely remove genomic DNA, has been carried out with NucleoSpin® RNA silica gel-based membrane technology like described in manufacturer's protocol.
A pre-treatment of the required labware with the ready-to-use RNase away® solution served as quick and safe removal of RNases. In order to further protect RNA from degradation, RNase-free reaction tubes and RNase-free water were used.

2.3.2 Determination of RNA Concentration

Each sample was diluted with RNase-free water (1:20) and transferred into a cuvette. Before the concentration of the eluated RNA was measured photometrically at the wavelength of maximum absorption of nucleic acids (RNA, DNA): λ= 260 nm (OD_{260}), the photometer SmartSpec™ Plus had been calibrated with RNase-free water.

2.3.3 Reverse Transcription

Reverse transcription (RT) was carried out by using the Qiagen's Onmiscript® RT kit. Thus, complementary DNA (cDNA) was obtained from the isolated RNA.
After addition of the RT-mastermix, each sample was incubated at 37° C for 60 min and at 93° C for 10 min thereafter. The reaction tubes were shortly centrifuged, put on ice and diluted with sterile water to a volume of 100 µl. The cDNA samples were stored at -20° C.

RT-mastermix (for 1 µg RNA)	Omniscript® Reverse Transcriptase [4 U]
	dNTP-Mix [0.5 mM]
	Oligo(dT) [1 µM]
	RNase inhibitor [0.25 U]
	ad 20 µl RNase-free H_2O

2.3.4 Polymerase Chain Reaction

2.3.4.1 Conventional PCR

5 µl of the cDNA-dilution (see chapter 2.3.3) were mixed with 45 µl PCR-mastermix.

The DNA amplification run was conducted in a thermal cycler with the following program:

Reaction steps	*Temperature [° C]*	*Time [sec]*
Denaturation	94	45
Annealing	53	30
Elongation	72	60

After 40 runs, an extended elongation at 72° C for 10 min finished the PCR procedure.

In the following, DNA amplificates were separated and analyzed by gelelectrophoresis.

PCR-mastermix (for 5 µl cDNA)	5 µl 10 x reaction buffer
	1.5 µl $MgCl_2$ [50 mM]
	1 µl desoxynucleotide (dNTP)-Mix [10 mM]
	2.5 µl primer (sense) [10 µM]
	2.5 µl primer (antisense) [10 µM]
	0.5 µl Taq® polymerase [5 U]
	ad 45 µl H_2O

2.3.4.2 Real-Time PCR (or Quantitative PCR)

Although the procedure of real-time PCR follows the principle of conventional PCR, this method is used to amplify and simultaneously quantify the DNA sequence of interest. Its key feature is detection of the DNA amplificates after each cycle (in "real time"). For this purpose, a fluorescent reporter (SYBR Green) serves as detection tool. SYBR Green specifically binds double-stranded DNA and fluoresces when bound to DNA.

Fluorescence becomes detectable at the threshold cycle (Ct), also named crossing point (CP). After reaching this point, the exponential replication of DNA is visualized by the fluorescent signal measured in each cell cycle when the greatest amount of amplificate products is present.

For the conduction of real-time PCR, 5 µl of each cDNA sample, previously diluted 1: 3 with water, was supplemented with 10 µl SYBR Green PCR-mastermix.

PCR was performed with the following program:

Reaction steps	*Temperature [° C]*	*Time [sec]*
Denaturation	95	30
Annealing	55	30
Elongation	72	60

Activation of the used Hot Star-Taq® DNA polymerase was achieved by an initial denaturation step at 95° C for 10 min.

SYBR Green PCR-mastermix	7.5 µl SYBR Green®
(for 5 µl cDNA)	0.45 µl primer (sense)
	0.45 µl primer (antisense)
	ad 10 µl H_2O

Finally, relative mRNA expression rates were calculated to avoid interpretation of non-comparable absolute values caused by general concentration variations among the different cDNA samples.

Amounts of mRNA expression are presented as relative quantification by normalizing CP values of the target genes to the respective CP values of the housekeeping gene glyceraldehyde-3-phosphate dehydrogenase (GAPDH) which was measured in parallel:
Δ CP = CP (gene of interest) – CP (GAPDH).
For selected experiments, a second normalization was followed by setting the Δ CP value of each sample in relation to the Δ CP value of the control. Thereby, percent values could be calculated which revealed changes of the mRNA level of each sample to the mRNA level of the control (100 %).

2.3.5 Agarose Gelelectrophoresis

The DNA base pair length of the amplified fragments can be analyzed by agarose gel electrophoresis. During this process, the negatively charged phosphate backbone of the DNA moves towards the positively charged anode after application of an electric field. The fragments are separated in accordance to their migration velocity. Next to size and conformation of the DNA molecules, further factors can affect this migration, i.e. the dimension of the gel pores (agarose concentration), the used voltage, temperature and ionic strength of the buffer.

Ethidium bromide, a fluorescent dye which intercalates into the major grooves of the DNA, was added to the agarose gel. After the gel had been cast into a horizontal gel carrier, it was placed into the electrophoresis chamber and covered with 0.5 x TBE buffer. Before pipetted into the wells of the gel (= loading of samples), each DNA sample had been supplemented with 5 µl loading buffer. This buffer contained Ficoll which raises the density and enables the DNA sample to sink to the bottom of the well and bromphenol blue which serves as a colored dye to monitor the progress of the electrophoresis.
A DNA size standard was pipetted into the first gel lane. Each further lane was loaded with 20-25 µl of the sample-buffer-mixture. The electrophoresis process was started by applying a constant electric field strength of 1500 V/m. After the run had been finished (60-70 min), the gel was exposed to UV-light making DNA strands visible.

agarose gel	agarose in 0.5 x TBE buffer [1.2 %] ethidium bromide [0.33 µg/ml]
loading buffer	Ficoll 400® [15 %] bromphenol blue [0.25 %] 0.5 x TBE buffer
5 x TBE buffer	tris [0.45 M] boric acid [0.45 M] EDTA [0.012 M]

2.4 Protein Analysis

Methods evaluating protein expression levels included Western blot analysis (detection of protein expression levels and quantification of receptor knockdown), phospho Western blot analysis (analysis of signaling pathways) and co-immunoprecipitation (analysis of heterodimeric insulin-, IGF-1 receptors).

2.4.1 Preparation of Total Protein Lysates from Cells

2.4.1.1 Western Blot Analysis and Immunoprecipitation

After dissemination of 3 x 10^5 cells in 2 ml culture medium per well (6-well plates) and incubation for 24 h, medium was removed gently and cells were washed twice with ice-cold 1 x PBS. Cellular proteins were extracted in 200-300 µl lysis buffer.

lysis buffer	RIPA buffer
	PMSF [1 mM]
	pepstatin A [0.7 μg/ml]
	leupeptin [0.5 μg/ml]
radioimmunoprecipitation assay buffer	tris-HCl [pH 7.4] [50 mM]
(RIPA buffer)	NaCl [150 mM]
	sodium deoxychlorate [0.5 %]
	Nonidet P-40 [1 %]
	SDS [0.1 %]
	EDTA [2 mM]

2.4.1.2 (phospho) Western Blot Analysis

2 x 10^5 cells were seeded in a volume of 1.5 ml culture medium per well (6-well dish). After 24 h cultivation, a starving period of 24 h followed. Hence, stimulating effects of FCS-compounds on receptor tyrosin kinases (RTK) activity were eliminated. Subsequently, test compounds (insulin, IGF-1, TGF-β) or water (control) were pipetted carefully onto the wells and plates were gently moved in a circular pattern for a homogenous distribution of the added solutions. After incubation at 37° C for 15 min, the supernatant was removed and cells were washed twice with ice-cold 1 x PBS. Cell lysis was carried out with 200-300 μl phosphatase inhibitor-containig lysis buffer to prevent dephosphorylation during the process of protein preparation.

lysis buffer for phospho proteins	lysis buffer
	NaF [35 mM]
	Na_3VO_4 [1 mM]

2.4.2 Determination of Protein Concentration by Lowry Method

The Lowry method (Lowry et al., 1951) is a copper-based protein assay. It represents a technique by which the total level of proteins in a solution can be determined. The colorimetric assay combines the Biuret- with the Folin-Ciocalteau-reaction:

In the first step (Biuret reaction), peptides containing three or more amino acid residues form an instable colored chelate complex with cupric ions (Cu^{2+}) under alkaline conditions.

The second step is a reduction of the Folin-Ciocalteu reagent (a mixture of phosphotungstic acid and phosphomolybdic acid) by the copper-peptide complex. The color of the product molybdenum blue continues to intensify during 15 min of incubation at room temperature. Samples are measured at λ= 750 nm.

10 µl of the cell lysate samples (see chapter 2.4.1) were pipetted into 1.5 ml eppendorf tubes and supplemented with 40 µl 0.1 % Triton® X-100 solution. The Lowry working reagents (DC Protein Assay Kit) were added to the lysates in accordance with the manufacturer's protocol and incubated for 15 min at room temperature.

The calibration curve was prepared by measurement of BSA standards of 50, 100, 300, 700, 1100 and 1500 µg/ml (in 0.1 % Triton® X-100).

2.4.3 Sodium Dodecyl Sulfate Polyacrylamid-Gelelectrophoresis and Ponceau Red Staining of Gels

Sodium Dodecyl Sulfate Polyacrylamid-Gelelectrophoresis (SDS-PAGE) is commonly used to separate proteins based on their length in an electric field.

The charge of the proteins is covered by the anionic detergent SDS. Corresponding to the molecular weight, amounts of SDS are bound to the polypeptide chains. The negatively charged samples are strongly attracted towards the anode in the electric field. In order to avoid effects on mobility by different protein conformations, the samples are heated with a surplus of SDS leading to a destruction of the secondary and tertiary structures of the proteins. Moreover, 2-mercaptoethanol which serves as reducing agent is added to the protein samples.

In the first step, 25 µg of each sample were mixed with Roti®-Load 1 (1/4 of the total volume), a 2-mercaptoethanol-containing reducing sample buffer, and denaturated at 70° C for 10 min. Meanwhile, a precast polyacrylamide gel was placed into the electrophoresis chamber which was filled with 1 x MOPS SDS running buffer.
As reference for the protein sizes, 5 µl of a prestained protein ladder (PageRuler™) were added to the samples. Attached to a power supply, the electrophoresis run was conducted with a constant voltage of 200 V at a current of 60 mA for 90 min.

2.4.4 (phospho) Western Blotting and Immunodetection

Western blot analysis includes the transfer of electrophoretically separated proteins onto polyvinylidene fluoride (PVDF) membranes. By immunodetection, viz. detection with monoclonal or polyclonal antibodies, the proteins can be identified and quantified.
In the preparation, the blotting sponge pads were equilibrated in transfer buffer. The PVDF membrane was moistened with methanol for 1-3 sec (activation), washed with water for 1 min and preincubated with transfer buffer for 20 min. After the electrophoretic run had been finished, the protein gel was removed from the gel cassette and washed for 5 min in transfer buffer.
Thereafter, the Western blot was assembled. Avoiding trapped bubbles, the PVDF membrane was put on the protein gel and encosed by filter paper. Two sponges formed the frames of the transfer sandwich.
The Western blot was fixed in a chamber filled with 4° C cold transfer buffer. Attached to the power supply, proteins were electrically transferred onto the membrane during the blotting process at a constant current of 250 mA and a voltage of 100 V for 90 min.
Afterwards, the membrane was positioned in a flat vessel and stained with the azo dye Ponceau S. Due to reversible binding of Ponceau S to positively charged amino groups, all proteins are stained to an equal extent on the membrane allowing an evaluation of the quality of the previous blotting process. By a washing step with TBS, Ponceau Red was removed and the stained protein bands were decolored.
Incubation at 4° C for at least 1 h in 5 % nonfat milk powder blotting solution followed to block non-specific protein-binding sites.

The first step of the immunodetection was exposure of the membrane to a specific primary antibody (see chapter 1.10) for 1.5 h at room temperature in 5 % nonfat milk powder solution or over night at 4° C in 5 % BSA blotting solution (for the respective antibodies in accordance to the manufacturer's protocol). After two washing steps with 0.1 % TBST and two blocking steps for 20 min each, the membrane was exposed to a horseradish peroxidase (HRP)-conjugated secondary antibody which was diluted in 5 % nonfat milk powder blotting solution (see chapter 1.10). During 1 h of incubation at room temperature, the secondary antibody which is directed against the host species was used to bind the antigen/antibody complex.

Then, the membrane was washed four times with TBST 0.1 % for overall 1 h. The target protein became visible by HRP-caused chemiluminescence. Therefore, the membrane was wetted for 1 min with BM Chemiluminescence Blotting Substrate (POD) detection solution, foil-wrapped and fixed in a film cassette. An x-ray film visualized the luminescent products on the membrane. Exposure times differed depending on the primary antibody (see chapter 1.10).

BSA blotting solution [5 %]	5 g BSA ad 100 ml TBST 0.1 %
nonfat milk powder blotting solution [5 %]	5 g nonfat dried milk powder ad 100 ml TBST 0.05 %
Ponceau red stain	Ponceau S [0.2 %] trichloroacetic acid [3 %]
TBS [pH 7.4]	tris [50 mM] Natriumchlorid [150 mM] HCl aqua bidest
TBST [0.1 %]/ TBST [0.05 %]	1 ml Tween 20/ 0.5 ml Tween 20 ad 1 l TBS
transfer buffer	tris [25 mM] glycine [192 mM] methanol [20 %]

2.4.5 Stripping of Detected Membranes

For detection with a further antibody, e.g. the housekeeping reference, a membrane preparation had been conducted before a next immunodetection was carried out:
After drying, the PDVF membrane was moistened with methanol for 1 sec and watered afterwards. It was treated with NaOH solution for 5 min to detach the antigen/antibody-binding of the previous immunodetection. A washing step with water for 5 min removed last NaOH residues. A protein blocking step over night at 4° C in 5 % blotting solution concluded the stripping process.

NaOH solution	NaOH pellets [0.2 M] aqua bidest

2.4.6 Densitometric Analysis

Amounts of proteins were quantified via densitometric analysis with ImageJ program. Intensities of the ECL-developed bands were measured as arbitrary units.

Loading varieties within different gel pockets (see chapter 2.4.3) were eliminated by normalizing each target protein to its respective housekeeping protein (see chapter 2.4.5). By this, absolute protein amounts were obtained.

A further standardization was done to obtain relative protein amounts which allowed a comparison of a particular treatment to the control level on protein expression.

Therefore, protein amounts were set into relation to the absolute protein amount of the control. Hence, each sample is expressed as percentage of the control level (100 %).

2.4.7 Co-Immunoprecipitation

By the use of immunoprecipitation (IP), a target protein is precipitated with a specific antibody that is immobilized onto insoluble sepharose beads. This leads to isolation and concentration of the particular protein out of the cell lysate.

The expression of heterodimeric IGF-1/insulin receptors was studied with co-immunoprecipitation (Co-IP) analysis, an extended technique of IP which is to detect protein-protein-interactions with two specific antibodies. Therefore, a special protocol for NSCLC cells was established.

In order to capture one component of the HR, the cell lysate (corresponding to 100 µg protein) was incubated with an IGF-1 or insulin receptor antibody (dilution see chapter 1.10). While shaking gently at 4° C over night, the antibody bound its specific target. The next day, 50 µl sepharose were added to the mixture and placed for 4 h on a smooth shaker (4° C). After centrifugation for 10 min at 10,000 rpm at 4° C, the supernatant was discarded and the pellet was washed three times with 100 µl tris-HCl [pH 7.4] to dissolve the antigen-antibody complex from the sepharose beads.

Subsequently, gelelectrophoresis and Western blot were carried out as described above (see chapter 2.4.4). Immunodetection was conducted with the relevant other antibody as used in the precipitation process (insulin or IGF-1 antibody). It follows that both receptor proteins, incorporated into HR, were captured and detected.
Antibody-untreated samples were used as negative controls. For the positive controls, protein samples were treated with the IR or the IGF-1R antibody, exclusively.

tris-HCl pH 7.4	10 mM tris-HCl
	HCl
	aqua bidest

2.5 Knockdown Assays

2.5.1 Transfection

Transfection describes a process of introducing nucleic acids into eukaryotic cells. To knockdown (KD) the gene of interest, small interfering RNA (siRNA) are channelled into the target cells. Due to interference with the complementary RNA of the target gene, siRNA leads to its degradation resulting in no translation of the protein.
The insertion of siRNA can be achieved by various techniques. In the following, the chemical-based lipofection method is described in more detail.

2.5.1.1 Lipofection

By use of lipofection reagents like Lipofectamine® (cationic liposome formulations) siRNA can be transfected into cells.
In this process, the negatively charged nucleic acid molecules are enclosed by the positively charged transfection reagent. Like the cell membrane, liposome vesicles are enveloped by a phospholipid bilayer. Thus, cell fusion of the siRNA-containing vesicles is reached.

NSCLC cells were seeded in FCS-containing, penicillin/streptomycin-free medium with a density of 3 x 10^5 cells per 6-well dish. After 24 h of incubation (confluence of cells: 30-50 %), growth medium had been aspirated and wells were washed with serum-free medium to remove last residues of FCS. The following transient transfection was conducted with Silencer® Select siRNAs directed against the IR (see chapter 1.8.2). Lipofectamine® was used to transfer siRNAs into the cells. In first experiments, concentrations of transfection components and incubation times were chosen in accordance with the manufacturer's protocol. However, to accommodate the transfection protocol to the cell lines tested, various modifications were carried out to establish a valide knockdown protocol.

For each well, 1.5 µl Lipofectamine® were gently mixed with 98.5 µl Opti-MEM® and incubated for 5 min at room temperature. In parallel, 1.25 µl siRNA (= 40 µmol) or 2.5 µl (= 20 µmol) non-coding siRNA control were diluted with Opti-MEM to a total volume of 50 µl and incubated at room temperature for 5 min. Thereafter, both solutions had been mixed and incubated for another 20 min before they were added to the cells. A 12 h exposure time with the transfection solution was followed by 12 h of incubation in starving medium. Thereafter, RNA-preparation, Westen blot analysis or [^{3}H]-thymidine incorporation was conducted.

2.5.2 Lentiviral Transduction

Stable KD of specific genes can be achieved by viral carriers. They contain short hairpin RNA (shRNA) which is complementary to the target RNA and thus able to silence gene expression via RNA interference (RNAi).

Establishment of IR KD and IGF-1R KD in NSCLC cells was performed by transduction with lentiviral vectors (LVs) expressing U6 promoter-driven shRNA against IR or IGF-1R. By the use of two plasmids with a different property in IR KD efficiency, effects of a strong KD were compared to effects of a weak KD. pLKO.1-U6-CMV-GFP-PGK-Puro (LV-GFP) and pLKO.1-U6-sh-ctr-PGK-Puro (LV-sh control) were used as controls. LV-GFP contains an U6 promoter without transgene and a CMV promoter-driven GFP expression cassette. LV-sh control contains U6 promoter-driven non-coding shRNA. The LVs for KD of IR and IGF-1R carry shRNA under control of the U6 promoter that targets different

regions of human IR and IGF-1R. All LV constructs were purchased from Sigma-Aldrich (Munich, Germany).

Generation and packing of viral vectors were carried out by the collaborating partner workgroup Pfeifer (Institute of Pharmacology and Toxicology, University of Bonn).

For LV transduction, 1.5 x 10^5 cells per 6-well dish for protein analysis or 2 x 10^4 cells per 24-well dish for mRNA analysis were seeded and incubated for 4 h until cells adhered. Medium was removed and replaced by 1 ml (for 6-well plate) or 0.4 ml (for 24-well plate) transduction medium, containing 150 ng (per 6-well) or 20 ng (per 24-well) RT LVs. 72 h after transduction (day (d) 3), cells were used for analysis or virus-mixture was replaced by starving medium and cells were incubated for 24 h (d 4) or 48 h (d 5). The KD was studied on mRNA and protein level (see chapter 2.3 and 2.4)

transduction medium	growth medium polybrene [3 µg/ml]

2.6 Analysis of Cell Survival

2.6.1 Cell Count

Measurement with CedEx XS revealed cell survival after viral transduction. For determination of cell count, cells were washed twice with PBS and trypsinized 72 h (d 3) after virus treatment (see chapter 2.5.2). The cell pellet which was received after centrifugation was resuspended in 1 ml growth medium. 10 µl of this solution were pipetted into a CedEx XS counting chamber. Cells were counted afterwards. Each sample was measured in triplicates. In order to perform cell count at d 4 and d 5, virus-containing medium was replaced by serum-free medium at d 3 and an incubation time of 24 h and 48 h, respectively followed before cell number was measured.

Results are presented as absolute cell number per ml.

2.6.2 Caspase Assay

Detection of Caspase 3/7 activity was conducted with Caspase-Glo® 3/7 Assay. As caspases activities were studied in both, IR or IGF-1R knockdown and cytokine-treated samples, different protocols were established .

An amount of 1 x 10^4 cells per 96-well plate was seeded into microplates in a volume of 200 µl growth medium.

For an analysis of effects of cytokines on apoptosis, cells had been set on starving medium for 24 h before incubated for 48 h with 100 nM of the test compounds.

Samples treated with water served as negative controls. Tumor necrosis factor α (TNFα)-treated cells were used as positive controls.

Implications of IR KD in programmed cell death were studied by Caspase-Glo® 3/7 assay at d 3 after LV transduction. Both, LV-sh control and untreated cells were used as negative controls. The chemotherapeutic drug gemcitabine, used in the therapy of NSCLC, was selected as positive control.

Background luminescence was detected by a blank reaction which contained the Caspase-Glo® 3/7 Reagent and cell culture medium without cells. Before the assay was conducted, Caspase-Glo® 3/7 Reagent had been freshly prepared. 100 µl of this reagent were pipetted into each well to a total volume of 200 µl. The microplates were mixed gently on a plate shaker for 1 min. After 1 h incubation at room temperature, luminescence signals representing caspases activities were measured.

All samples were measured in quadruplicates. Activation levels of caspases in cytokine-stimulated samples are shown as percentage of untreated control levels. Caspases activities of IR KD samples are represented as percentage of LV-sh control cell levels.

Caspase-Glo® 3/7 Reagent (homogenous solution)	10 ml Caspase-Glo® 3/7 Buffer 1 bottle Caspase-Glo® 3/7 Substrate (lyophilized)

2.7 Analysis of Gene Expression Profiles

1 µg of H292, H226 and H460 total RNA (see chapter 2.3.1) was used as starting material for linear T7-based amplification of sample RNA.

Following operations were carried out by Miltenyi Biotec (Gladbach, Germany). The analysis based on quadruplicate measurement (four biological replicates on four independent arrays). Microarray raw data (light intensity) were translated by logarithmic transformation.

For statistical analysis, ratios of IR KD vs. LV-sh control expression levels were calculated. No change in gene expression is signified by zero, induction by a positive and suppression by a negative sign.

2.8 Statistical Analysis

Data were analyzed using Prism 5.0 software (GraphPad Software Inc.). Arithmetic means and standard error of the mean (SEM) were calculated and are presented in the "Result" section (see chapter IV) .

One-way ANOVA (analysis of variance) was used to determine how a certain response is affected by one factor; e.g. response to three different concentrations of insulin in a cell line. Thereby, insulin treatment is the only factor. Due to three different concentrations of insulin, the factor is said to have three levels.

Analysis with *two-way ANOVA* was conducted to examine how a response is affected by two factors; e.g. response to three different concentrations of insulin in LV-sh-IRa-treated *and* LV-sh control samples. Insulin treatment is one factor and virus treatment (yes/no) the other.

If the F-test reports a P value of < 0.05, the null hypothesis (H_o), indicating that samples show *no* significant differences in their means, can be rejected.

In order to analyze in more detail which group differed to which statistical extent from another group, post-hoc tests were performed. Among multiple comparison tests, Bonferroni method allows a comparison of multiple independent groups, whereas Dunnett method compares independent groups to a common control group.

An error probability of $p < 0.05$ represents a significant (*), $p < 0.01$ highly significant (**) and $p < 0.001$ most highly significant (***) difference of the means.

IV Results

1 Basic Configuration of NSCLC Cells

In order to evaluate implications of insulin and the insulin receptor in lung carcinoma promotion, three NSCLC cell lines, each representing a different cancer subtype (see Materials 1.3.1 for details), were included in this study.
Various cell screening experiments were performed previously to reveal relevant *basic characteristics* of the different cell lines.

1.1 Basal Proliferation Rates

The individual extent of cell proliferation - independent from external stimuli - was analyzed by measurement of [^{3}H]-thymidine incorporation under basal conditions (i.e. starving conditions).
H460 cell line showed the highest [^{3}H]-thymidine incorporation rate (25700 dpm) which was 5-fold higher than that of H226 cells (5800 dpm) (Fig. 8). H292 cells revealed the lowest [^{3}H]-thymidine incorporation rate (2400 dpm) which was significantly below that of H226 and H460 cells.

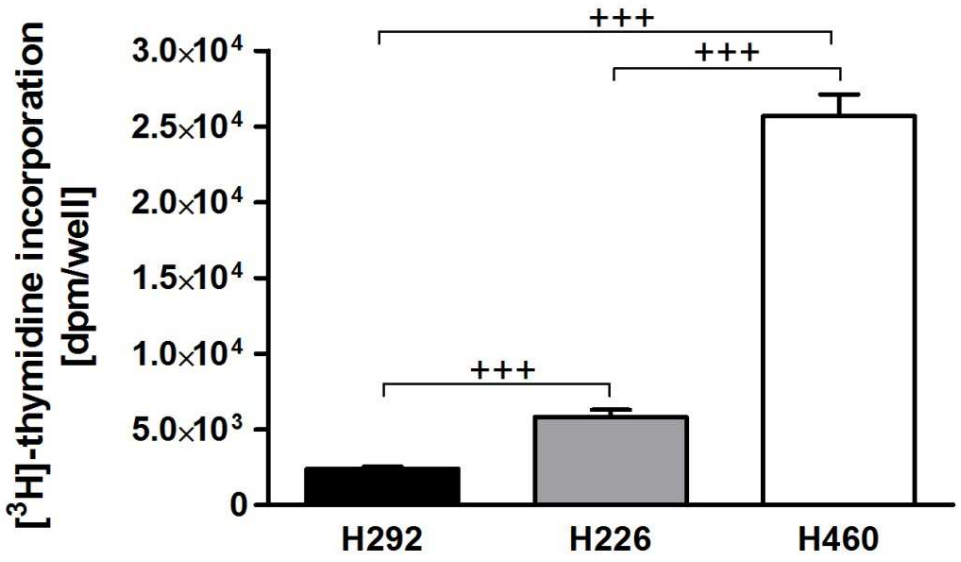

Figure 8: Basal [^{3}H]-Thymidine Incorporation Rate in H292, H226 and H460 Cells.

Cells were cultured in growth medium and provided with starving medium for 24 h afterwards. Thereafter, [^{3}H]-thymidine (37 MBq/ml) was pipetted onto each well. During 24 h of incubation, radioactive-labelled thymidine was incorporated into newly synthesized DNA strands. Radioactivity was recorded as dpm per well by liquid scintillation spectometry. The bar graphs show means + SEM of N= 6 (H460 cells) or N= 11 (H292, H226 cells) experiments. Significance of differences: +++ $p < 0.001$

1.2 Expression of Insulin and IGF-1 Receptors

Knowledge of the presence and the expression levels of insulin and IGF-1 receptors in H292, H226 and H460 cells is essential to comprehend implications of both receptors in cancer cell progression and effects caused by receptor knockdown.

Quantitative real-time PCR and Western blot analysis revealed in parallel that IR and IGF-1R were present in all cell lines tested. In H292 cells, expression levels of both receptors were most pronounced (Fig. 9). The IR expression in H226 cells was at a slightly lower level as compared to H292 cells, i.e. 80 % of H292 mRNA (Fig. 9A) and 76 % of H292 protein level (Fig. 2C, left bar chart). H460 cells revealed the lowest IR expression level within the cell lines tested, i.e. 30 % and 44 % of H292 mRNA (Fig. 9A) and protein level, respectively (Fig. 9C, left bar chart).

IGF-1R expression in H226 cells was 10 % of mRNA (Fig. 9A) and 43 % of protein level (Fig. 9C, right bar chart) compared to H292 cells. H460 cells were positioned in between; their IGF-1R expression was 20 % of H292 mRNA (Fig. 9A) and 58 % of H292 protein level (Fig. 9C, right bar chart).

Besides, the IR/IGF-1R ratio was calculated. qPCR data revealed that the IGF-1R/IR ratio was highest in H292 (10:1) and H460 (5:1) cells. Expression of both receptors hardly differed in H226 cells (Fig. 9A).

(A) mRNA Expression Levels of Insulin and IGF-1 Receptors

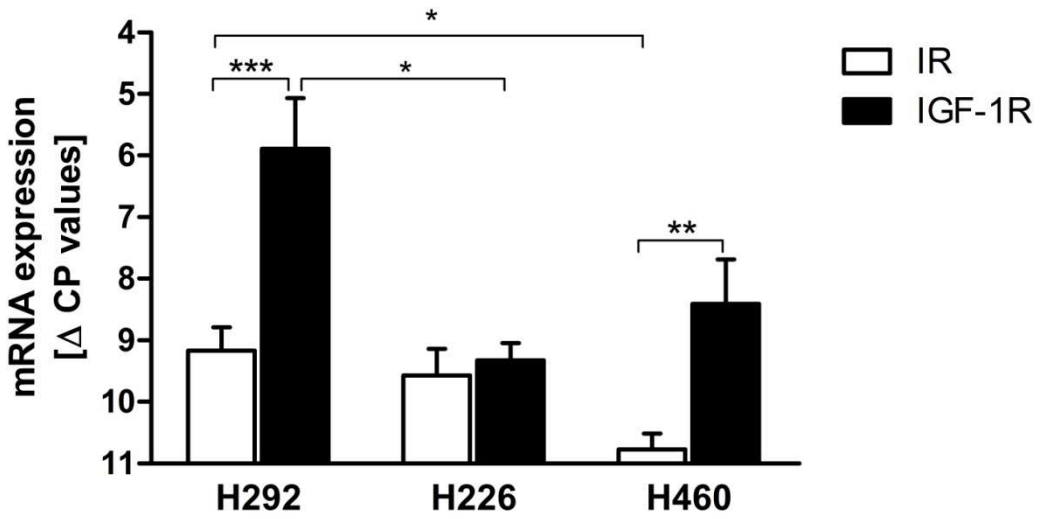

(B) Protein Expression of Insulin and IGF-1 Receptors

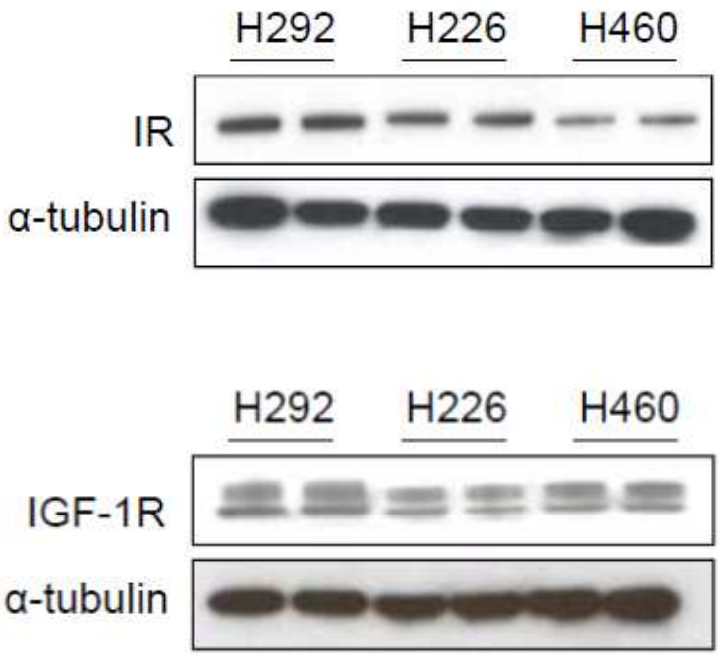

(C) Protein Expression of Insulin and IGF-1 Receptors (Densitometric Analysis)

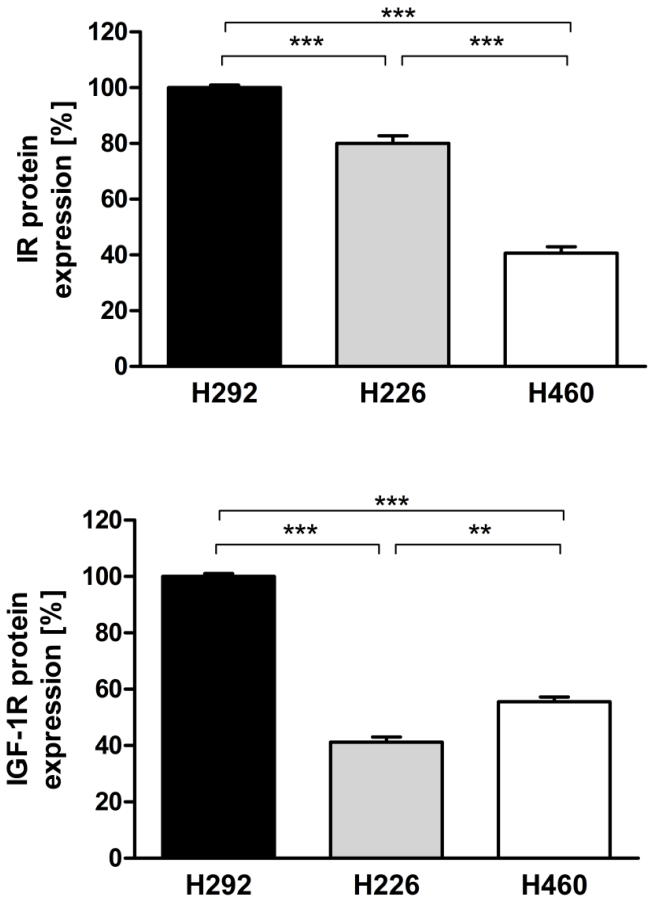

Figure 9: Basal Expression of Insulin and IGF-1 Receptors in H292, H226 and H460 Cells.

IR and IGF-1R *mRNA* expression levels are presented in (A). Cells were cultured in growth medium for 48 h before total RNA extraction was conducted. qPCR was carried out with IR and IGF-1R primers listed in Materials 1.9. The bar charts show N= 2-4 experiments (measured in triplicates). Amounts of mRNA expression levels are shown as Δ CP (relative quantification) by normalizing CP values of target genes (IR or IGF-1R) to CP values of GAPDH levels (see Methods 2.3.4.2). A representative Western blot result shows IR and IGF-1R *protein* expression levels in the NSCLC cells tested (B, upper panels). Cellular protein extraction was conducted after cells had been incubated for 24 h in growth medium. Anti-insulin or anti-IGF-1 receptor antibodies (see Materials 1.10) were used for immunodetection. After film processing, membranes were stripped, blotted over night and incubated with anti-α-tubulin antibody the next day. The housekeeping α-tubulin protein was used as internal control (B, lower panels). The exposure time was 1 min for IR antibody detection and 1 sec for IGF-1R and α-tubulin antibody detection. Densitometric analysis of Western blot analysis is presented in (C). The bar graphs show means + SEM of N= 4 experiments. Significance of differences: * $p < 0.05$, ** $p < 0.01$, *** $p < 0.001$

1.3 Analysis of Insulin Receptor Splicing Isoforms

By performance of PCR with primer pairs spanning Exon 11, presence of IR splicing variants IR-A and IR-B were studied in the three NSCLC cell lines. Amplificates of IR-A and IR-B were separated by agarose gel electrophoresis and assigned to each isoform based on their molecular weight.

Both splicing variants were present to a roughly equal extent in H292 cells (Fig. 10). In H226 cells, the PCR product corresponding to IR-B was markedly higher expressed as those corresponding to IR-A. Vice versa, in H460, IR-A appeared to be the predominant isoform.

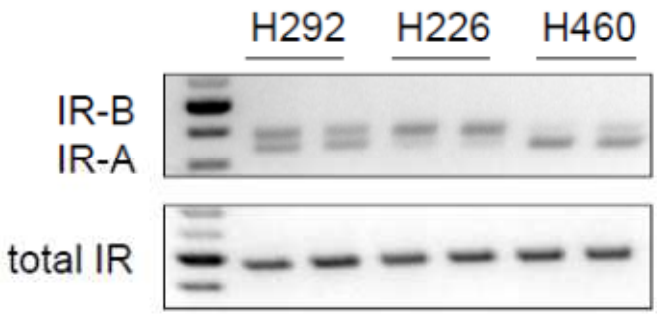

Figure 10: Expression of Insulin Receptor Splicing Isoforms IR-A and IR-B in H292, H226 and H460 Cells.

An incubation period of 48 h in growth medium was preceded before RNA extraction was performed. To distinguish between IR-A (-Ex11) and IR-B (+Ex11) sequences, conventional PCR was carried out with a splicing variants sensitive primer pair (see Materials 1.8, NM_001079817) (panel above). Total IR served as internal reference. Therefore, a primer pair (see Materials 1.8, NM_000208) spanning IR without differentiating between both isoforms (also used in experiments presented in Fig.9A) was used. Shown is one representative result of N= 3 analysis.

1.4 Presence of Heterodimeric IR/IGF-1 Receptors

Next to IR homodimers, *heterodimeric receptors* (see Introduction 2.2) form a special receptor phenotype that is frequently present in cancer cells.

In order to detect whether NSCLC cells build these hybrid receptors, co-immunoprecipitation was carried out in H292, H226 and H460 cells. As described in the "Materials and Methods" section (see chapter 2.4.6), the precipitation step was performed with an anti-IGF-1R (Fig. 11A) or an anti-IR antibody (Fig. 11B). Correspondingly, the immunoprecipitated proteins were detected with the respective other antibody, i.e. anti-IR (Fig. 11A) or anti-IGF-1R (Fig. 11B). Precipitation and detection with the same antibody, i.e. anti-IGF-1R (Fig. 11A) or anti-IR (Fig. 11B), was performed in parallel and served as positive control. Samples treated with sepharose but without antibody were chosen as negative control.

Both approaches of IR and IGF-1R antibody-mediated immunoprecipitation resulted in positive findings (Fig. 11A, B); taken together, ten independent experiments clearly evidenced presence of HR in all cell lines tested.

(A) Immunodetection with Anti-Insulin Receptor Antibody

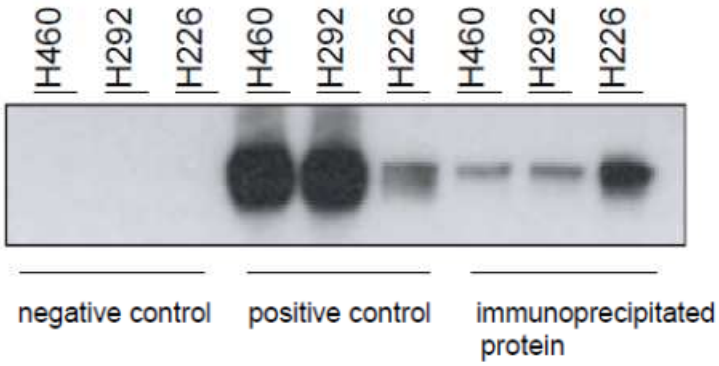

(B) Immunodetection with Anti-IGF-1 Receptor Antibody

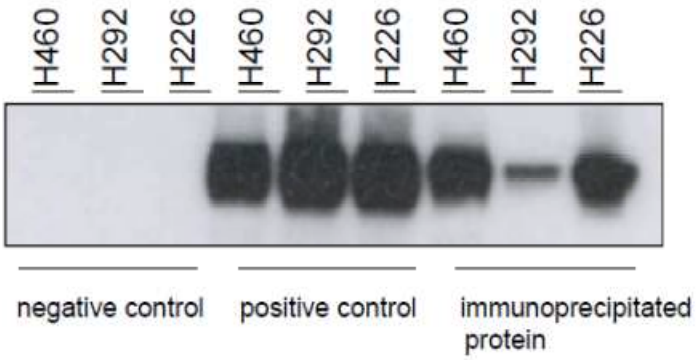

Figure 11: Heterodimeric Insulin/IGF-1 Receptors in NSCLC cells.

Whole protein isolation was performed after cells were cultured for 24 h in growth medium. Procedure of co-immunoprecipitation followed. (A): 100 µg of proteins were incubated with anti-IGF-1R antibody (see Materials 1.9.3) over night in order to collect IGF-1R proteins out of the cell lysate (immunoprecipitated protein). For the positive control, samples were treated with anti-IR antibody over night. Antibody-untreated samples were used as negative control. Detection was carried out with anti-IR antibody (see Materials 1.9.1). (B): Application of anti-IR and anti-IGF-1R antibodies was used inversely compared to (A); immunoprecipitated proteins were incubated with anti-IR antibody (see Materials 1.9.3) and positive control was exposed to anti-IGF-1R antibody. The membrane was immunodetected with anti-IGF-1R antibody. The exposure time was 1 min and 1 sec for IR antibody and IGF-1R antibody detection, respectively. All NSCLC cells tested showed presence of heterodimeric insulin/IGF-1 receptors. Shown are 2 representative Western blot images of N= 10 experiments.

2 Influences of Insulin and IGF-1 on Mitogenic Processes

2.1 Effects on Cell Proliferation

[^{3}H]-thymidine incorporation studies were performed to examine effects of insulin in comparison to IGF-1 on the proliferation rate in NSCLC cells.

After exposure of H292 cells to 1 nM insulin, [^{3}H]-thymidine incorporation was slightly elevated to 117 %. Significantly enhanced incorporation rates were caused by 100 nM and 1 μM insulin to 178 % and 280 %, respectively (Fig. 12A). An insulin-mediated increased cell proliferation was also observed in H226 cells, albeit the concentration-response curve appeared to be right-shifted compared to H292 findings. This indicates a reduced potency of insulin in H226 cells. An insulin concentration of 1 μM caused an overall stimulation to 200 % (Fig. 12A). In contrast, in H460 cells, insulin failed to enhance [^{3}H]-thymidine incorporation (Fig. 12A).

In order to illuminate IGF-1 effects on cell proliferation and to compare effects of insulin to those of IGF-1, cells were incubated with IGF-1 in a concentration range from 1 nM to 10 nM (Fig. 12B). H292 cells responded with a significantly increased [^{3}H]-thymidine incorporation rate after treatment with 1 nM (143 %) and 10 nM (202 %) IGF-1. Although in H460 cells 1 nM IGF-1 did not lead to an enhanced cell proliferation rate, significant effects were observed by 3 nM (147 %) and 10 nM (179 %) IGF-1. Notably, IGF-1 failed to increase the [^{3}H]-thymidine incorporation rate in H226 cells (Fig. 12B).

(A)

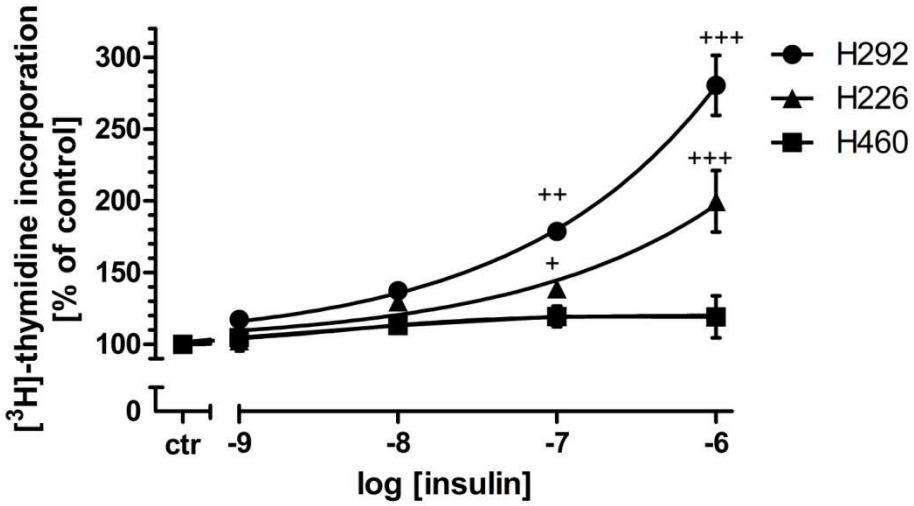

(B)

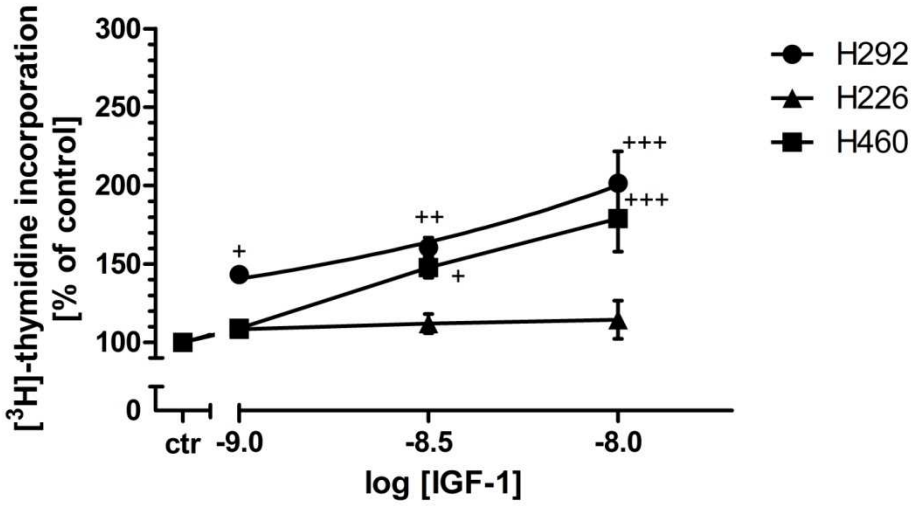

Figure 12: Effects of Insulin and IGF-1 on [^{3}H]-Thymidine Incorporation in NSCLC Cell Lines.

Cells were seeded and cultured in growth medium for 24 h. An incubation time in starving medium for 24 h followed. After this wash-out period, test compounds in concentrations of 1 nM- 1 μM insulin (A) or 1 nM- 10 nM IGF-1 (B) were added to the wells. Treatment of cells with vehicle-only (water) was paralleled in each experiment serving as control (ctr). Results of mostly N > 6 experiments are expressed as percentage of ctr of the individual cell proliferation as means ± SEM. Significance of differences: + $p < 0.05$, ++ $p < 0.01$, +++ $p < 0.001$ of the respective cell preparation control.

2.2 Activation of Mitogenic Signaling Pathways

2.2.1 Insulin/IGF-1 Receptor Phosphorylation

The extent of receptor autophosphorylation upon insulin stimulation was tested by phospho (p) Western blot analysis. Due to the large structural homology of IR and IGF-1R at the relevant site, only a combined pIGF-1R/pIR antibody was available.

Regarding basal levels of pIGF-1R/pIR, differences within the cell lines became obvious (Fig. 13A). Only in H292, clearly activated receptors, identified by a visible pIGF-1R/pIR signal *in absence of insulin*, were observed (Fig. 13A, left). However, concentration-dependent phosphorylation of the tyrosine residues Y1135/1136 (IGF-1R) and Y1150/1151 (IR) after exposure to insulin in the nanomolar range was detected in all cell lines tested. Picomolar insulin concentrations did not increase receptor phosphorylation (data not shown).

Densitometric analysis allowed a more precise analysis of pIGF-1R/pIR levels (Fig. 13B). By detecting also slightest variations in the density distribution within the Western blot membrane, basal levels of pIR/IGF-1R could be measured and taken as internal reference. Compared to respective controls, 10 nM of insulin caused significant receptor autophosphorylation in H292 and H226 cells to 264 % and 225 %, respectively but only slight autophosphorylation in H460 cells to 131 %. Exposed to 100 nM insulin, IGF-1R/IR autophosphorylation was induced significantly in the three cell lines (H292 cells: 355 %, H226 cells: 388 %, H460 cells: 277 % compared to vehicle-treated control).

(A)

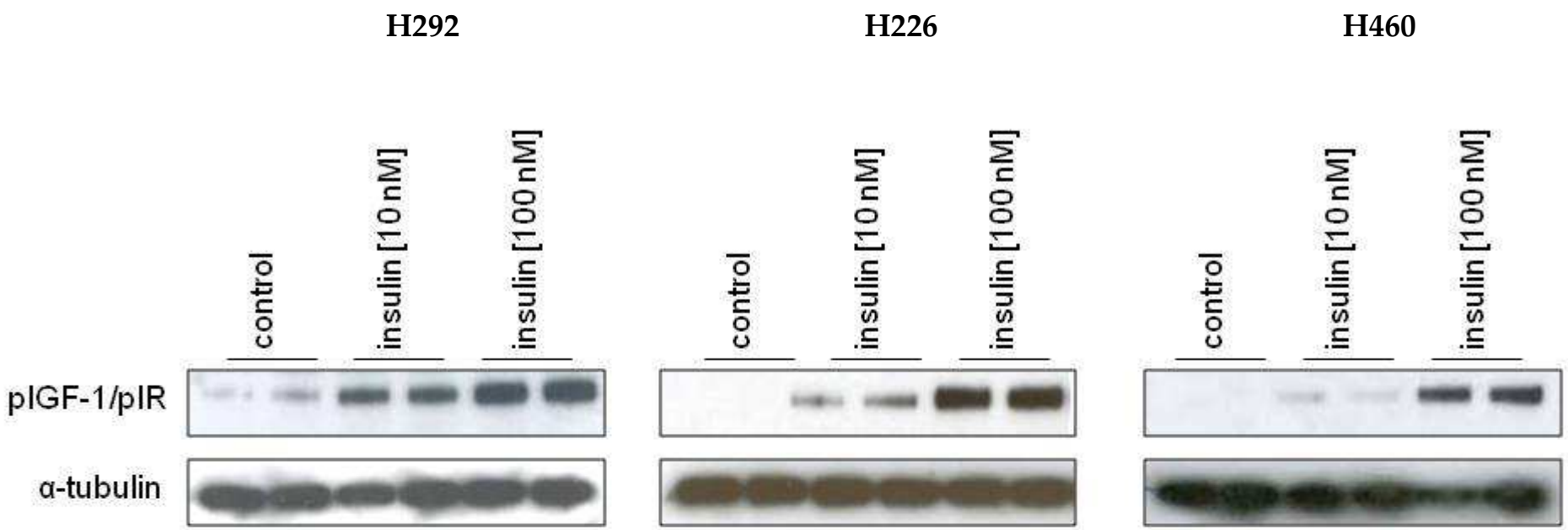
H292
H226
H460
control
insulin [10 nM]
insulin [100 nM]
pIGF-1/pIR
α-tubulin

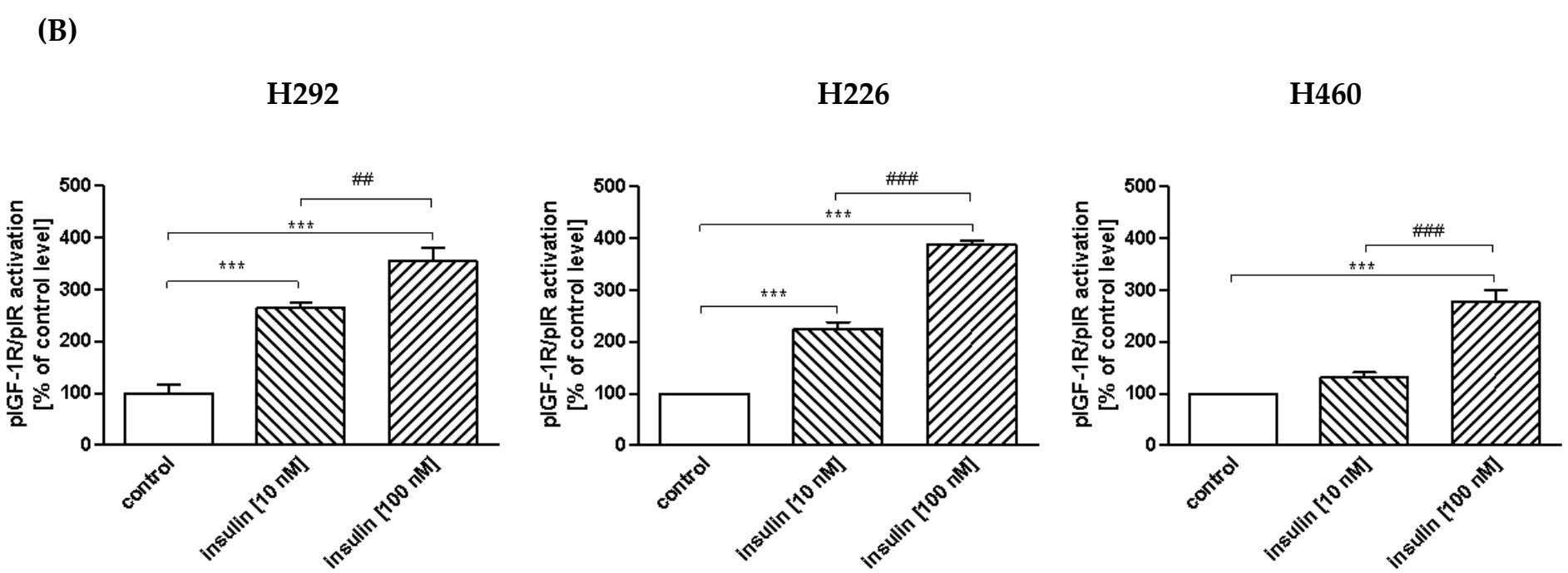

Figure 13: Effect of Insulin on IGF-1R/IR phosphorylation in NSCLC cells.

Western blot analysis revealed concentration-dependent autophosphorylation of IGF-1R/IR caused by insulin (A). Serum-starved cells were treated with 10 nM or 100 nM insulin for 15 min. Signals of phosphorylated tyrosine residues were detected (upper panels). Use of α-tubulin antibody was chosen as housekeeping reference control (lower panels). The exposure time was 1 min and 1 sec for pIGF-1R/pIR antibody and α-tubulin antibody detection, respectively. Densitometric analysis is presented in (B). The bar graphs show mean + SEM of N= 4 experiments, expressed as percentage of the control level. Significance of differences: *** $p < 0.001$; ## $p < 0.01$, ### $p < 0.001$

2.2.2 Akt Phosphorylation

Akt phosphorylation under basal conditions (i.e. in absence of insulin) was identified in H226 and H460, but not detectable in H292 cells (Fig. 14A). Beyond, 100 pM- 100 nM insulin induced Akt-signaling in a concentration-dependent manner in the three NSCLC lines.
Beyond, it was aimed to compare insulin-mediated effects to IGF-1-mediated effects on Akt phosphorylation. Therefore, cells were also exposed to 10 nM of IGF-1. Results of Akt protein analysis indicated that IGF-1 and insulin stimulation did not differ from each other (Fig. 14B).

(A)

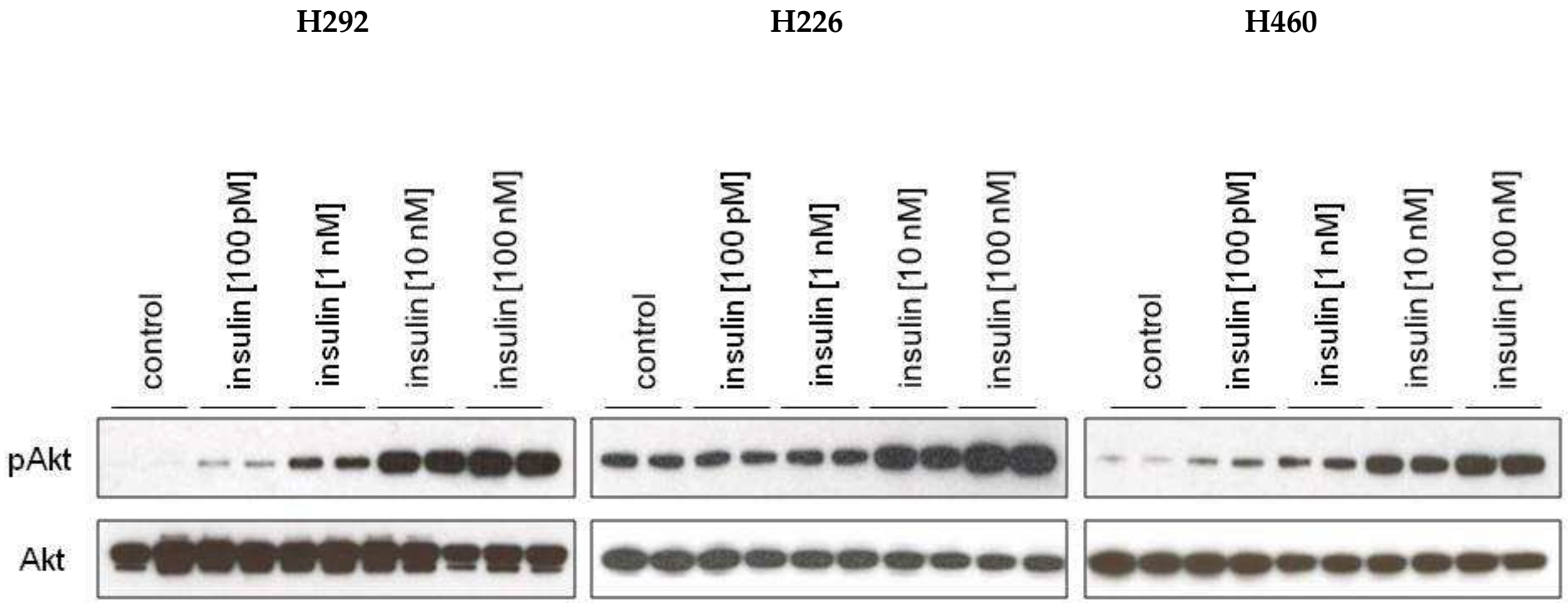
H292
H226
H460
control
insulin [100 pM]
insulin [1 nM]
insulin [10 nM]
insulin [100 nM]
pAkt
Akt

(B)

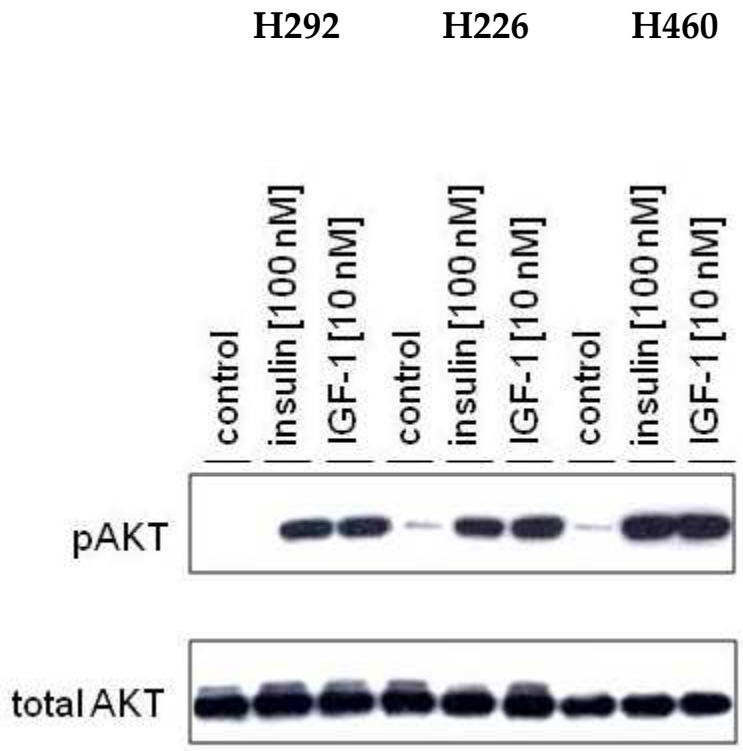

Figure 14: Effects of Insulin and IGF-1 on PKB/Akt Phosphorylation in H292, H226 and H460 cells.

Western blot analysis (N= 4) revealed protein expression levels of phospho Akt (A, B upper panels) and total Akt (A, B lower panels) in NSCLC cells. After a starving period of 24 h, cells were exposed to 100 pM- 100 nM insulin (A) or 100 nM insulin and 10 nM IGF-1 (B) for 15 min before cellular protein extraction was conducted. Concentration-dependent increase in phosphorylation levels of Akt after insulin treatment is presented in (A). Insulin-caused Akt phosphorylation is compared to IGF-1-caused phosphorylation in (B). The exposure time was 1 sec for pAkt and Akt antibody detection.

2.2.3 ERK/MAPK Phosphorylation

In contrast to basal Akt phosphorylation, constitutively phosphorylated ERK1/2 proteins were present in all cell lines tested. However, only in H292 cells, ERK/MAPK was clearly activated by insulin (Fig. 15A). 100 nM insulin and 10 nM IGF-1 induced p44/42 phosphorylation to an equal extent in these cells. In H226 cells, p44/42 phosphorylation was not influenced by insulin but however by IGF-1 (Fig. 15B). Insulin and IGF-1 failed to increase ERK1/2 phosphorylation in H460 cells (Fig. 15B).

Densitometric data quantified Western Blot observations. Both, 100 nM insulin and 10 nM IGF-1 led to a significant p44/42 phosphorylation to 197 % and 204 %, respectively in H292 cells (Fig. 15C, left). In H226 cells, 10 nM IGF-1 (126 %) but not 100 nM insulin (109 %) enhanced ERK1/2 phosphorylation significantly (Fig. 15C, middle). However, neither insulin nor IGF-1 markedly influenced ERK/MAPK in H460 cells (Fig. 15C, right).

(A)

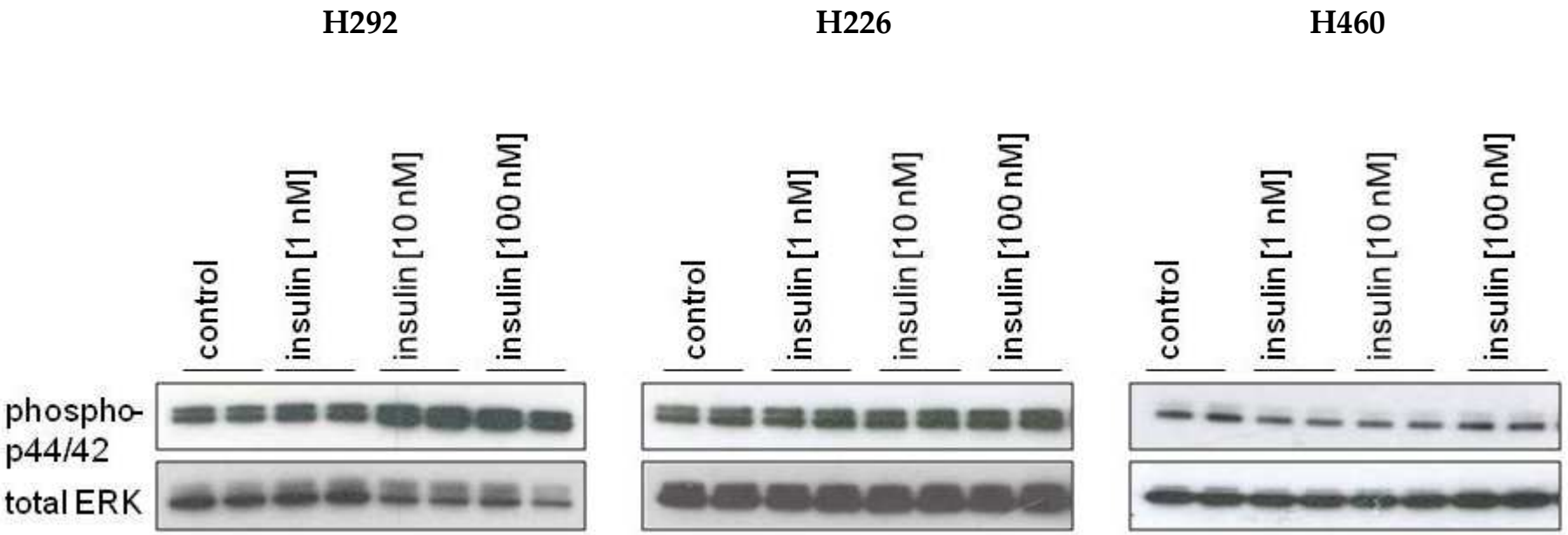
H292
H226
H460
control
insulin [1 nM]
insulin [10 nM]
insulin [100 nM]
phospho-p44/42
total ERK

(B)

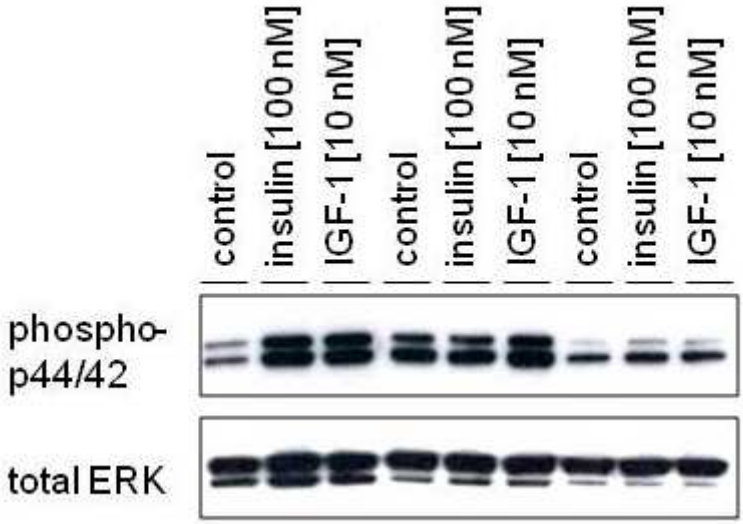
H292
H226
H460
control
insulin [100 nM]
IGF-1 [10 nM]
control
insulin [100 nM]
IGF-1 [10 nM]
control
insulin [100 nM]
IGF-1 [10 nM]
phospho-p44/42
total ERK

(C)

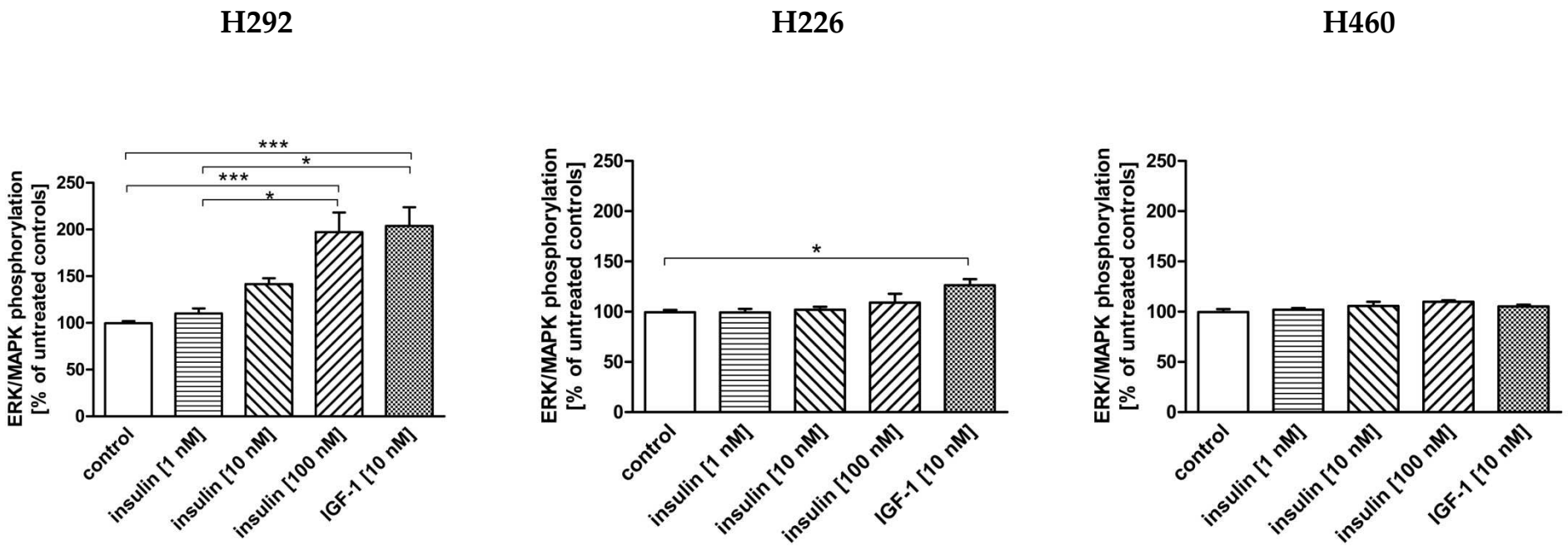

Figure 15: Effects of Insulin and IGF-1 on ERK/MAPK Signaling in H292, H226 and H460 cells.

Cells were cultured in growth medium and placed in starving medium for 24 h afterwards. Test compounds were added and cells were incubated for 15 min before protein preparation was conducted. Western blot analysis reveal ERK1/2 MAPK proteins in NSCLC cells after exposure to insulin in a concentration range from 1 nM- 100 nM (A) and 100 nM insulin compared to 10 nM IGF-1 (B). Phosphorylation levels of p44/42 proteins are shown in the upper panels. Expression of the housekeeping protein total ERK (internal loading control) is presented in the lower panels. The exposure time was 1 min and 1 sec for phospho p44/42 and total ERK antibody detection, respectively. Densitometric analysis (C) shows quantification of p44/42 phosphorylation in each cell line. The bar graphs show means + SEM of N > 3 experiments, measured in duplicates. Results are expressed as percentage of the control. Significance of differences: * $p < 0.05$, *** $p < 0.001$

3 Influences of TGF-β on Mitogenic Processes

3.1 Effects of TGF-β Compared to Insulin on [^{3}H]-Thymidine Incorporation

In H292 and H226 cells, insulin increased cell proliferation to a marked extent in concentrations from 100 nM onwards (see chapter 2.1).

In addition, [^{3}H]-thymidine incorporation was measured after cell exposure to 100 nM insulin and 1 ng/ml (0.08 nM) TGF-β. Thereby, effects of TGF-β on proliferation and possible interactions with insulin could be analyzed. H460 cells were not included in this study since proliferation of this line was not influenced by insulin (see chapter 2.1).

Figure 16 shows a significant increased [^{3}H]-thymidine incorporation rate after incubation with 100 nM insulin in H292 to 173 % (Fig. 16A) and in H226 cells to 126 % (Fig. 16B) which is in line with previous data (Fig. 12). In contrast, TGF-β led to a decreased [^{3}H]-thymidine incorporation rate to 64 % and 60 % in H292 and H226 cells, respectively. Simultaneous treatment with both substances revealed a proliferation rate approximately at control levels.

(A) [^{3}H]-Thymidine Incorporation Rate in H292 Cells

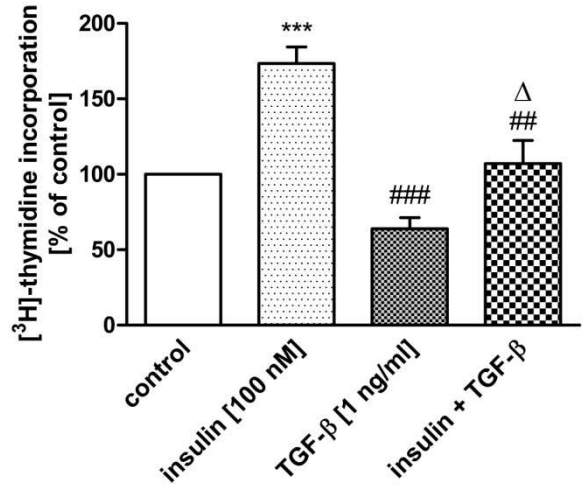

(B) [^{3}H]-Thymidine Incorporation Rate in H226 Cells

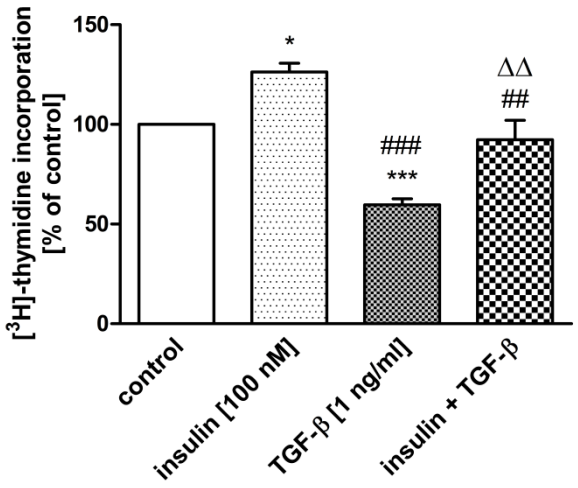

Figure 16: Effects of Insulin and TGFβ on [^{3}H]-Thymidine Incorporation in H292 and H226 Cells.

Cells were treated and prepared as described in Figure 12. Insulin [100 nM] and/ or TGF-β [1 ng/ml] were used as test compounds. Treatment of cells with vehicle-only (water) was paralleled in each experiment (controls). Bar graphs show mean + SEM of N= 5 experiments presented as percentage of controls. Significance of differences: * $p < 0.05$, *** $p < 0.001$ vs. control; ## $p < 0.01$, ### $p < 0.001$ vs. insulin; Δ $p < 0.05$, ΔΔ $p < 0.01$ vs. TGF-β

3.2 Expression of EMT Markers after TGF-β Treatment

In order to obtain a detailed overview of the expression profile of the EMT markers N-Cadherin (CDH2) and Endothelin (ET-1) in NSCLC cells, basic mRNA expression levels (Fig. 17) and mRNA expression levels after treatment with test compounds TGF-β, insulin and IGF-1 (Fig. 18) were measured.

Highly significant differences in ET-1 and CDH2 basic expression were detected within the cell lines tested (Fig. 17). H460 cells expressed ET-1 most pronounced, i.e. 4-fold and 128-fold higher than in H292 and H226 cells, respectively. The CDH2 mRNA level in H226 cells was 3-fold and 256-fold higher than in H292 and H460 cells, respectively.

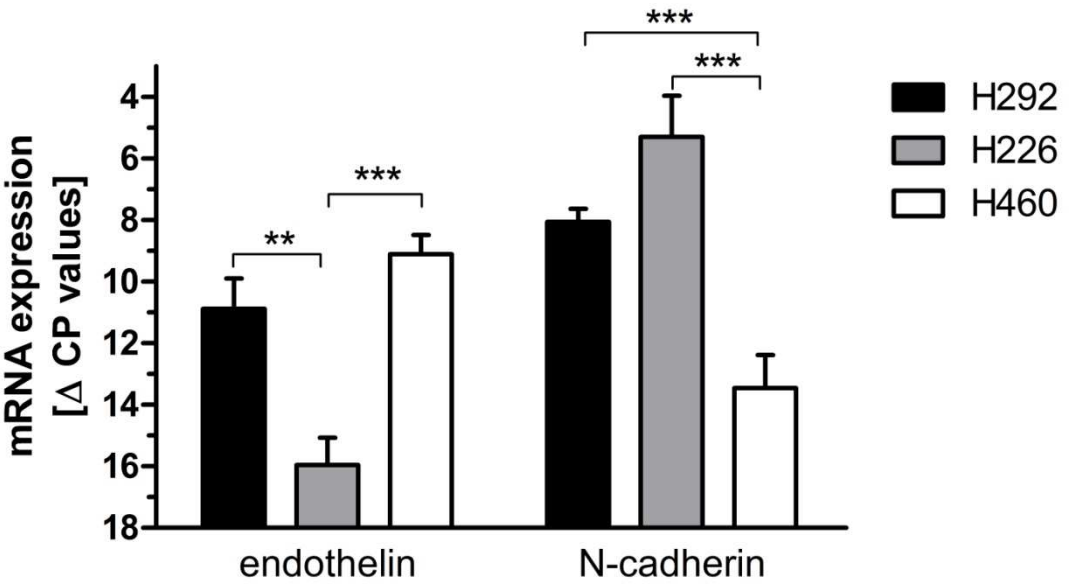

Figure 17: Basic mRNA Expression Rate of Endothelin and N-Cadherin in NSCLC Cell Lines.

Preparation and conduction of qPCR was proceeded as described in Figure 9A. Endothelin and N-cadherin primers are listed in Materials 1.8. Amounts of mRNA expression are shown as Δ CP (relative quantification) by normalizing CP values of target genes to CP values of GAPDH levels (see Methods 2.3.4.2). The bar charts show means + SEM of N= 5 experiments (measured in triplicates). Significance of differences: ** $p < 0.01$, *** $p < 0.001$

In H292 cells, ET-1 mRNA expression was markedly increased by TGF-β to 603 % (Fig. 18). In contrast, insulin and IGF-1 decreased the mRNA expression rate to 35 % and 36 %, respectively. Notably, TGF-β effects were significantly attenuated by insulin (to 261 %) and by IGF-1 (to 138 %) in samples which were exposed to the respective substance combination. ET-1 mRNA expression was increased to 303 % after TGF-β treatment in H226 cells. However, neither insulin nor IGF-1 had significant impacts on mRNA expression in these cells. In accordance to findings in H292 cells, in H226 cells, insulin and IGF-1 diminished TGF-β effects (303 %) to 201 % and 256 %, respectively. H460 cells presented a differing ET-1 expression profile after exposure to the test compounds. Contrary to H292 and H226 cells, TGF-β enhanced the ET-1 mRNA expression only slightly to 140 %, whereas insulin and IGF-1 strongly induced ET-1 mRNA to 217 % and 205 %, respectively. With combinations of TGF-β and insulin (237 %) and TGF-β and IGF-1 (280 %), the ET-1 mRNA expression level was most strongly upregulated.

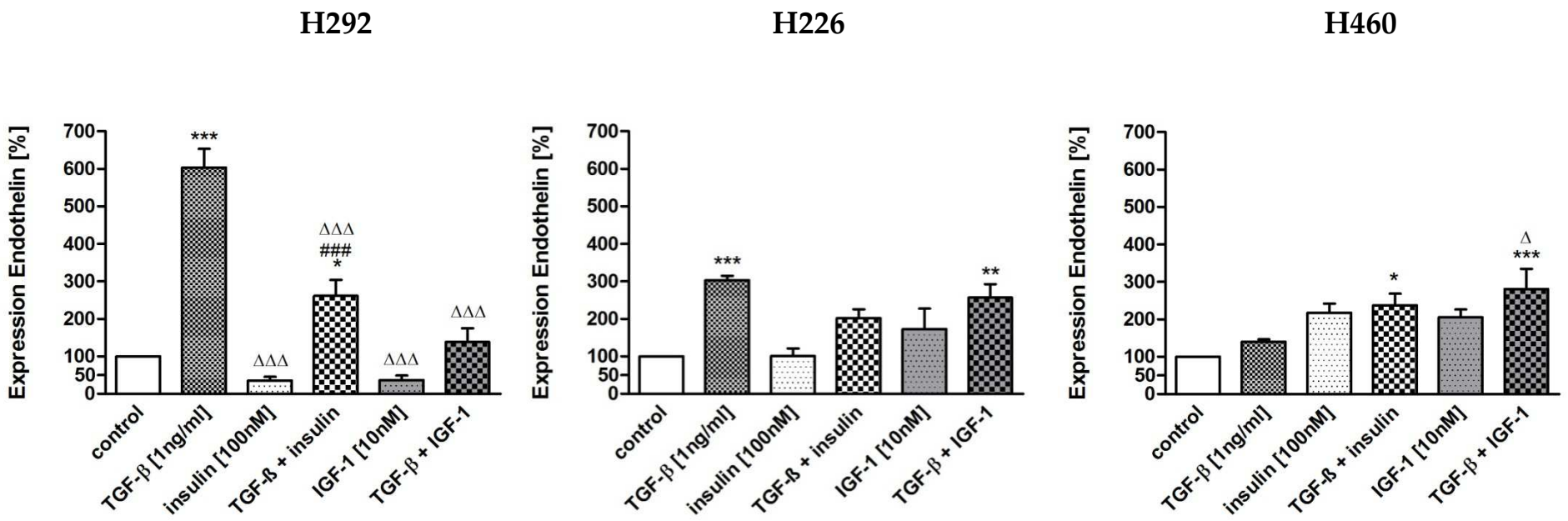

Figure 18: Effects of TGF-β, Insulin and IGF-1 on Endothelin mRNA Expression Levels in NSCLC Cells.

Cells were cultured in growth medium and placed in starving medium for 24 h subsequently. Test compounds were added and cells were incubated for 24 h before RNA preparation and qPCR was conducted as described in Figure 17. Amounts of endothelin mRNA expression levels after substance treatment are shown as percentage of controls (100 %). Therefore, a second normalization was followed by setting the Δ CP value of each sample in relation to the Δ CP value of the control (see Methods 2.3.4.2). The bar graphs show means + SEM of N= 6 experiments. Significance of differences: * $p < 0.05$, ** $p < 0.01$, *** $p < 0.001$ vs. control; ### $p < 0.001$ vs. insulin; Δ $p < 0.05$, ΔΔΔ $p < 0.001$ vs. TGF-β

The CDH2 mRNA expression profile revealed similar tendencies like the ET-1 expression profile after incubation with the test substances in H292 cells (Fig. 19). TGF-β caused an increase in CDH2 mRNA expression to 660 %. Insulin and IGF-1 led to a decrease to 76 % and 58 %, respectively. Again, both combined with TGF-β reduced the effect of the latter (TGF-β + insulin: 232 %, TGF-β + IGF-1: 360 %). Remarkably, in H226 cells, TGF-β and IGF-1 exposure had equal effects on the CDH2 mRNA expression; i.e. mRNA levels were upregulated to 230 % by TGF-β and IGF-1. However, the substance combination of TGF-β and IGF-1 induced CDH2 mRNA expression only to 168 %. Insulin had no impact on CDH2 expression, whereas combined with TGF-β the mRNA level was significantly reduced (189 %) compared to the TGF-β effect (230 %). The same findings were obtained in H460 cells after exposure to TGF-β (209 %), insulin (97 %) and their combination (163 %). However, IGF-1 alone and both together (IGF-1 and TGF-β) had no significant effects on CDH2 expression.

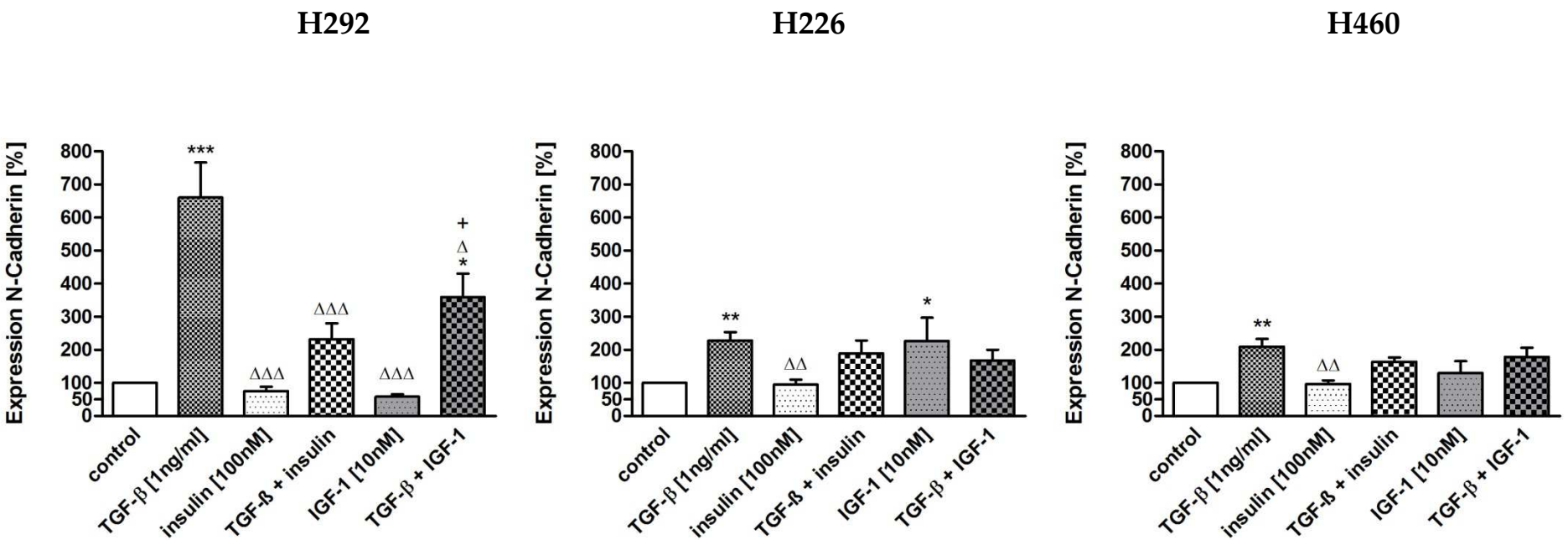

Figure 19: Effects of TGF-β, Insulin and IGF-1 on N-Cadherin mRNA Expression Levels in NSCLC Cells.

Experiments were conducted as described in Figure 18. The bar graphs show means + SEM of N= 6 experiments, expressed as percentage of controls (see Fig. 18). Significance of differences: * $p < 0.05$, ** $p < 0.01$, *** $p < 0.001$ vs. control; Δ $p < 0.05$, ΔΔ $p < 0.01$, ΔΔΔ $p < 0.001$ vs. TGF-β; + $p < 0.05$ vs. IGF-1

4 Effects of Insulin and IGF-1 Receptor Knockdown

4.1 Receptor Knockdown Methods

4.1.1 Non-viral Transfection

It was aimed to establish an insulin and IGF-1 receptor knockdown protocol for NSCLC cell lines with lipofection as transfection method. siRNAs directed against the targets IR (siRNA s7479, siRNA s7478) and IGF-1R (siRNA s7212) (see Materials 1.8.2.) were used for lipofection. Initially, H292 cells were used exclusively in order to proof whether a KD of IR can be achieved in NSCLC cells.

qPCR data revealed that siRNAs s7479 and s7478 significantly knocked down IR mRNA expression (data not shown). To verify the KD on protein level, Western blot analysis was performed (Fig. 20A, left). Densitometric quantification of Western blotting indicated that siRNAs s7479 and s7478 led to a downregulation of IR proteins to 41 % and 32 %, respectively compared to non-coding (nc) siRNA-treated samples (Fig. 20A, right).

However, IGF-1R KD with siRNA s7212 was less pronounced. Densitometric analysis of Western blot analysis revealed a protein downregulation to 56 % compared to nc controls (Fig. 20B, right).

(A) Knockdown of Insulin Receptor in H292 Cells

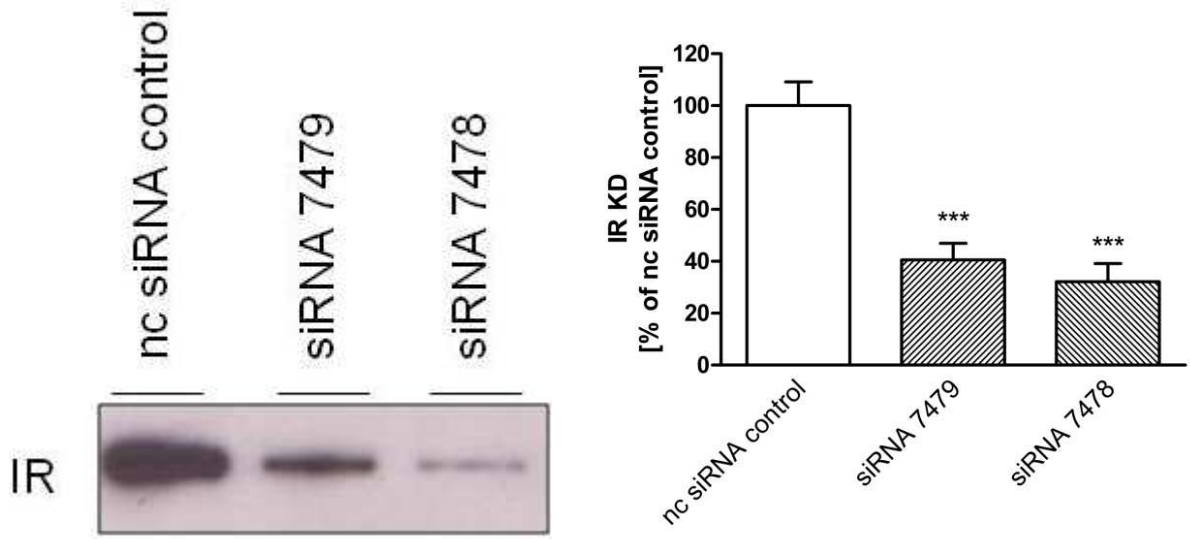

(B) Knockdown of IGF-1 Receptor in H292 Cells

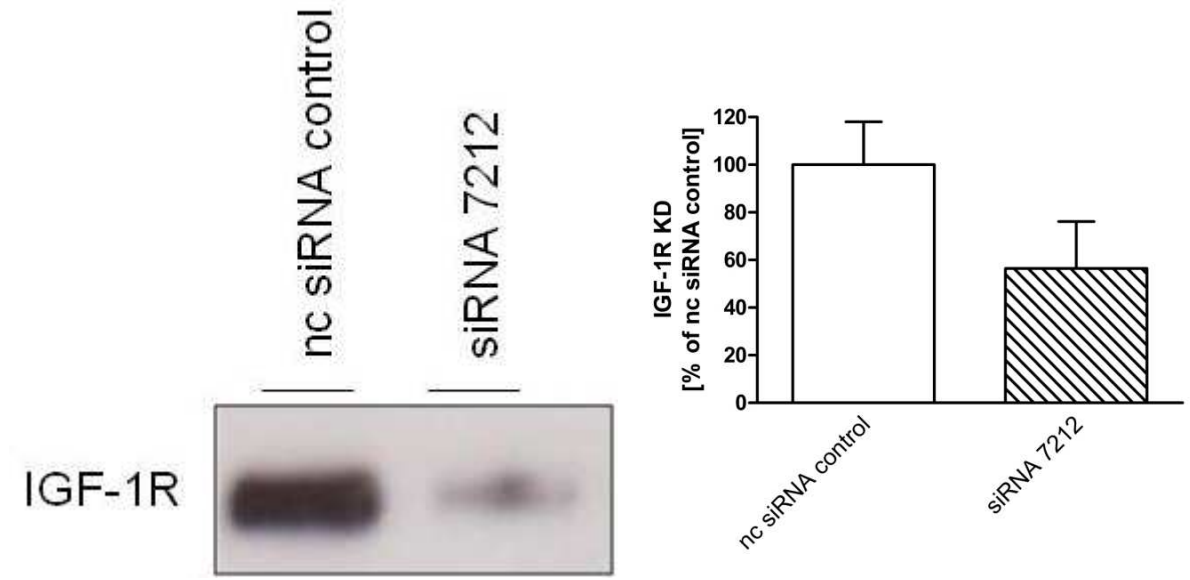

Figure 20: Insulin and IGF-1 Receptor Knockdown via Lipofection in H292 Cells.

Cells were cultured for 24 h in FCS-containing, penicillin/streptomycin-free medium. The transient transfection was conducted with Silencer® Select siRNAs directed against IR or IGF-1R (for details see Materials 2.5.1.1). Western blot analysis reveals KD of IR (A, left) and IGF-1R (B, left) after transfection. The exposure time was 1 min for IR antibody and 1 sec for IGF-1R antibody detection. The bar graphs of the densitometric analysis show means + SEM of N= 6 IR KD experiments (A, right)

and means + SEM of N= 3 IGF-1R KD experiments (B, right). Data are expressed as percentage of the non-coding siRNA controls. Significance of differences: *** $p < 0.001$ vs. control

In pre-tests, aiming to verify the compatibility of the experimental setting, the vehicle Lipofectamine® appeared to impair insulin- and IGF-1-mediated influences on cell proliferation. Both, vehicle-only (Lipofectamine®)- and water-treated controls showed a comparable [^{3}H]-thymidine incorporation rate (Fig. 21). Thus, Lipofectamine® did not influence the basal proliferation rate in H292 cells. Beyond, however, no changes were measured by insulin or IGF-1 in the Lipofectamine®-containing setting (Fig. 21).

Without any transfection agents, insulin and IGF-1 led to a significantly increased [^{3}H]-thymidine incorporation rate in H292 cells (Fig. 12), whereas in presence of Lipofectamine®, insulin failed to elevate the cell proliferation distinctly. Compared to the control level, an increase to 107 % (10 nM) and 109 % (100 nM) was found.

In IGF-1-treated cells, a slightly diminished [^{3}H]-thymidine incorporation rate (1 nM: 91 %, 3 nM: 86 %) was detected.

As a consequence of the unsuitability of Lipofectamine® as transfection reagent for these experiments, lipofection was not used as KD method for further studies.

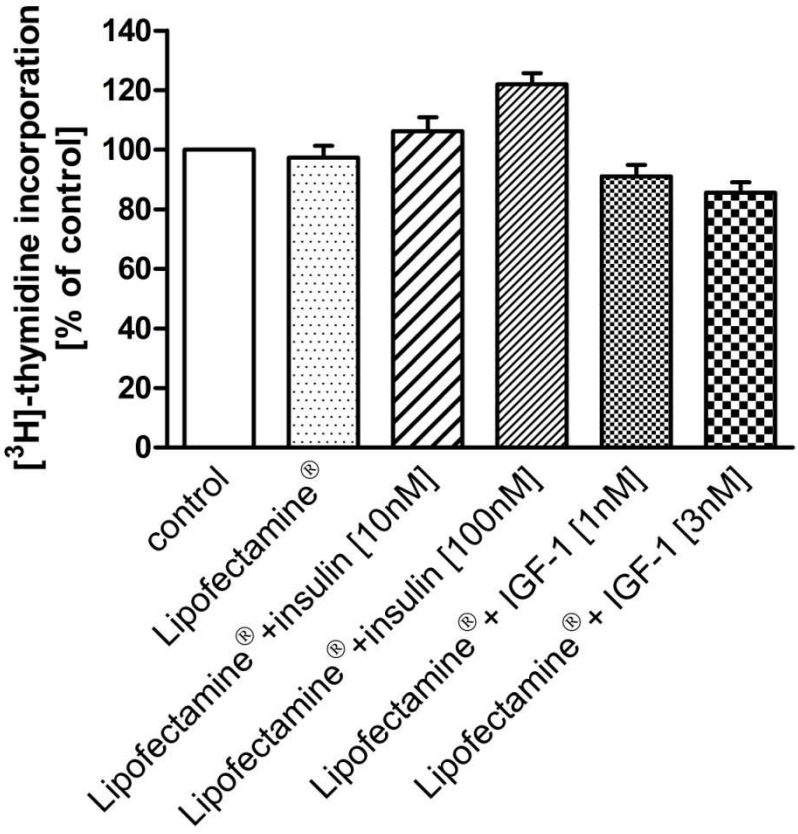

Figure 21: Influence of Lipofectamine® on [3H]-Thymidine Incorporation in H292 cells.

Cells were cultured and prepared as described in Methods 2.5.1.1, albeit no siRNA was given to the transfection solution. The following protocol included exposure to 10 nM/ 100 nM insulin or 1 nM/ 3 nM IGF-1, [3H]-thymidine incubation and measurement of radioactivity (see Fig. 12). Treatment of cells with vehicle-only (water or Lipofectamine®) was paralleled in each experiment as control. The bar graphs show means + SEM of N= 6 (insulin) or N= 3 (IGF-1) experiments. Data are expressed as percentage of the arithmetic average of controls.

4.1.2 Lentiviral Transduction of shRNAs

Lentiviral transduction was established with shRNAs complementary to the target genes IR and IGF-1R (see Materials 1.8.3). In order to check the effectiveness of the lentiviral transduction protocol for NSCLC cells, transduction with GFP-containing plasmids was performed in parallel to each KD experiment. Hence, GFP-treated cells served as positive transduction control and fluorescence of GFP indicated virus infestation of the cells (Fig. 22A).

Vector LV-sh-IRa (LV-sh-NM208a) knocked down the IR mRNA highly significant in H292, H226 and H460 cells; on d 4, IR was diminished to 10 %, 7 % and 19 % in H292, H226 and H460 cells, respectively (Fig. 22B). However, in accordance to the manufacturer's information, LV-sh-IRb (LV-sh-NM208b) led to a less marked IR KD. In H292 and H460 cells, IR mRNA expression was reduced to 37 % and 26 %, respectively. In H226 cells, IR mRNA expression was decreased to 60 % after LV-sh-IRb treatment (Fig. 22B).

KD effects of LV-sh-IRa were also studied on protein level by Western blot and densitometric analysis (Fig. 22C, D). Treatment with LV-sh-IRa led to a marked reduction of IR proteins in all cell lines tested. Western blotting displayed a knockdown to 8 % in H292, 1 % in H226 and 1 % in H460 cells (Fig. 22D).

(A) Lentiviral Transfection Control with GFP

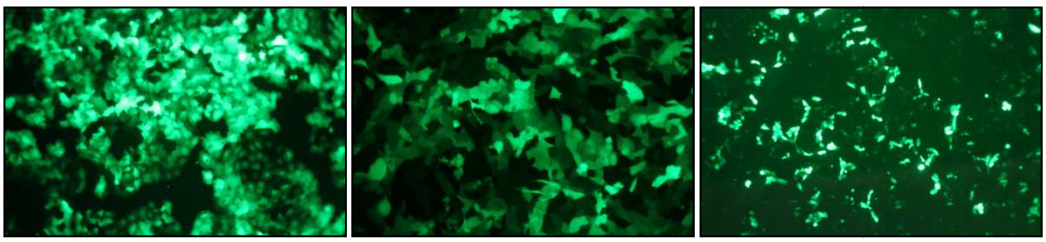

(B) Insulin Receptor mRNA Knockdown after Lentiviral Transduction

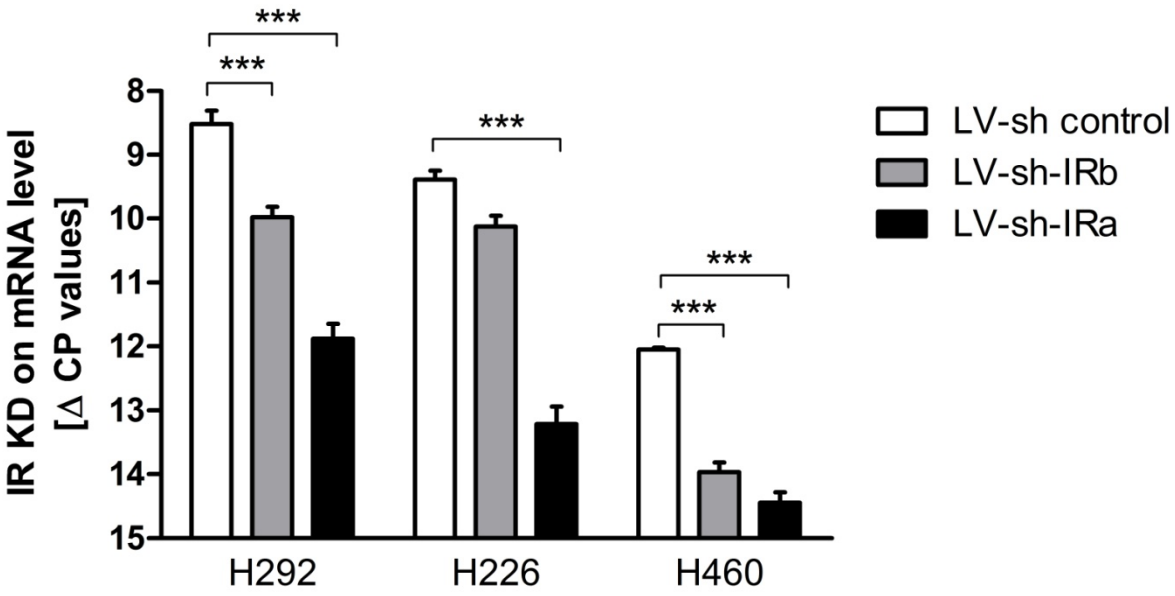

(C) Insulin Receptor Protein Knockdown after Lentiviral Transduction

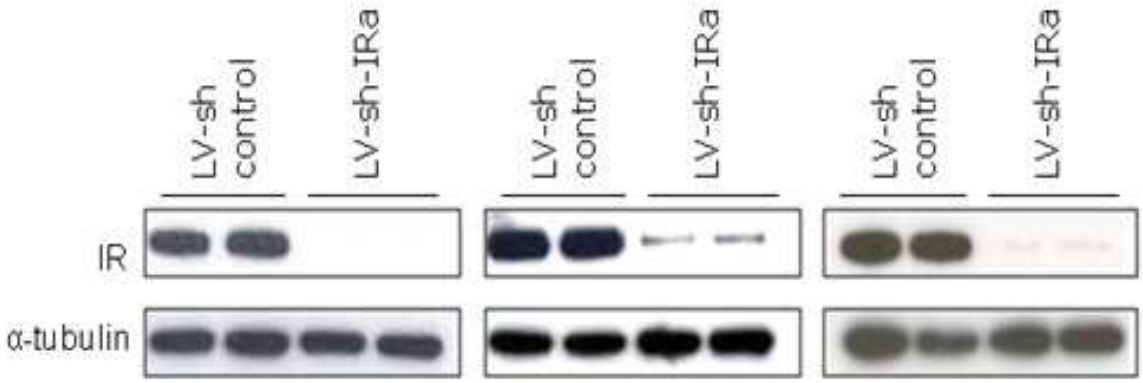

(D) Insulin Receptor Protein Knockdown after Lentiviral Transduction (Densitometric Analysis)

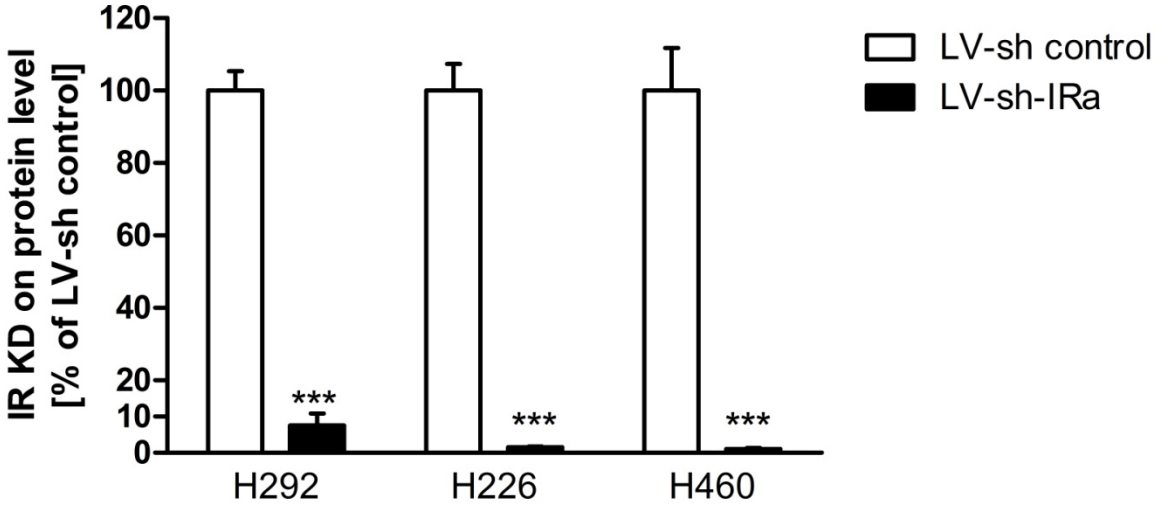

Figure 22: IR KD in NSCLC Cells after Lentiviral Transduction.

Establishment of IR KD in NSCLC cells was performed by transduction with LVs expressing U6 promoter-driven shRNAs against IR (see Methods 2.5.2 for details). LV-sh control was used as control. 72 h after transduction, virus-mixture was replaced by starving medium and cells were incubated for 24 h (d 4) before qPCR or Western blotting followed. A representative image of GFP controls on d 4 is shown in (A). IR *mRNA* expression levels in LV-sh-IRa- and LV-sh-IRb-treated cells compared to LV-sh control are presented in (B). qPCR was carried out with IR primer listed in Materials 1.9. Amounts of mRNA expression are shown as Δ CP (relative quantification) by normalizing CP values of IR to CP values of GAPDH levels (see Methods 2.3.4.2). A Western blot image shows IR *protein* expression levels in IR KD cells compared to controls (C). Anti-insulin receptor antibody (see Materials 1.10) was used for immunodetection. Anti-α-tubulin antibody detection served as internal control. The exposure time was 1 min and 1 sec for IR antibody and α-tubulin antibody detection, respectively. Densitometric analysis of Western blot analysis is presented in (D). The bar graphs show means + SEM of N= 4 experiments. Significance of differences: *** $p < 0.001$

The IGF-1R was knocked down by two independent shRNAs (see Materials 1.8.3: LV-sh-NM875a, LV-sh-NM875b). During the testing stage it became visible that both shRNAs did not differ in their KD capacity (data not shown). Therefore, LV-sh-NM875b, declared as LV-sh-IGF-1R in following figures, was used for further experiments. At d 4 the IGF-1R mRNA expression was decreased to 56 %, 53 % and 16 % in H292, H226 and H460 cells, respectively (Fig. 23A).

Verification of the IGF-1R KD on protein level was proved by Western blotting (Fig. 23B).

Quantification yielded an IGF-1R protein KD to 14 % (H292 cells), 33 % (H226 cells) and 52 % (H460 cells) (Fig. 23C).

(A) IGF-1 Receptor mRNA Knockdown after Lentiviral Transduction

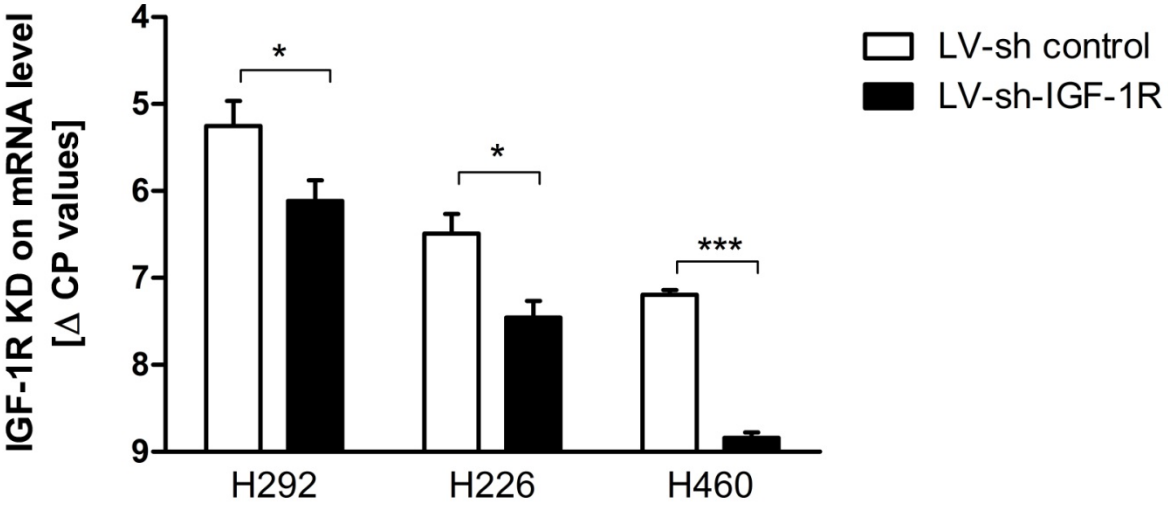

(B) IGF-1 Receptor Protein Knockdown after Lentiviral Transduction

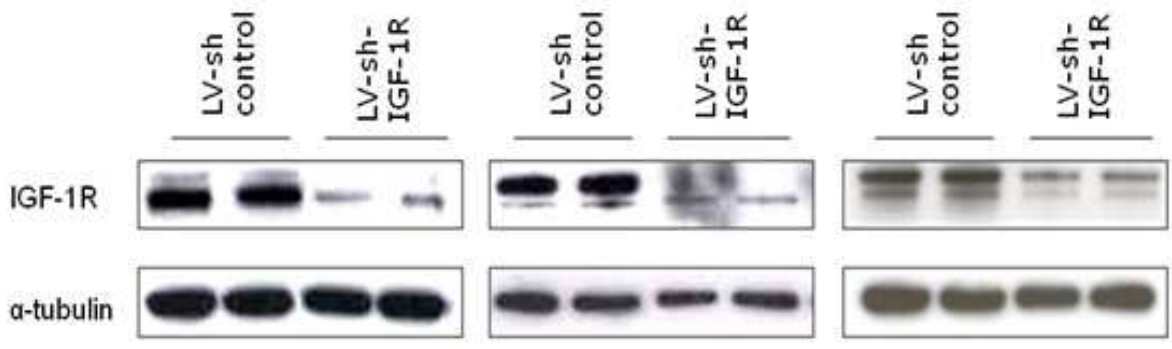

(C) IGF-1 Receptor Protein Knockdown after Lentiviral Transduction (Densitometric Analysis)

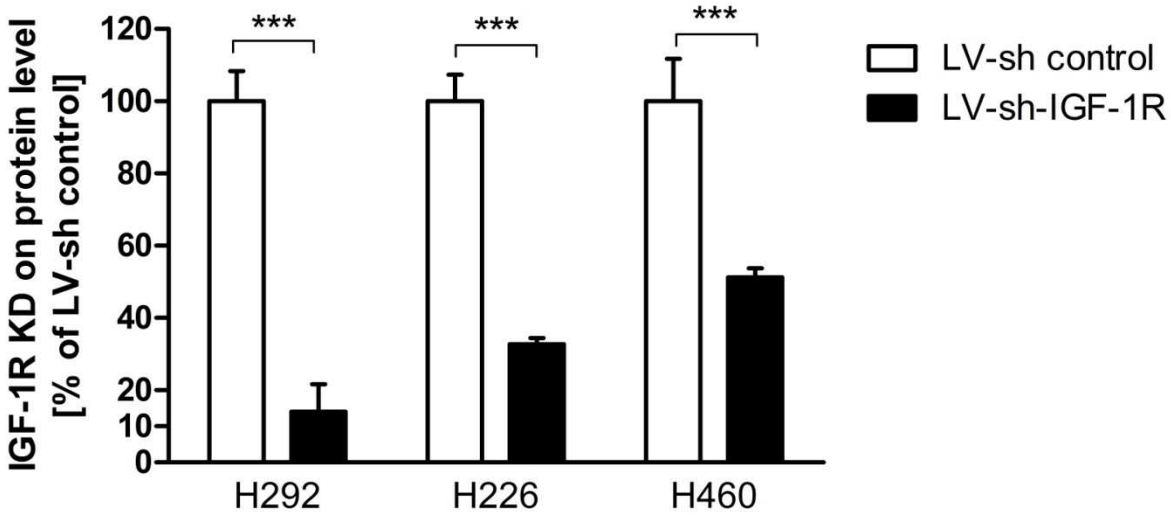

Figure 23: IGF-1R KD in NSCLC Cells after Lentiviral Transduction.

Establishment of IGF-1R KD in NSCLC cells was performed by transduction with LV expressing U6 promoter-driven shRNA against IGF-1R (LV-sh-IGF-1R) (see Methods 2.5.2).
IGF-1R *mRNA* expression level in LV-sh-IGF-1R cells compared to LV-sh control is presented in (A). qPCR was carried out with the IGF-1R primer pair listed in Materials 1.9. Amounts of mRNA expression are shown as Δ CP (relative quantification) by normalizing CP values of IGF-1R to CP values of GAPDH levels (see Methods 2.3.4.2).
A representative Western blot image presents IGF-1R *protein* expression levels in IGF-1R KD cells compared to controls (B). Anti-IGF-1R antibody (see Materials 1.10) was used for immunodetection. The exposure time for IGF-1R antibody and α-tubulin antibody detection was 1 sec. Densitometric analysis of Western blot analysis is presented in (C). The bar graphs show means + SEM of N= 4 experiments. Significance of differences: * $p < 0.05$, ***$p < 0.001$

4.2 Cell Death after Insulin Receptor Knockdown

It became visible that NSCLC cells die upon IR KD; 72 h (d 3) after viral transduction, IR KD cells appeared less confluent via microscopic examination compared to untreated or LV-sh control cells. This phenomenon, found in all lines tested, became even more pronounced at d 4 and led to a most prominent cell death at d 5.

Conduction of cell count confirmed and quantified these observations of a time-dependent increased cell death. At d 5, the number of LV-sh-IRa-treated cells was 2 % in H292, 29 % in H226 and 7 % in H460 compared to respective LV-sh controls (Fig. 24).

In the following, it was aimed to study whether the reduced cell number is a consequence of a strong IR KD. Therefore, cells with a moderate IR KD (LV-sh-IRb) and an IGF-1R KD (LV-sh-IGF-1R) were analyzed for comparison. In four independent experiments cell count remained stable after IGF-1R KD in H292, H226 and H460 cells (data not shown). Partial IR KD also caused a time-dependent decrease in H292 and H226 cell survival, albeit to a lesser extent (d 5: 31 % and 46 %, respectively). In H460 cells, no major difference in cell number after transduction with LV-sh-IRa and LV-sh-IRb was measured (Fig. 24).

4.2.1 Apoptosis Induction After Insulin Receptor Knockdown

Performance of a luminescence-based caspase 3/7 assay was carried out to analyze whether the decline in cell number could be a consequence of apoptosis (Fig. 25). Both, untreated and LV-sh control cells served as negative controls. Gemcitabine-treated cells were chosen as positive (i.e. caspase-activating) control.

IR KD activated caspases 3/7 significantly in comparison to the negative controls in the three cell lines. However, the strongest upregulation was found in H292 cells; LV-sh-IRa enhanced caspase activity to 550 % which was even above the caspase activity level of the positive control (453 %). In H226 cells, IR KD provoked an increase to 430 %, whereas gemcitabine enhanced caspase activity to 845 %. The comparably lowest but still significant impact of IR KD on caspase activity was found in H460 cells (increase to 140 %). As observed in H226 cells, effects of gemcitabine were significantly stronger than effects of the receptor KD (increase to 417 %).

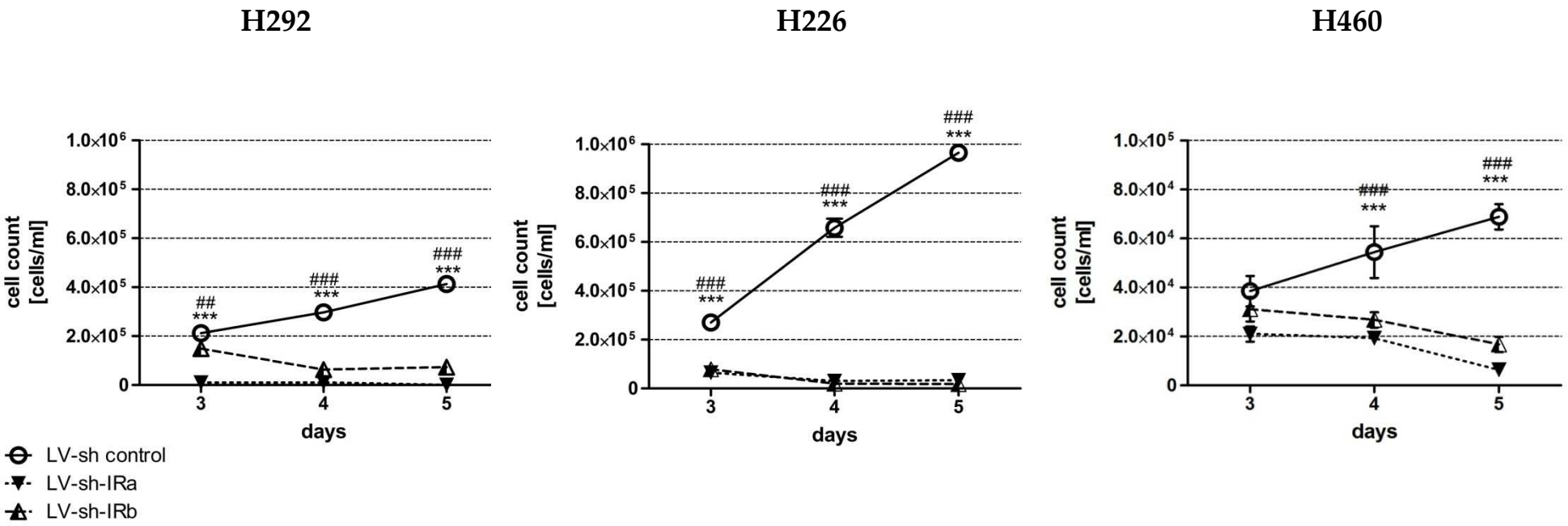

Figure 24: Decrease in NSCLC Cell Survival Caused by Stable Transduction with LV-sh-IRa and LV-sh-IRb.

Cells were seeded and incubated for 4 h before LV transduction was performed (for details see Methods 2.5.2). At d 3 after virus treatment cells were trypsinized and prepared for cell count (see Methods 2.6.1). Cell count at d 4 (d 5) was performed by replacing virus-containing medium by serum-free medium at d 3. An incubation time of 24 h (48 h) under starving conditions followed. Each sample was measured in triplicates. Results (absolute cell number per ml) are presented as means ± SEM of N= 4 experiments. Significance of differences: *** $p < 0.001$ LV-sh-IRa vs. LV-sh control; ### $p < 0.001$ LV-sh-IRb vs. LV-sh control

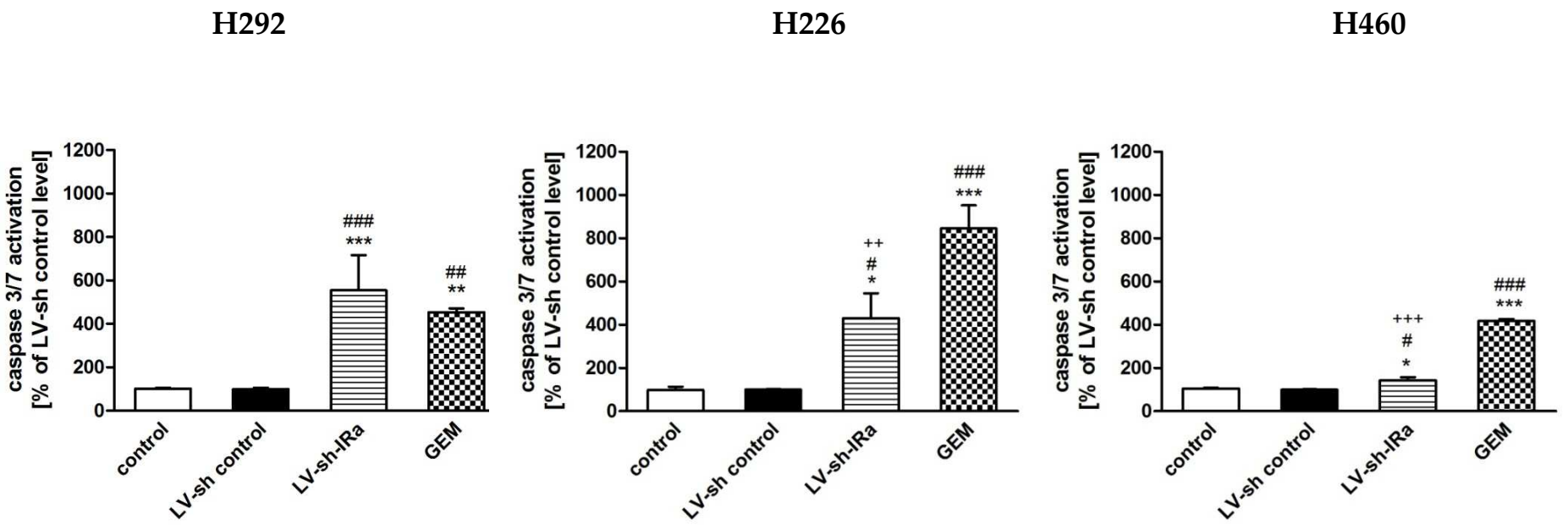

Figure 25: Effects of IR KD on Caspase 3/7 Activation in NSCLC Cells.

Detection of Caspase 3/7 activity was conducted by the use of Caspase-Glo® 3/7 Assay. Effects of IR KD on caspases activity were measured at d 3 after LV transduction. Both, LV-sh control and untreated cells served as negative controls. The chemotherapeutic drug gemcitabine was selected as positive control. A blank reaction, including Caspase-Glo® 3/7 Reagent and cell culture medium without cells was required in order to detect background luminescence.
The results, presented as percentage of LV-sh controls, are means + SEM of N= 3 experiments. Significance of differences: * $p < 0.05$, ** $p < 0.01$, *** $p < 0.001$ vs. control; # $p < 0.05$, ## $p < 0.01$, ### $p < 0.001$ vs. LV-sh-control; ++ $p < 0.01$, +++ $p < 0.001$ vs. gemcitabine

4.3 Effects of IGF-1 Receptor Knockdown on EMT and Cell Proliferation

4.3.1 IGF-1 Receptor Knockdown Induced EMT

Cells transduced with the LV-GFP and the LV-sh control virus showed an inconspicuous and intact epithelial morphology (Fig. 26A). In contrast, LV-sh-IRa-treated cells were marked by a damaged and injured phenotype. Beyond, as described in chapter 4.2, the cell confluence was markedly reduced. Notably, in H292 IGF-1R KD cells a visible cell transformation became obvious. The typical epithelial cell appearance was no longer clearly pronounced. Instead, cells became more smooth muscle-like, i.e. their phenotype displayed a mesenchymal morphology (Fig. 26A). EMT could be the underlying mechanism of this observed cell transformation. Thus, mRNA expression levels of ET-1, CDH2 and fibronectin were measured (Fig. 26B). The mRNA expression levels of the target genes in LV-sh control cells were used as reference.

ET-1 expression was significantly upregulated in both, IR-KD and IGF-1R KD cells to 492 % and 408 %, respectively. However, CDH2 and fibronectin mRNA levels were significantly elevated in IGF-1R KD cells to 390 %. Fibronectin expression was equally pronounced in IR KD and control cells, whereas CDH2 expression was elevated to 200 % in IGF-1 KD cells.

(A) Microscopic Observation of H292 Cell Morphology

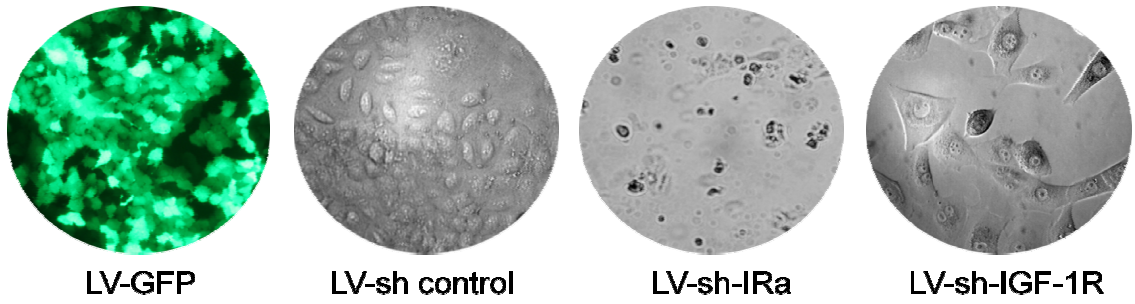

(B) mRNA Expression of EMT Marker

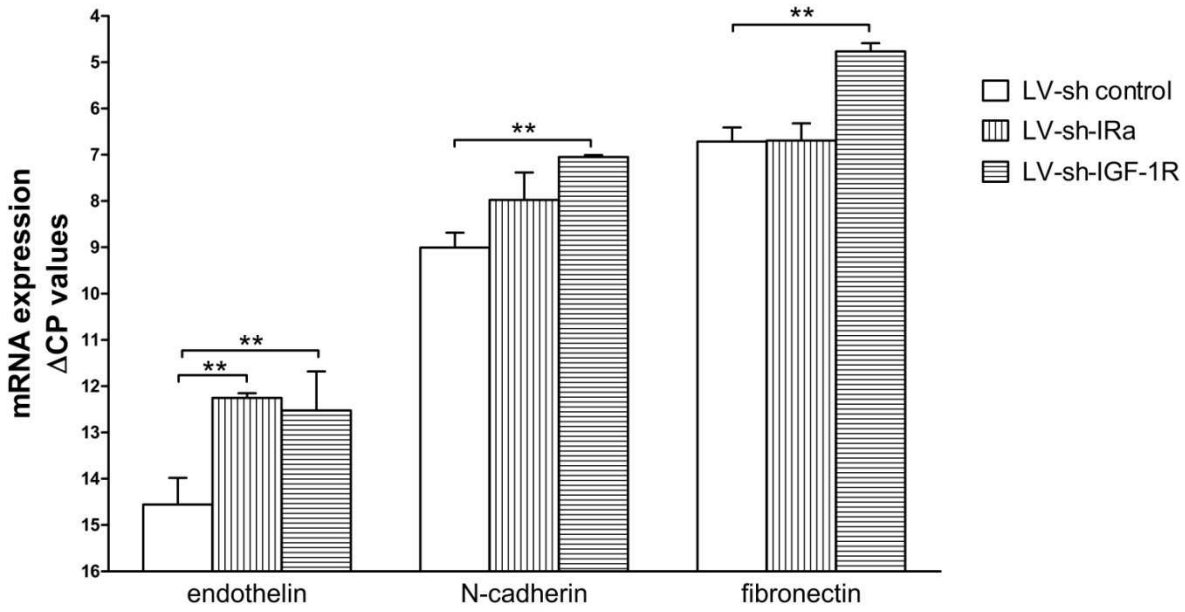

Figure 26: Effects of IGF-1R KD on EMT in H292 Cells.

Lentiviral transduction was performed as described previously. Cells were analyzed at d 4. One representative microscopic image out of N= 4 is shown in (A). qPCR was conducted to quantify mRNA expression levels of EMT markers (ET-1, CDH2, fibronectin) (B). Primers are listed in 1.9. Amounts of mRNA expression are shown as Δ CP (relative quantification) by normalizing CP values of target genes to CP values of GAPDH levels (see Methods 2.3.4.2). The bar graphs show of means + SEM of N= 3 experiments. Significance of differences: ** $p < 0.01$

4.3.2 Increased Proliferative Effects of Insulin in IGF-1R KD Cells

Insulin markedly empowered cell proliferation in H292 cells (Fig. 12). However, it remained unclear to which extent mitogenic insulin effects are mediated via *IGF-1R* activation. Therefore, [^{3}H]-thymidine incorporation was analyzed in *H292 IGF-1R KD cells* after incubation with insulin in concentrations of 100 nM and 1 μM (Fig. 27).

The basal cell proliferation (i.e. without insulin stimulation) of IGF-1R KD cells did not differ decisively from that of LV-sh control cells. However, the [^{3}H]-thymidine incorporation rate in insulin-treated IGF-1R KD cells was significantly higher than in insulin-treated LV-sh control cells. Exposed to 100 nM insulin, the incorporation rate was increased to 226 % in IGF-1R KD cells but only to 140 % in LV-sh control cells. A concentration of 1 μM insulin increased the [^{3}H]-thymidine incorporation to 185 % and 262 % in LV-sh control and IGF-1R KD cells, respectively.

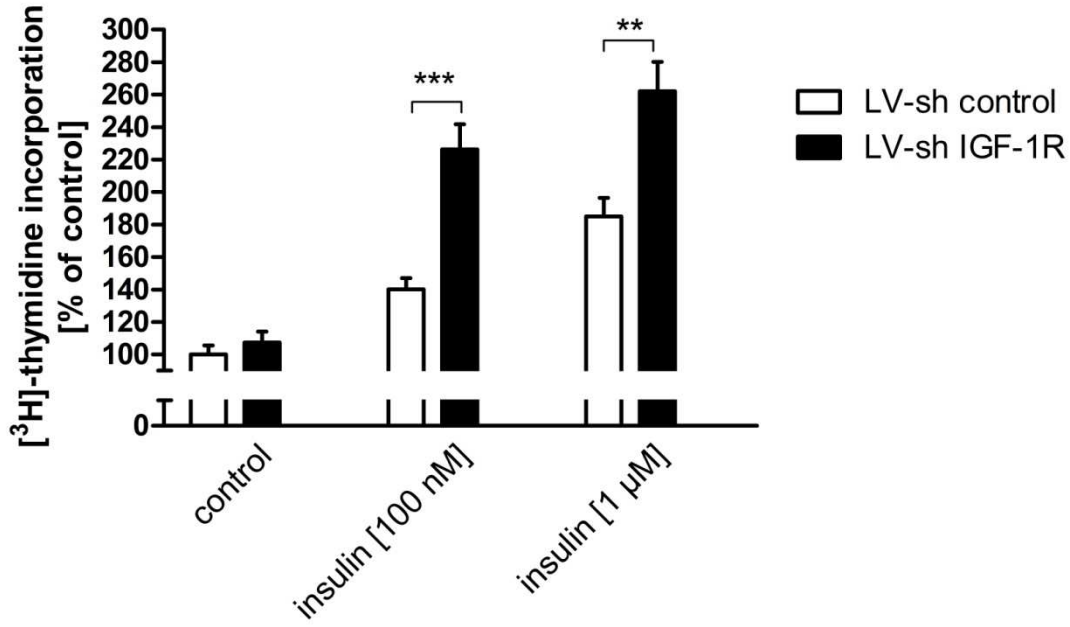

Figure 27: Increased Insulin-Induced [^{3}H]-Thymidine Incorporation Rate in H292 IGF-1R KD Cells.

Lentiviral transduction was followed by [^{3}H]-thymidine incorporation assay as described in Figure 12. Radioactivity was recorded as dpm per well by liquid scintillation spectometry. Water-treated samples served as controls in LV-sh control and IGF-1R KD cells. Results of N= 3 experiments are expressed as means + SEM. Significance of differences: ** $p < 0.01$, *** $p < 0.001$

4.4 Impaired Mitogenic Signaling Pathways in Knockdown Cells

4.4.1 Phosphorylation of Insulin Receptors

Changes in basal and insulin-induced IR/IGF-1R phosphorylation levels after IR KD were examined with phospho Western blotting (Fig. 28) in H292, H226 and H460 cells. Next to detection of the phosphorylated receptor proteins, detections with IR and IGF-1R antibodies (see Materials 1.10.1) were performed in parallel. Thereby, the IR KD could be proved (middle panels) and beyond, possible changes in IGF-1R protein expression could be captured (lower panels).

After stimulation with 10 nM and 100 nM insulin, pIR/pIGF-1R levels remained largely unchanged in H292 IR KD cells compared to LV-sh control cells (upper panels). Thus, even low insulin concentrations (10 nM) caused a clear IR/IGF-1R phosphorylation in H292 IR KD cells. Notably, there were no signs of a compensatory IGF-1R upregulation.

In H226 and H460 IR KD cells, potency and maximal effect of insulin with regard to receptor autophosphorylation were slightly diminished (upper panels). However, clear phosphorylation signals after treatment with 100 nM insulin were still observed.

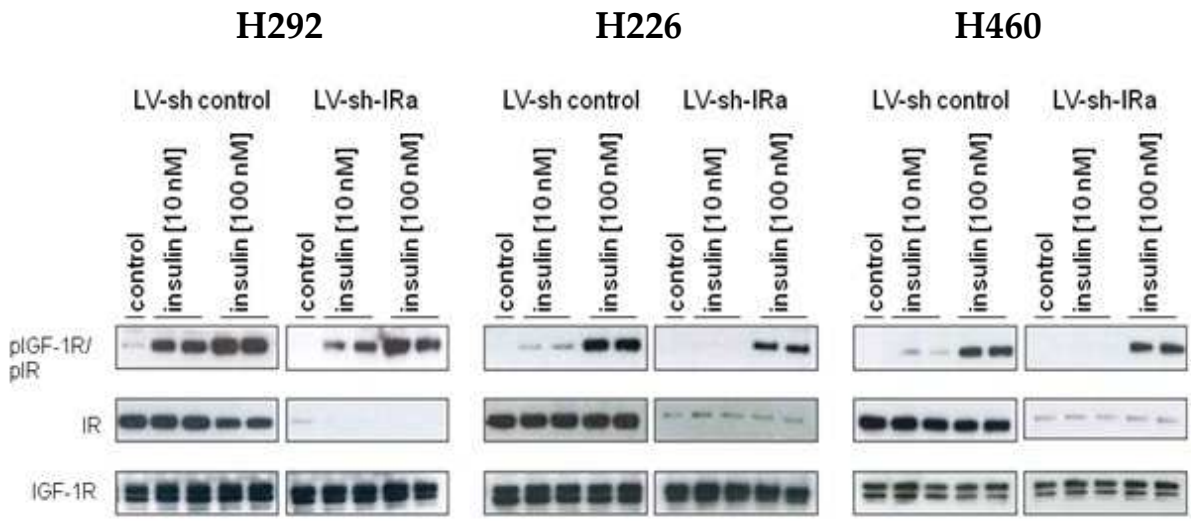

Figure 28: Phosphorylation of IR/IGF-1R in H292, H226 and H460 IR KD Cells.

Receptor protein activation was analyzed at d 4 after lentiviral transduction. Western blot experiments represent pIGF-1R/pIR protein expression after insulin stimulation in LV-sh control cells and LV-sh-IRa-treated cells (upper panels). IR (middle panels) and IGF-1R (lower panels) protein detection served as controls. Antibodies are listed in Materials 1.10. The exposure time was 1 sec for IGF-1R antibody and 1 min for pIGF-1R/pIR and IR antibody detection. N= 3 (H292 cells) or N= 2 (H226 and H460 cells) experiments were performed.

4.4.2 Akt Phosphorylation

As described in chapter 2.2.2, insulin induced Akt phosphorylation in a concentration-dependent manner.

In order to examine if or to which extent IR KD and IGF-1R KD change activation of Akt-signaling after insulin exposure, phospho Western blotting was performed in H292, H226 and H460 cells (Fig. 29A, B, C).

Compared to LV-sh control cells, IR KD resulted in a reduction of insulin-induced Akt phosphorylation in all cell lines. Although LV-sh-IRa downregulated the IR significantly (Fig. 22), pAkt signals were still detectable.

Since H292 cells revealed the highest expression rate of IR among the NSCLC cells tested (Fig. 9), it was to analyze whether in this cell line partial KD shows any changes in insulin-induced Akt-signaling like compared to LV-sh controls. Indeed, transduction with LV-sh-IRb also resulted in (slightly) decreased Akt phosphorylation levels.

Further studies with LV-sh-IGF-1R-transduced cells indicated that the activity of Akt signaling does not depend on IGF-1R in H292 and H226 cells; there were no changes in insulin-induced pAkt signals in IGF-1R KD compared to LV-sh control cells (data not shown).

In H460 cells, IGF-1R KD diminished insulin-caused Akt phosphorylation to the same extent as IR KD (Fig. 29C).

(A) Akt Signaling in LV-sh-IRa and LV-sh-IRb-Transduced H292 Cells

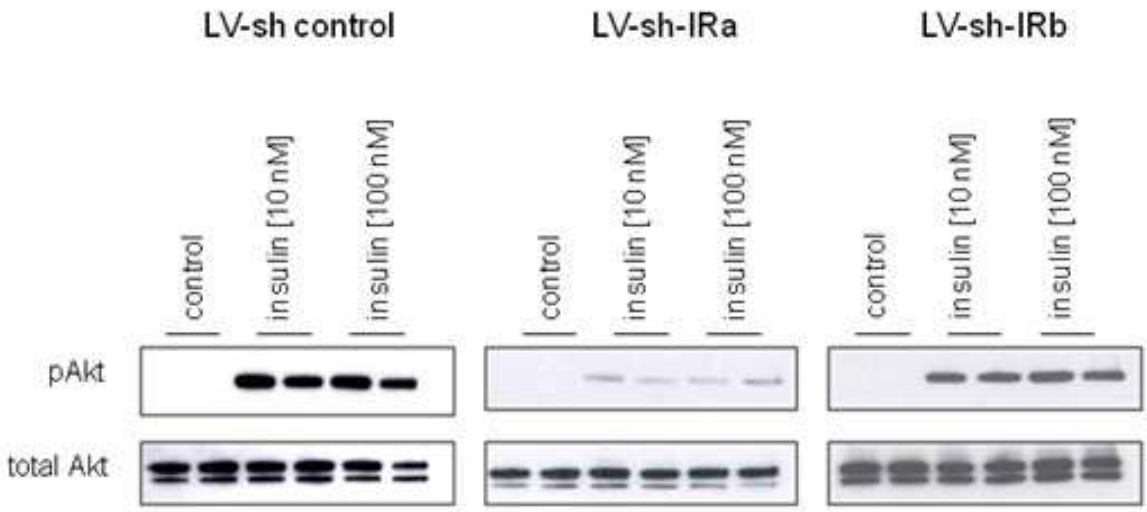

(B) Akt Signaling in LV-sh-IRa-Transduced H226 Cells

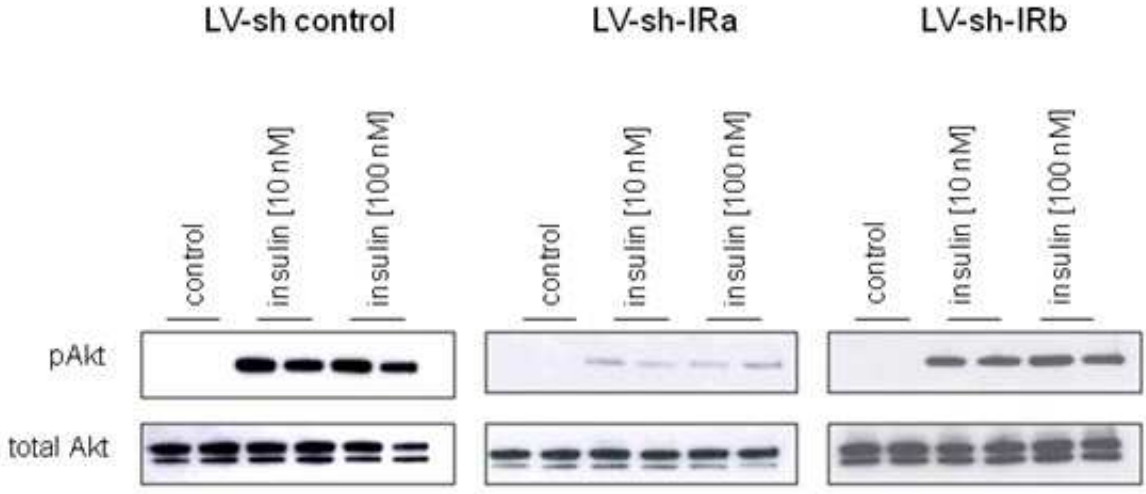

(C) Akt Signaling in LV-sh-IRa and LV-sh-IGF-1R-Transduced H460 Cells

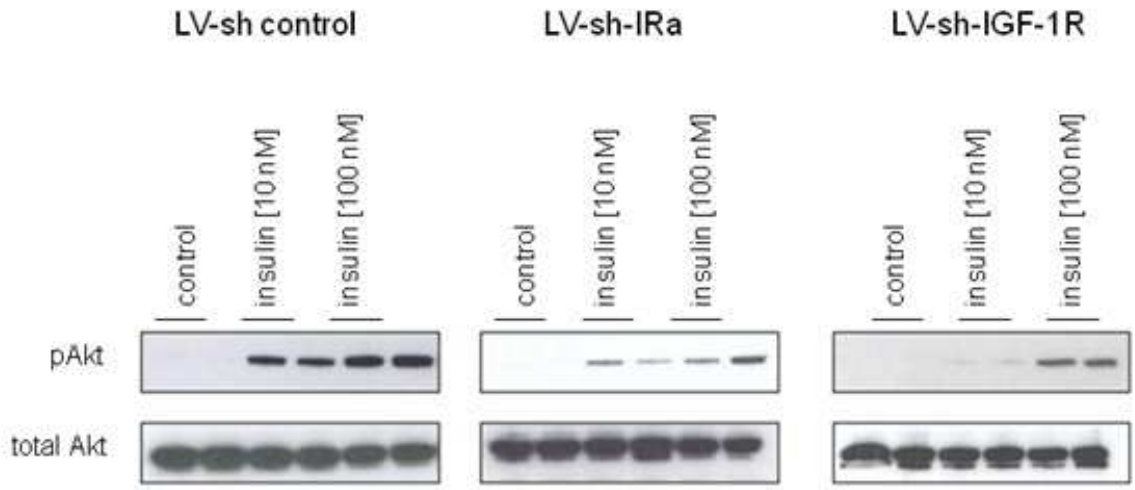

Figure 29: Akt Signaling in H292, H226 and H460 KD Cells.

Cell preparation for protein analysis was carried out at d 4 after lentiviral transduction. Western blot analysis revealed expression of pAkt (upper panels) and total Akt (lower panels) in IR KD cells compared to the controls in the three NSCLC cell lines. In H460 cells an additional Western blot experiment of IGF-1R KD cells is shown (C). Lentiviral transduction was carried out as described previously. Western blotting was performed with antibodies used before (see Fig. 14). The exposure time was 1 sec for pAkt antibody and Akt antibody detection. N= 4 (H292 cells) or N= 2 (H226 and H460 cells) experiments were performed.

4.4.3 ERK/MAPK Phosphorylation

MAPK analysis was only studied in cell line H292, because in H226 and H460 cells, insulin failed to affect this mitogenic pathway (Fig. 15).

In H292 LV-sh-IRa-transduced cells, both, basal ERK/MAPK phosphorylation and its insulin-dependent activation were markedly less pronounced than in controls (Fig. 30A). Especially stimulatory effects of insulin were significantly reduced by 67 % in 10 nM and 64 % in 100 nM treated samples (Fig. 30A, densitometric analysis). Notably, the basal phospho p44/42 level was diminished by partial IR KD. Beyond, only slightly decreased insulin-induced phospho p44/42 protein levels could be identified compared to LV-sh controls.

As previously observed in Akt signaling studies (see chapter 4.4.2), IGF-1R KD did not affect any changes in basal or insulin-induced ERK/MAPK signaling (data not shown).

In H226 cells, IGF-1R KD markedly reduced basal and insulin-stimulated ERK/MAPK signaling. Effects of IR KD were less pronounced but still visible (Fig. 30B).

IR KD revealed a specific feature in H460 cells; opposed to H292 and H226 cells, phosphorylation of ERK1/2 was upregulated in LV-sh-IRa cells. The same phenomenon was found after KD of IGF-1R (Fig. 30C).

(A) ERK/MAPK Signaling in LV-sh-IRa- and LV-sh-IRb-Transduced H292 Cells

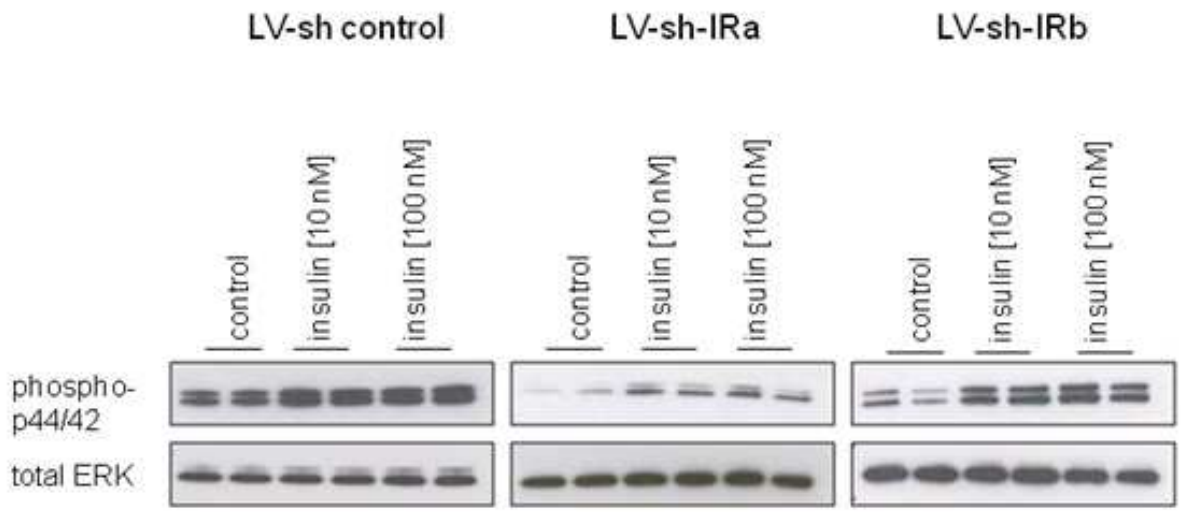

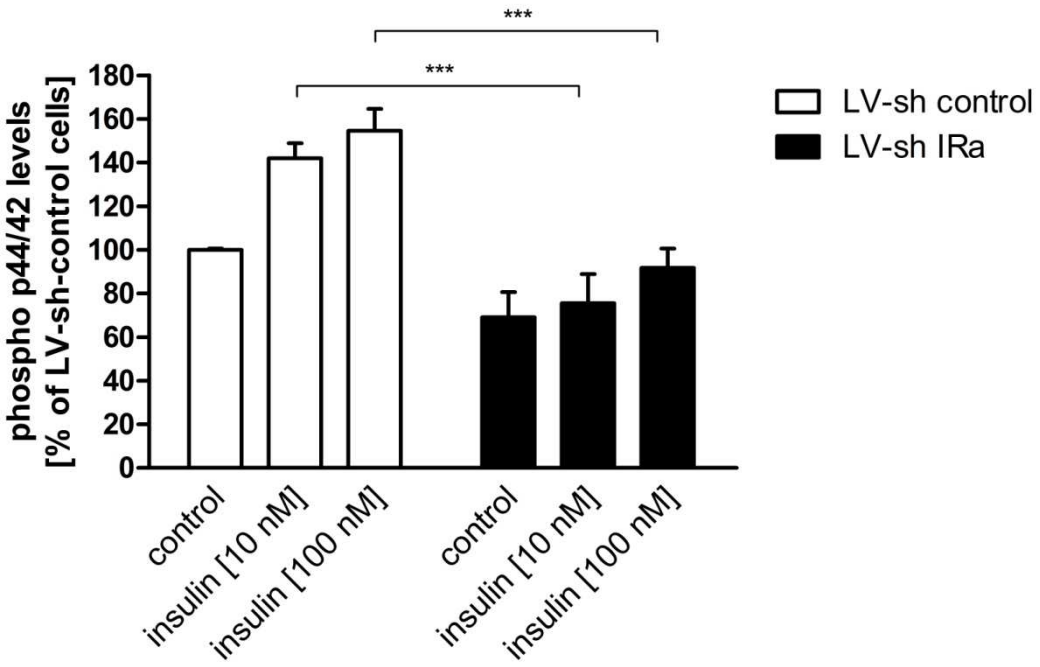

(B) ERK/MAPK Signaling in LV-sh-IRa and LV-sh-IGF-1R Transduced H226 Cells

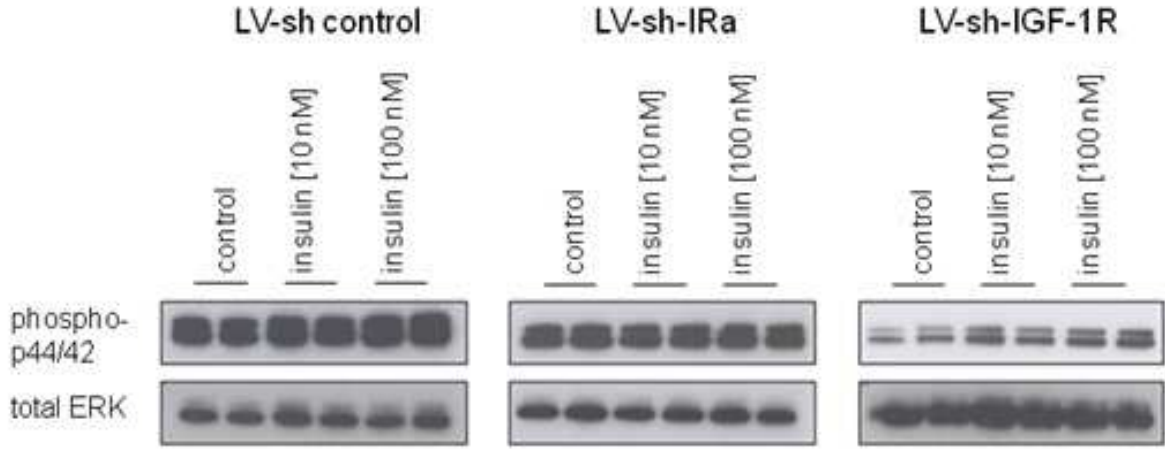

(C) ERK/MAPK Signaling in LV-sh-IRa- and LV-sh-IGF-1R-Transduced H460 Cells

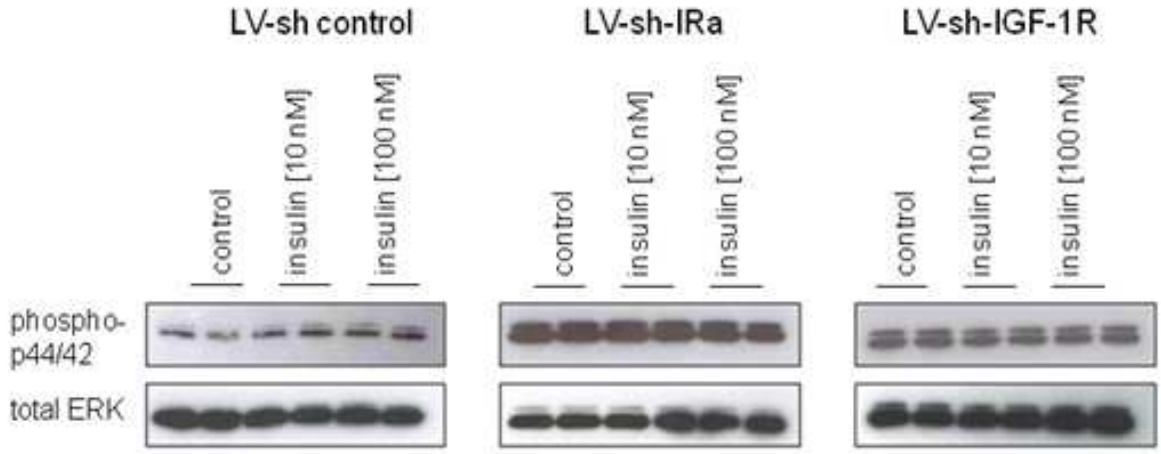

Figure 30: ERK/MAPK Signaling in H292, H226 and H460 KD Cells.

Protein extraction was conducted at d 4 after transduction. Representative Western blot experiments show expression of phospho p44/42 (upper panels) and total ERK (lower panels) in IR KD cells compared to LV-sh controls in the three NSCLC cell lines. Densitometric analysis of ERK/MAPK phosphorylation levels in H292 cells is presented in (A). An additional Western blot experiment of IGF-1R KD cells is shown in H226 (B) and H460 cells (C). Lentiviral transduction was performed as described before. Western blotting was carried out with antibodies used previously (see Fig. 15). The exposure time was 1 min and 1 sec for phospho p44/42 and total ERK antibody detection, respectively. The bar graphs show means + SEM of N= 4 (H292 cells) or N= 2 (H226 and H460 cells) experiments. Significance of differences: ***$p < 0.001$

4.5 Microarray-Based Gene Expression Profiling of Insulin Receptor Knockdown Cells

4.5.1 Altered Gene Expression in IR KD Cells

It became evident, that downregulation of the IR has several effects of its own which differed between the investigated NSCLC cell lines. In order to obtain an overview of gene expression alterations evoked by the almost complete loss of IR, genome-wide gene profiling was performed. Hereby, marked changes in the group of cytokines became evident. Figure 31B contrasts all cytokines which were strongly induced by the IR KD. Changes of gene expression in IR KD cells compared to LV-sh control samples are presented as fold-change values (see Methods 2.7). With respect to apoptosis-involved cytokines, IL24 was upregulated most strongly, particularly by 78-, 5- and 160-fold in H292, H226 and H460 cells, respectively. TNF expression levels were elevated by 9-, 5-, 3-fold in H292, H226 and H460 cells, respectively. Additionally, in H292 cells, IR KD caused a 10-fold upregulated IL20 gene expression. In the field of chemokines, members of the CXCL family, known to be involved in angiogenesis, were markedly upregulated in the three NSCLC cells (for details see Fig. 31B). Beyond, elevated levels of several insulin- and IGF-family members, like insulin-induced genes (INSIG-1-2), insulin-like factors (INSL-3-5) or IGF-like factors (IGFL-1-3) were also found in the three cell lines (Fig. 31B). The expression of IGFL-1 was upregulated 14-fold in H292 IR KD cells. However, the IGFL-1 receptor (IGFL-1R) was downregulated in the NSCLC cell lines tested, by 0.4-fold in H292 and H226 cells and by 0.2-fold in H460 cells. An appreciable 2-fold increase in IGF-2 and IGF-2R gene expression was detected in H460 cells.

(A) Upregulated Expression of Apoptosis-Involved Cytokines in Insulin Receptor Knockdown Cells

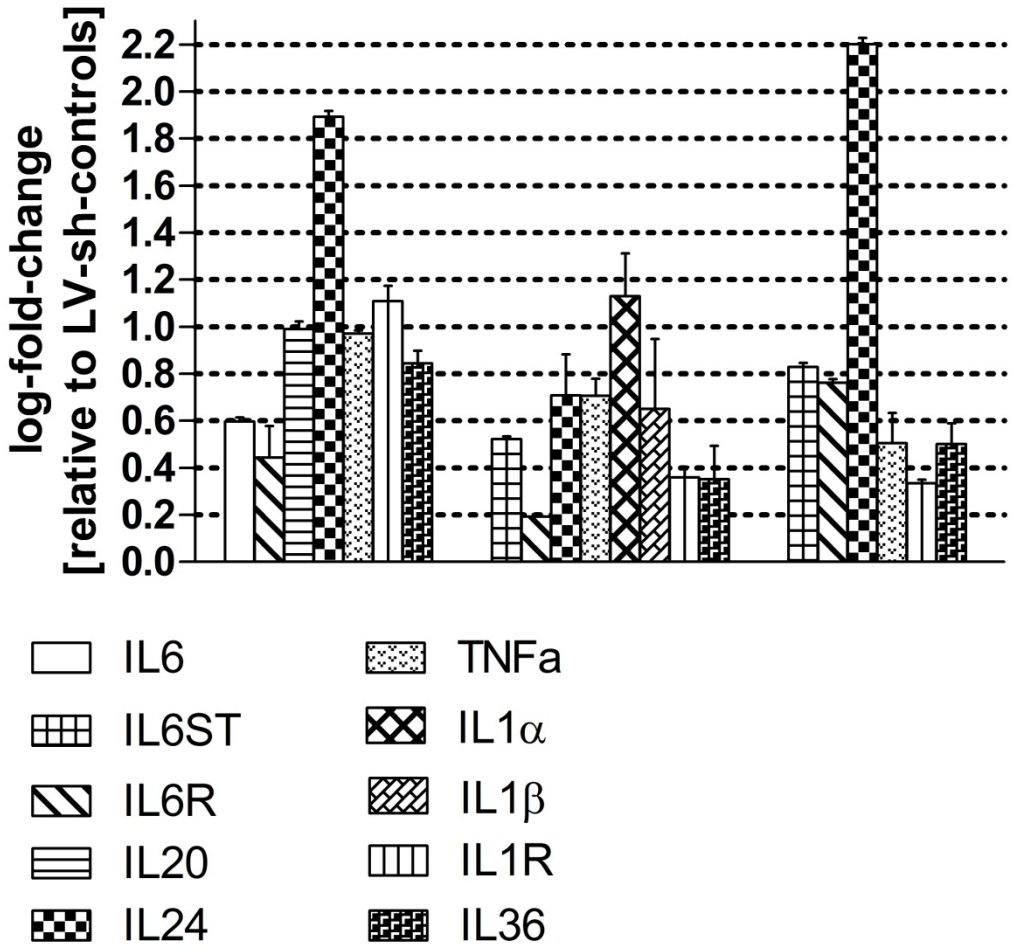

(B) Overview of Most Strongly Altered Genes in Insulin Receptor Knockdown Cells

	Genes	Mean Fold Change ± SEM	Genes	Mean Fold Change ± SEM	Genes	Mean Fold Change ± SEM
	Cell line H292		*Cell line H226*		*Cell line H460*	
1. Cytokines						
A: Interleukins						
Interleukin 10 family	IL20	10 ± 0,76				
	IL24	78,03 ± 4,53	IL24	5,10 ± 2,48	IL24	160,32 ± 10,6
Interleukin 1 family	IL37	8,27 ± 0,5	IL1α	13,64 ± 6,42	IL18	6,60 ± 0,25
	IL36γ	6,99 ± 0,79	IL1β	4,21 ± 4,19	IL36β	3,16 ± 0,65
	IL1R2	12,87 ± 2,25	IL1RAP	13,03 ± 0,73	IL1RAP	6,42 ± 0,42
B: Chemokines						
CXCL Family	CXCL2	10,11 ± 0,55	CXCL2	7,19 ± 0,49	CXCL2	3,33 ± 0,49
	CXCL3	5,12 ± 0,32	CXCL3	42,16 ± 6,15	CXCL3	13,68 ± 3,2
			CXCL5	5,71 ± 0,36	CXCL5	7,01 ± 0,21
C: TNF	TNF	9,4 ± 0,26	TNF	5,08 ± 0,86	TNF	3,19 ± 0,78
2. Insulin Family	IR	0,1 ± 0,004	IR	0,21 ± 0,01	IR	0,34 ± 0,02
	INSL-3	2,6 ± 0,08	INSL-3	2,26 ± 0,12	INSL-3	4,04 ± 0,35
	INSIG-1	3,2 ± 0,08	INSIG-1	2,35 ± 0,3	INSL5	8,49 ± 2,13
	INSIG-2	2,3 ± 0,04	INSIG-2	1,59 ± 0,09	INSIG-1	3,58 ± 0,34
					INSIG-2	2,80 ± 0,17
3. IGF-1 Family	IGFL-1	14,1 ± 0,15	IGFLR1	0,43 ± 0,01	IGFLR1	0,21 ± 0,02
	IGFLR1	0,4 ± 0,006	IGFL3	6,22 ± 1,05	IGFL3	4,13 ± 0,9
	IGFL3	4,1 ± 0,29			IGFBP1	13,15 ± 0,99
					IGFBP3	3,27 ± 0,17
					IGF2	2,09 ± 0,13
					IGF2R	2,20 ± 0,03

Figure 31: Altered Gene Expression in H292, H226 and H460 IR KD Cells.

Microarray-based gene expression analysis revealed genes which were most strongly up-, or downregulated in IR KD cells. The bar graph (A) presents changed expression levels of cytokines known to be involved in programmed cell death. Overview of most strongly altered genes in IR KD cells are presented in table (B) as functional clusters. For details, see Methods 2.7. Mean fold changes ± SEM are given compared to sh control levels (four samples of each cell line).

5 Induction of Apoptosis

5.1 Effects of IL6, IL20, IL24 and TNF on Caspases Activity

In order to further verify a possible correlation between IR KD and programmed cell death, NSCLC cells were treated with cytokines that were most strongly induced in the microarray chip *and* known to be associated to apoptosis: IL6, IL20, IL24 and TNFα (Fig. 31).
After cytokine-exposure, caspase 3/7 assays were performed to examine activation levels of caspases indicating induction of apoptosis (Fig. 32). A significant activation of caspases was caused by TNF in all three cell lines (H292: 237 %, H226: 130 % and H460: 231 %). IL6 activated caspases 3/7 significantly in H292 and H226 cells to 123 % and 114 %, respectively. The same tendency was found after IL24 exposure (H292: 127 %, H226: 116 %). Besides, in H292 cells, IL20 caused an increase in caspase activity to 140 %.

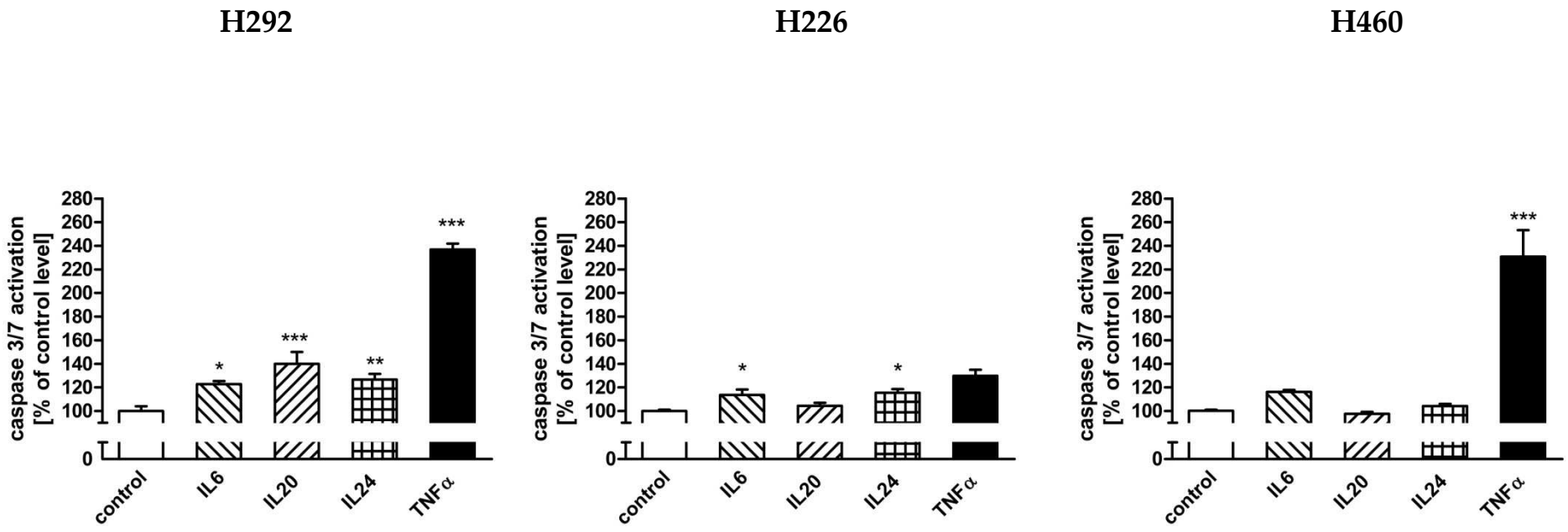

Figure 32: Effects of Apoptosis-Inducing Cytokines on Caspase 3/7 Activity in H292, H226 and H460 Cells.

Cells were exposed to 100 nM of the test compounds (IL6, IL20, IL24 or TNFα) for 48 h. Subsequently, Caspase-Glo® assay was measured. The bar graphs show means + SEM of N= 4 experiments. Significance of differences: ** $p < 0.01$, *** $p < 0.001$ vs. control

V Discussion

As described in the introduction, there is a lack of clarity about insulin action and its signaling in tumor-promoting processes at present. Therefore, it is of clinical relevance to illuminate the role of insulin and the IR in malignant cells in more detail.
Steadily increasing rates of T2DM patients and detected correlations between hyperinsulinemia and neoplasms underline the necessity of these concerns.

In light of the recently approved inhaled insulin formulation Afrezza® in the United States of America, effects of insulin, particularly in comparison to IGF-1, have to be analyzed in cells derived from the respiratory system. Although there are warnings & precautions about the use of Afrezza® for patients with active lung cancer, there is *no contraindication* that clearly prohibits an inhaled insulin therapy for patients with malignancies and people with an increased risk for tumor development (MannKind Corporation, 2014).
Presence of a few mutated cells (precancerous conditions) may occur in any organism. However, those cells are combated by the immune system under normal conditions. It remains unclear whether steadily increased insulin levels – as present in the lungs during a therapy with inhaled insulin – might favor the progression of mutated cells. This could lead to the manifestation of a carcinoma.
In order to evaluate insulin action and involvement of the IR in mutated cells, the present study was conducted with *malignant human lung cancer cells*.
NSCLC includes different epithelial cancer types that account for the vast majority of lung cancers (see Introduction 1.2.2) (American Cancer Society, 2015). To get a differentiated and more precise overview of the impacts of insulin and its receptor, three NSCLC cell lines, each representing a different subtype, were analyzed.

1 Effects of Insulin and IGF-1 in NSCLC Tumor Cell Promotion

As typical for cancer cells, each NSCLC subtype revealed a cell-specific basic configuration including differences in their basal proliferation levels, activity of mitogenic signaling pathways and IR, IR splicing variants and IGF-1R expression levels.
Notably, different IR-A/IR-B and IR/IGF-1R ratios were also found in H292, H226 and H460 cells. Likewise, in literature it has been described that amounts of IR and IGF-1R do not correlate with each other in NSCLC cells (Kim et al., 2012).
Based on these findings it could be expected that insulin and IGF-1 might have independent roles in malignancies and are implicated to a different extent in H292, H226 and H460 cell tumor promotion.

1.1 Concentrations of Insulin in the Lungs after Inhaled Administration

The observed effects in the presented experiments were achieved by insulin concentrations in the nanomolar range. These concentrations are also locally present in the lungs after inhaling insulin. For the currently approved Afrezza® the single-dose of insulin ranges from 4 units (~ 0.35 mg/ 60 nM insulin) to 24 units (~ 2.10 mg/ 360 nM insulin) (FDA, 2014). 39 % of inhaled insulin reach the epithelial lining fluid of the lower respiratory tract (product information Afrezza: http://www.accessdata.fda.gov/drugsatfda_docs/label/2014/022472lbl.pdf) which displays a volume between 20-40 ml (Rennard et al., 1986). Consequently, *local* insulin peak concentrations are in a range between *585 nM and 7 µM*.
Insulin is inhaled several times per day and its degradation proceeds slowly due to low amounts of insulin-degradating enzymes (IDE) in the lungs (Kuo et al., 1993). Therefore, constantly increased insulin concentrations remain in the lower respiratory system. It follows that an experimental setting with nanomolar insulin concentrations imitates a therapeutic situation in human bronchial epithelial cells.

1.2 Tumor Cell Proliferation

1.2.1 Insulin Supports Proliferation Particularly in Slow-Proliferating Cell Lines

Famous hallmarks of tumorigenesis are accumulation of various mutations in genes that control cell proliferation and autocrine secretion of growth hormones. As a result, cancer cells divide more rapidly and become less dependent on external growth stimuli (see Introduction 1.2.1).

Cell line H292 belongs to the NSCLC subtype *mucoepidermoid carcinoma (MEC)*. MEC is a heterogeneous group of malignant tumors that can be divided into low, high and intermediate grade neoplasms in correspondence to the respective biological potential (Goode et al., 1998) ranging from slow-proliferating to highly aggressive and metastatic (Nance et al., 2008). [^{3}H]-thymidine incorporation assays indicated that H292 cells reveal the slowest basal proliferation rate within the three cell lines tested. However, in line with previous studies (Mayer et al., 2012), insulin markedly induced the cell proliferation rate. Exposed to even *low nanomolar* concentrations of either insulin or IGF-1 (1 nM onwards), H292 cells responded with enhanced [^{3}H]-thymidine incorporation rates. Thus, regarding their proliferative features, H292 cells appear to exhibit a low malignant tumor behavior marked by dependence on external growth stimuli.

The NSCLC subtype *squamous cell carcinoma (SCC)* is mostly associated with smoking and it displays a high malignant behavior (Hirano et al., 1994) due to its potential to spread even in an early stage (Steward & Kleihues, 2003). However, manifestation of an apparent tumor takes about three to four years. This indicates that SCC tend to grow more slowly compared to other tumor types (Steward & Kleihues, 2003). In the SCC cell line H226, the [^{3}H]-thymidine incorporation rate under basal conditions was 2.5-fold higher than in H292 cells. Accordingly, in H226 cells, ERK1/2 and Akt were active even under starving conditions which was not the case in H292 cells. External supplied IGF-1 did not further stimulate cell proliferation. This reveals an IGF-1-independent cell proliferation behavior in H226 cells. However, insulin in *higher nanomolar* concentrations (100 nM onwards) led to significantly increased rates of [^{3}H]-thymidine incorporation.

H460 cells belong to *large cell lung carcinoma (LCLC)*. It is well studied that LCLC tend to grow rapidly and reveal an aggressive malignant tumor cell behavior (Eldridge, 2015). Results from [^{3}H]-thymidine incorporation analysis showed that H460 cells had the highest basal proliferation level within the cell lines studied, i.e. ~ 10-fold and ~ 5-fold higher than H292 and H226 cells, respectively. In accordance, ERK1/2 and Akt were basal phosphorylated in H460 cells. The external growth stimulus insulin did not influence [^{3}H]-thymidine incorporation rates. Despite its fast autonomous cell growth, IGF-1 in concentrations from 3 nM onwards continued to increased the [^{3}H]-thymidine incorporation rate.

In summary, each cell line revealed biological behavior patterns that fit to commonly described characteristics of tumor cells (Hanahan et al., 2000). It became evident that H292, H226 and H460 cells exhibit a characteristic basal proliferation rate whose intensity corresponds to presence or absence of basal Akt activity. Moreover, a coherency between autonomous cell growth and magnitude of dependence on external applied IGF-1 and insulin could be observed.

Although human insulin has not been in the focus of cancer research yet, it should not be underestimated regarding its mitogenic potential in NSCLC cells. [^{3}H]-thymidine incorporation assays clearly evidenced that the anabolic hormone empowers the proliferation rate in two of the three NSCLC cell lines, namely the comparably slow-proliferating H292 and H226 cells. Albeit IGF-1 is commonly described to possess a greater mitogenic activity than insulin (Siddle et al., 2001), particularly in H226 cells, insulin but not IGF-1 had strong effects on the cell proliferation rate.

Now that inhaled insulin is available, it appears to be relevant to further study impacts of insulin on proliferation in normal HBE cells, pre-malignant HBE cells and other lung cancer cells. Previous studies already reported that micromolar insulin concentrations enhanced proliferation of normal HBE cells (Mayer et al., 2012), smooth muscle cells and fibroblasts (Warnken et al., 2010).

Against the background of steadily increasing rates of T2DM patients, it also becomes necessary to analyze insulin action in cells of other tissues. For instance, it has already been

shown that insulin increases cell proliferation significantly in MCF-7 breast cancer cells (Chappell et al., 2001).

Further studies have to be conducted in order to expand knowledge about insulin and to draw general conclusions on insulin as mitogenic hormone.

1.2.2 Insulin- and IGF-1-Induced Cell Proliferation Correlates to Receptor Expression

It was to clarify whether insulin and IGF-1 receptor expression levels influence insulin- and IGF-1-mediated proliferative effects and thus serve as markers in cancer cell characterization. Within the cell lines tested, H292 expressed both receptors most strongly and in accordance, cell proliferation was enhanced most significantly by insulin and IGF-1.

In H226 cells, IR was expressed to a slightly smaller extent than in H292 cells although its expression was still clearly detectable. [^{3}H]-thymidine incorporation was also induced significantly by insulin whereas the effect size was reduced compared to H292 cells. Concomitant with low IGF-1R expression levels, even higher concentrations (10 nM) of IGF-1 failed to increase [^{3}H]-thymidine incorporation in H226 cells.

IR were expressed to a very low amount in H460 cells, markedly below H292 and H226 expression levels. Probably as a consequence thereof, even supraphysiological insulin concentrations (1 μM) did not lead to any influences on [^{3}H]-thymidine incorporation. In accordance, strong IGF-1R expression was paralleled by IGF-1-induced cell proliferation in H460 cells.

These findings clearly reveal dependence of effective insulin-/IGF-1-induced cell proliferation on IR/IGF-1R expression levels in NSCLC cells. Similar correlations were observed in other tissues, such as in MCF-7 breast cancer cells (Milazzo et al., 1992). In this cell line, insulin markedly increased cell proliferation (see chapter 1.2.1) and the IR expression level was 6-fold higher than in its non-malignant counterparts.

In order to specify the above-mentioned hypothesis, analysis of possible correlations between expression of *IR splicing isoforms* and the magnitude of insulin-/IGF-1-triggered proliferation was analyzed.

Being predominantly expressed in tumor tissues, IR-A is widely known to mediate *mitogenic* insulin effects. This has concretely been proved for breast and prostate cancer cells (Singh et

al., 2014). In contrast, IR-B is described to trigger *metabolic* insulin effects. Its expression is predominant in (non-malignant) insulin-responsive tissues, mostly liver, adipose tissue and skeletal muscles (Singh et al., 2014). Consequently, it was to be expected that cell proliferation of IR-A-expressing NSCLC cell lines is more sensitive towards insulin stimulation. Interestingly, proliferation of the two IR-A-expressing cell lines H292 and H460 appeared to be strongly influenced by IGF-1. As the IR binds IGF-1 with a 50- to 100-fold lower affinity than insulin (0.1 nM) (Varewijck & Janssen, 2012), it has to be investigated whether IGF-1 could even influence cell proliferation via IR-A-binding. In H226 cells, IR-B was the predominant IR splicing isoform, whereas IR-A was hardly detectable. Notably, insulin clearly increased the [^{3}H]-thymidine incorporation rate in H226 cells.

From these findings two hypothesis can be proposed. First, it could be assumed that insulin might also trigger *mitogenic* effects via *IR-B signaling* in absence of IR-A. This would contradict the general characterization of mitogenic IR-A and metabolic IR-B action.

Second, there is evidence that cancer cells probably also trigger *mitogenic IGF-1 effects* via *IR-A* activation. Since the binding affinity of IGF-1 to homodimeric IR is comparably low (see above), binding to heterodimeric IR/IGF-1R could be the underlying mechanism. This hypothesis is supported by Belfiore et al. (2009). It is stated that IR-A overexpression is accompanied by an increased formation of IR-A/IGF-1R HR (HR-A) which leads to increased IGF-1-binding sites. In addition, HR-A were shown to bind IGF-1 with an equal affinity like IGF-1R (0.1 nM) (Pandini et al., 2002).

Indeed, cell lines H292 and H460 expressed IR-A and HR to a proper amount. It can therefore be hypothized that in both cell lines, increased [^{3}H]-thymidine incorporation rates after IGF-1 exposure might be caused by HR-A activation.

1.3 The Role of Insulin in Mitogenic Signaling

The first step of insulin-triggered signaling constitutes autophosphorylation of the IR upon ligand-binding leading to an activation of downstream effector pathways.

Since insulin in higher nanomolar concentrations also binds IGF-1R (K_D ~ 200 nM) (Kurtzhals et al., 2000), it appeared necessary to analyze to which extent *total IR and IGF-1R activation* is triggered by insulin.

Insulin led to a concentration-dependent phosphorylation of IR/IGF-1R in H292, H226 and H460 cells although with differences in the activation potency. Even 10 nM caused a significant receptor autophosphorylation in H292 and H226 cells. In this concentration insulin mainly binds IR indicating that the observed protein signal derived from *IR activation*. IR activation by low insulin concentrations is supported by presence of high IR levels in H292 and H226 cells.

Clear visible receptor autophosphorylation by 100 nM insulin was observed in the three cell lines tested and can be attributed to IR *and* IGF-1R activation (see above) (Kurtzhals et al., 2000). Analysis of pIR/pIGF-1R levels in IR KD cells underline an activation of IGF-1R by insulin. Besides, as H460 cells only weakly express IR, it appears plausible that the phospho-signal caused by 100 nM insulin mainly derived from IGF-1R activation.

In contrast to H226 and H460 cells, H292 exhibited basal phosphorylated IR/IGF-1R. While there was no correlation between basic receptor expression and receptor phosphorylation levels as described in literature (Kim et al., 2012), negative correlations between pIR/pIGF-1R and the downstream effector Akt could be observed. This phenomenon has also been described previously (Chandarlapaty et al., 2011). Consistent with this reported coordinated feedback, in H292 cells, basal presence of pIR/pIGF-1R was accompanied by absence of basal Akt phosphorylation. In H226 and H460 cells, the opposite basal phosphorylation levels could be detected. These findings fit to the phenomenon of constitutive feedback inhibition of upstream signaling pathways by Akt and display a possible mechanistic feature of NSCLC cells in order to steer mitogenic signaling.

Western blot analysis indicated that Akt was phosphorylated in a precise concentration-dependent manner in the cell lines tested by 1 nM- 100 nM insulin. Notably, 100 nM insulin led to a comparable Akt phosphorylation like 10 nM IGF-1. This indicates that a concentration of insulin which could be achieved in the lungs after inhalation induces mitogenic Akt signaling with the same potency as supraphysiological levels of IGF-1.

Interestingly, in H292 and H460 cells, even 100 pM insulin caused Akt phosphorylation, whereas 100 pM insulin did not lead to IR phosphorylation. It is known that cancer cells exploit mitogenic signaling transduction more efficiently than non-malignant cells; for instance, enhanced expression levels of downstream docking proteins can trigger an

amplification of following signaling pathways. In this context, increased levels of IRS could play a crucial role in Akt signaling amplification - as already observed in MCF-7 breast cancer cells (Surmacz, 1995).

Taken these findings together, the Akt signaling pathway turned out to be highly sensitive towards insulin stimulation in H292, H226 and H460 cells. As Akt triggers numerous cancer-supporting processes, these results further underline that insulin represents a potential harmful mediator in cancer cells.

All cells exhibited presence of basal phosphorylated ERK1/2 proteins which demonstrates a certain independence of MAPK activation from external stimuli (Hanahan et al., 2000). In fact, in the NSCLC cell lines studied, physiological concentrations of insulin and IGF-1 - that certainly activate the cognate RTK - failed to increase MAPK phosphorylation.
In cell line H460, even higher nanomolar concentrations of insulin and IGF-1 did not (further) phosphorylate ERK1/2 proteins. In H226 cells, 100 nM insulin had no influence on MAPK activation, whereas 10 nM IGF-1 increased phospho p44/42 proteins.
Consequently, insulin and IGF-1 appear to play a minor role in mitogenic MAPK signaling in H226 and H460 cells. These findings are in good agreement with previous studies in MCF-7 cells (Dufourny et al., 1997). Vice versa, Dufourny et al. reported that activation of MAPK signaling is not required for insulin and IGF-1 action on growth promotion. This also fits to observations in H226 and H460 cells. No coherencies between insulin and IGF-1 effects on MAPK phosphorylation and on [^{3}H]-thymidine incorporation could be detected. Contrary to IGF-1, insulin increased [^{3}H]-thymidine incorporation but failed to enhance MAPK phosphorylation in H226 cells. Vice versa, in H460 cells, only IGF-1 increased the [^{3}H]-thymidine incorporation rate. However, IGF-1 failed to enhance MAPK phosphorylation.
In accordance to the common scientific consensus, MAPK is considered to be one main downstream effector of the IR and the IGF-1R. Therefore, insulin and IGF-1 are widely known to induce phosphorylation of mitogenic ERK1/2 signaling (Siddle et al., 2001). However, this contradicts the results from MCF-7, H226 and H460 cells. An insulin- and IGF-1-induced MAPK activation was only detected in cell line H292. Accordingly, in H292 cells, insulin and IGF-1 induced the [^{3}H]-thymidine incorporation rate clearly.

Those conflicting data of the roles of insulin and IGF-1 in MAPK signaling are most likely caused by the complexity of insulin and IGF-1 signaling in malignant cells (Taniguchi et al., 2006) and by an uncoupling of mitogenic downstream effectors from upstream regulation. It follows that MAPK activation in cancer cells is a cell-specific matter which can hardly be generalized.

1.4 Insulin and IGF-1 Action Placed in a Broader Context of Tumor Promotion in NSCLC Cells

IGF-1 and insulin only represent two out of numerous growth stimuli. Currently, epidermal growth factors (EGF) (Hendler & O., 2001), fibroblast growth factors (FGF) (Marek et al., 2009), cyclooxygenases (COX) (Krysan et al., 2005; Sharma et al., 2010) and lysine specific demethylase 1 (LSD-1) (Lv et al., 2012) are counted among the most prominent peptides that empower tumor progression next to IGF-1 in NSCLC cells. However, entire knowledge about their signal transduction including feedback mechanisms is still largely uncovered. Hence, cancer cells make use of a complex molecular machinery which has to be further investigated.

From this point of view, it is obvious that measurement of proliferation and detection of Akt and ERK signaling do not reflect the whole complex interaction of cancer-promotive processes in tumor cells. However, important insights into insulin action could be obtained in this study which contributes to a better understanding of its role in different NSCLC cell lines. Contrary as assumed in literature, findings have shown that insulin - even in physiological concentrations - revealed precise mitogenic features in two cell lines tested (H292 and H226 cells). Besides, due to its large impact on Akt phosphorylation in the three cell lines, insulin might also trigger cancer-supporting features in (apparently) high autonomous malignant cells.

2 Effects of TGF-β in NSCLC Tumor Cell Promotion

The transforming growth factor facilitates angiogenesis and metastasis due to initiation of cell remodelling processes (see Introduction 3.1.1.).
However, effects on tumor promotion in general, including cancer cell proliferation and its interaction with other growth factors are controversially discussed in literature and have therefore been researched in more detail in NSCLC cells in this study.

2.1 TGF- β and Insulin Reveal Opposite Impacts on Proliferation

[^{3}H]-thymidine incorporation assays revealed that TGF-β appears as opponent of insulin in cell proliferation in H292 and H226 cells.
As described above (see chapter 1.2.1), 100 nM insulin significantly increased [^{3}H]-thymidine incorporation rates in H292 and H226 cells. Exposed to 1 ng/ml TGF-β, a concentration in the physiological range (Wakefield et al., 1995), cell proliferation was decreased significantly below control levels in these cells.
This effect was also described in a previous study with H292 cells that was conducted with 10-fold higher concentrations of TGF-β (10 ng/ml) and insulin (1 μM) (Mayer et al., 2012). Notably, the present study indicates that proliferation-inhibiting effects of 1 ng/ml TGF-β did not markedly differ from effects of 10 ng/ml as shown by Mayer et al.
Being exposed to TGF-β and insulin simultaneously, insulin weakened TGF-β impacts on [^{3}H]-thymidine incorporation rates; an elevation to approx. control levels was found in H292 and H226 cells. Thus, anti-proliferative TGF-β action was cancelled by insulin. This apparent functional antagonism could indicate that insulin and TGF-β share a downstream target which is not described in literature yet.

2.2 Basal CDH2 and ET-1 Expression Levels Do Not Correlate in the NSCLC Cells Tested

ET-1 and CDH2 are two prominent EMT-supporting peptides (Rosanò et al., 2005). Particularly, ET-1 is known to promote the growth of epithelial cancer cells by facilitating angiogenesis and cell proliferation (Grant et al., 2003). CDH2 displays comparable features; CDH2-expressing NSCLC are associated with an aggressive tumor behavior accompanied by poor prognosis for patients (Hui et al., 2013).

Initially, analysis of basic CDH2 and ET-1 profiles was required to study effects of TGF-β on their expression rates (see chapter 2.3). H292, H226 and H460 cells turned out to be ET-1- and CDH2-expressing cells. These characteristics are not specific for the average of epithelial cancer cells (Nakashima et al., 2003; Nieman et al., 1999). In consequence, all cell lines studied rather display aggressive tumor behaviors, viz. likely to spread into other tissues.

Constitutive mRNA expression levels of both peptides varied significantly within H292, H226 and H460 cells. H226 cells expressed CDH2 most strongly within the cell lines. In contrast, ET-1 was only rarely expressed. Since previous studies demonstrated a correlation between CDH2 expression and invasion and motility (Nieman et al., 1999), cell line H226 fits well in the group of SCC cells, commonly described to be highly invasive (Steward & Kleihues, 2003).

The cancer type LCLC is associated with an intensely malignant behavior including a rapid onset of metastasis (see chapter 1.2.1). Although H460 cells showed the lowest CDH2 mRNA levels, ET-1 mRNA was most strongly expressed. Thus, CDH2 appears to play a minor role, whereas other EMT-facilitators, i.e. ET-1, could steer morphological remodelling processes.

H292 cells revealed marked presence of both, CDH2 and ET-1 mRNA, albeit their expression rates were below the respective highest CDH2-, or ET-1-expressing cell line. A rather metastatic behavior due to basal expression of EMT markers can thus be assumed for the MEC cell line H292.

In ovarian cancers, it has been observed that ET-1 upregulates CDH2 expression (Rosanò et al., 2006). This demonstrates a correlation between both EMT markers. Such correlations

could not be detected in the NSCLC cell lines; ET-1 and CDH2 levels appeared to be independent from each other.

Those conflicting observations between ovarian and lung cancer cells in general and NSCLC cell lines in particular underline that each tumor displays an individual cell architecture. Since EMT is triggered by numerous peptides, it seems difficult to draw comprehensive conclusions on EMT based on CDH2 and ET-1 expression exclusively.

However, the presented results give evidence of the *general ability* of NSCLC cells to undergo invasion and metastasis. This underlines their malignant characteristics.

2.3 TGF-β Induces CDH2 and ET-1 Expression to a Varying Extent in H292, H226 and H460 cells

In H292 and H226 cells, TGF-β significantly increased ET-1 and CDH2 expression levels. In H460 cells, TGF-β only induced CDH2 expression, whereas ET-1 expression remained uneffected. This might indicate that the canonical EMT pathway via TGF-β-triggered smad signaling transduction plays a minor role in H460 cells, while H292 and H226 cells are strongly influenced by TGF-β.

Next to TGF-β, IGF-2 has turned out to be crucial for EMT induction (Kalluri & Neilson, 2003; Larue & Bellacosa, 2005). Since H460 cells were more sensitive towards IGF-1R than IR activation (see chapter 1.2), an EMT induction via IGF-2-mediated IGF-1R pathway could be plausible. Accordingly, microarray data revealed a 40 % increased basal IGF-2R mRNA level of H460 cells compared to H292 and H226 cells. Although direct implications of IGF-2R in EMT have not been analyzed yet, this detail might further explain involvement of the IGF-2 network in EMT.

2.4 Controversial Roles of IGF-1 and Insulin in CDH2 and ET-1 Expression

Remarkably, as observed in [^{3}H]-thymidine incorporation studies, insulin had the opposite effect of TGF-β on ET-1 and CDH2 expression in H292 cells. Although insulin failed to

influence ET-1 and CDH2 mRNA levels in a significant way, it markedly reduced TGF-β effects. IGF-1 exhibited the same behavior pattern. This underlines that insulin and IGF-1 act in a similar manner in H292 cells as already observed in [^{3}H]-thymidine incorporation analysis.

A diminishing effect of insulin (1- 5 μM) on TGF-β (10 ng/ml)-induced CDH2 mRNA expression was also described in H292 cells before. Moreover, similar findings of a further EMT marker, namely fibronectin 1 (FN1), were found (Mayer et al., 2012).

A functional antagonism between TGF-β and insulin has thus been shown in proliferation and in effects on EMT marker expression in cell line H292. Apart from these findings, it has to be studied which clinical relevance arises from this finding. It further remains unclear whether the functional antagonism can be detected in other MEC cells. Performance of an extended research, e.g. by analyzing other EMT markers and cell lines, could illuminate whether insulin is commonly capable of antagonizing TGF-β effects in MEC cells. In contrast to H292 findings, *synergistic effects* between insulin/IGF-1 and TGF-β on ET-1 mRNA expression were detected in H460 cells. Exclusively in the combinations, the expression rate was significantly increased. TGF-β failed to increase and insulin/IGF-1 only slightly increased ET-1 mRNA levels. Synergistic interactions between IGF-1 and TGF-β regarding EMT induction were also described in MCF-7 breast cancer cells (Walsh & Damjanovski, 2011).

However, common principles of ET-1 and CDH2 mRNA regulation by insulin, IGF-1 and TGF-β in H226 and H460 cells could not be detected. In accordance, no consistent data can be found in literature; previous studies confirm that different cell lines reveal various mechanisms in steering EMT. These include action of TGF-β, IGF-1, ERK and Akt signaling transduction (Xie et al., 2004).

3 Lipofection Does not Serve as Appropriate Method for Insulin Receptor Knockdown Experiments

Transduction of siRNAs was performed as lipofection with the cationic liposome formulation Lipofectamine®. This method allowed a successful KD of IR and IGF-1R. However, an impaired action of insulin and IGF-1 on [^{3}H]-thymidine incorporation became evident subsequent to treatment with Lipofectamine®; no increase in proliferation followed after insulin and IGF-1 exposure.

An apparent non-responsiveness towards insulin stimulation in Lipofectamine®-treated cells was also described in another study (Pramfalk et al., 2004) which furthermore provided reasons for this observed phenomenon. Pramfalk et al. reported an interaction between the cationic lipid reagent and the IR; after *activating* the kinase activity, Lipofectamine® led to a downregulation of the receptor. In consequence, insulin had significantly reduced effects on glucose-uptake in Lipofectamine®-treated adipocytes and no effects at all in Lipofectamine®-treated rat myotubes and neuroblastoma cells compared to controls. These findings are in good agreement with [^{3}H]-thymidine incorporation assays in H292 cells presented in this study (see above). It therefore can be suggested that the interaction established by Pramfalk et al. also led to a failed insulin stimulation in Lipofectamine®-treated H292 cells.

Also IGF-1 had no influence on the [^{3}H]-thymidine incorporation rate in Lipofectamine®-treated H292 cells. Since the IGF-1R reveals a large homology to the IR, the same mechanism of Lipofectamine®-triggered activation and subsequent receptor downregulation can be assumed.

In consequence, lipofection did not represent a suitable method for IR and IGF-1R KD experiments. Alternatively, receptor KD with lentiviral shRNA was established in NSCLC H292, H226 and H460 cells. By this stable transfection, IR and IGF-1R were downregulated successfully. As opposed to lipofection, no conspicuities and disturbing factors could be observed in following KD experiments.

4 The Role of the Insulin Receptor and the IGF-1 Receptor in NSCLC Tumor Cell Promotion

4.1 Loss of Insulin Receptors Causes Apoptosis in NSCLC Cell Lines

4.1.1 NSCLC Cells Die upon Insulin Receptor Knockdown

Reduced IR expression levels strongly affected survival of the three cell lines. The observed time-dependent cell death was found after IR KD exclusively, while IGF-1R KD only caused *stagnation* of proliferation. These findings could indicate that reduced IR expression levels impair the cellular metabolism leading to necrosis or to initiation of programmed cell death. Importantly, the latter would represent a new finding for NSCLC cells and could have an important impact on illumination of the role of IR in cancer cell survival.

4.1.2 Increased Caspase Activity after Insulin Receptor Knockdown

Luminescence-based caspase 3/7 assay was performed to proof whether there is a coherency between IR signaling and apoptosis. Notably, IR KD significantly upregulated caspases activity resulting in apoptosis in all cell lines tested.

Numerous studies report an involvement of the IGF-1R in apoptosis prevention, e.g. in melanoma, glioblastoma, multiple myeloma and colon cancer cell lines (Jernberg-Wiklund & Nilsson, 2007; Resnicoff et al., 1995). Hence, it has generally been suggested that the IGF-1R respresents a central protector of programmed cell death after activation by IGF-1 or IGF-2 (Yu & Rohan, 2000). This was also observed in NSCLC cell lines (Hurbin et al., 2002). In contrast, the IR is not commonly described to be capable of mediating anti-apoptotic effects. Only in mouse fibroblasts lacking functional IGF-1R, it has been detected that reduced IR expression levels led to apoptosis (Prisco et al., 1999). However, clear anti-apoptotic mechanisms of IR signaling or vice versa, apoptosis-inducing mechanisms caused by absence of IR remain unclear.

In search of general mechanisms that lead to evasion of apoptosis in cancer cells, different signaling downstream targets have been analyzed in numerous studies. Notably, the

docking protein IRS-1 turned out to be a key mediator in anti-apoptotic signal transduction (Peruzzi et al., 1999). Frequently increased expression levels of IRS-1 are found in many cancer cells. IRS-1 is considered to amplificate IGF-1R signaling resulting in an enhanced apoptosis prevention (Prisco et al., 1999; Reuveni et al., 2013). Remarkably, it is not reported that IRS-1 also triggers apoptosis prevention upon upstream IR phosphorylation. This however would be a concern of interest due to the findings of this study.

Besides, a functional antagonism between IRS-1 and TGF-β on programmed cell death has been reported for human hepatocellular carcinoma cells (HCC) (Tanaka & Wands, 1996). Tanaka and Wands observed that TGF-β-induced apoptosis was annulled by either insulin or IGF-1. These HCC findings point out that interactions of TGF-β and insulin occur on various levels (see chapter 2.1) and give evidence of an involvement of IR signaling in cell survival.

Next to IRS-1 phosphorylation, the Akt signaling cascade has been proved to be a main pathway for IGF-1R-triggered apoptosis prevention (Fernandez, 2004). In contrast, MAPK failed to mediate anti-apoptotic effects (Kulik et al., 1997). Since IR signaling had no apparent impact on the p44/42 phosphorylation in H226 and H460 cells, the MAPK pathway can also be excluded as mechanistic link between IR KD and caspase activation in NSCLC cells. As shown before (see chapter 1.3), Akt signaling highly depended on insulin exposure and consequently could also play a role in programmed cell death in the NSCLC cell lines. KD data of H460 cells revealed similar (reduced) phosphorylation levels of Akt in *IR KD cells* and *IGF-1R KD cells* (see chapter 4.5.2). Consequently, a decreased Akt signaling most likely leads to a decreased cell proliferation which results in a reduced cell number compared to controls. But however, general impacts on *caspase activation* which was only found in IR KD cells cannot be confirmed.

Taken together, there were no apparent hints in literature and Akt/ MAPK pathway analysis of this study explaining the essential role of the IR in cell survival.

4.1.3 Enhanced Expression of Apoptosis-Inducing Cytokines as possible Mechanistic Link between Insulin Receptor Knockdown and Apoptosis

In order to find a possible link between IR KD and caspase activation in NSCLC cells, genome-wide gene profiling was performed in IR KD cells and LV-sh control cells. Remarkably, in all cell lines tested, the most strongly upregulated gene cluster comprised the group of cytokines. Further analysis revealed that those elevated cytokines have apoptosis-inducing features.

TNFα was one of the most strongly induced cytokines in all NSCLC cells tested. The latter is commonly known to be among the most potent cell death-inducing cytokines (Chen & Goeddel, 2002; Rath & Aggarwal, 1999) and its pro-apoptotic pathways are interesting targets for cancer therapy (Ghobrial et al., 2005).

Indeed, luminescence-based caspase 3/7 assay performed in TNFα-treated cells underlined that this cytokine significantly induced caspase activity in H292, H226 and H460 cells.

In literature, TNFα is described to interfere with the IR; acting as functional antagonist, it blocks insulin action (Hotamisligil et al., 1994). Others report that TNFα promotes inhibitory serine/threonin phosphorylation of IRS-1 and IRS-2 which impedes association between the docking proteins to IR and IGF-1R. This results in IR and IGF-1R signaling disruption (Rui et al., 2001). Thus, IRS-1-mediated anti-apoptotic signal transduction can be suppressed by TNFα. As IR and TNFα appear to have counteracting functions, it becomes possible that the IR suppresses TNFα expression which can be concluded from microarray data. In accordance to this hypothesis, basic IR expression levels (see chapter 1.2.2) were proportional to the extent of increased TNFα expression levels after IR KD within the cell lines. Since there are no hints in literature, it should be of interest to detect the underlying mechansims to proof this phenomenon.

Notably, IL24 was the most strongly induced gene in H292 and H460 IR KD cells and it was also markedly induced in H226 IR KD cells. The complex functions of IL24 are not well known yet, albeit precise anti-tumoral features, e.g. induction of apoptosis, have been identified as its key characteristics (Dash et al., 2014).

In H292 and H226 cells, IL24 significantly activated caspase activity which confirms its pro-apoptotic features. Thus, induced gene expression of caspases-activating cytokines after IR

KD - as proved for TNFα and IL24 in this study - is most probably the underlying mechanism for programmed cell death.

Only in H292 cells, IL20, a further apoptosis-inducing interleukin (Donnelly et al., 2004), significantly increased caspase activity. In accordance, IL20 was strongly upregulated in H292 IR KD cells.

The role of IL6 in apoptosis is controversially discussed in literature. Although pro-apoptotic features are reported in lung fibroblasts (Moodley et al., 2003), the general characteristics of IL6 are considered to be anti-apoptotic and thus pro-tumorigenetic (Grivennikov & Karin, 2008; Hirano et al., 2000). Since IL6 gene expression was enhanced in H292 IR KD cells, it was aimed to illuminate its role in H292 cells compared to H226 and H460 cells. Notably, in *all cell lines* it was observed that IL6 *increased* caspase activity.

Next to cytokine expression, IGFL-1 was upregulated significantly in H292 cells. According to the current state of knowledge, particularly in cancer cells, IGFL-1 functions are poorly understood yet. However, the protein generally has been observed to be involved in the pathogenesis of psoriasis which rather characterizes inflammatory features (Guo et al., 2014). Interestingly, IGFL-1 expression is known to be enhanced by TNFα (Lobito et al., 2011). This control by TNFα might indicate that IGFL-1 could also have pro-apoptotic features. Especially in H292 IR KD cells, distinctly elevated TNFα levels possibly caused induction of IGFL-1 expression. This in turn might represent a further mechanism leading to apoptosis.

Summarized, it appears plausible that upregulation of various caspase-inducing mediators serve as mechanistic link between IR KD and initiation of apoptosis. Vice versa, it is assumable that the IR actively prevents NSCLC cells from apoptosis by suppressing the expression of cytokines that steer programmed cell death.

Many genes with largely unknown or controversial functions, like IGFL-1, IL24 or IL6, have been found to be upregulated in IR KD cells. It remains indispensable to analyze their roles in cancer cells and their coherencies with the IR in more detail to define novel mediators in cancer involvement.

Especially in light of discovering new approaches in cancer therapy, the IR as potential inhibitor of the prominent cell death-inducer TNFα could be an interesting target for further research.

4.2 Insulin Receptor Knockdown Leads to Upregulated Gene Expression of Various Insulin and IGF Family Members

The IR KD did not lead to a compensatory upregulation of insulin, IGF-1 or IGF-1R gene expression. However, elevated levels of several insulin family members, i.e. INSL and INSIG became evident in H292, H226 and H460 cells. These peptide hormones have been recently discovered and only little is known about their functions. It is reported that INSL-3 is expressed almost exclusively in Leydig cells (Rossato et al., 2011). This contradicts results of microarray-based gene profiling indicating presence of INSL-3 in NSCLC cells. Moreover, INSL-3 was upregulated in IR KD cells. Since INSL-3 has been mainly associated with prostate carcinoma, the focus has been on illumination of its role in benign and malign prostate cancer cells (Klonisch et al., 2005). However, an involvement in tumor biology *in general* is suggested (Hombach-Klonisch et al., 2003). Hereby, it was observed that INSL-3 showed anti-proliferative features by downregulating growth-supporting Erb receptors and EGF (Klonisch et al., 2005). However, INSL-3 was found to increase cell motility (Klonisch et al., 2005) and to facilitate formation of anchorage-independent colonies (Hombach-Klonisch et al., 2010).

INSIG-1 and INSIG-2 were increased in the three NSCLC cell lines. Both are known to trigger metabolic homeostasis (Dong & Tang, 2010) but their role in cancer cells still remain unclear.

Interestingly, an increased gene expression of IGF-2 and IGF-2R was detected in H460 IR KD cells. These findings promote the hypothesis of a dominant role of the IGF-2/IGF-2R signaling transduction in H460 cells as discussed previously. Consequences of elevated IGF-2 and IGF-2R levels are most likely induction of EMT resulting in phenotypical changes of H460 cells after loss of IR (see chapter 2.3). As discussed above (see chapters 1.2.2 & 2.3), IR were only weakly expressed and IGF-2R were most strongly expressed in H460 cells compared to H292 and H226 cells. Remarkably, only in H460 cells, IR KD increased IGF-2R gene expression. It could be assumable that IR and IGF-2R expression levels influence each other. Such a compensatory controlling mechanism would be a novel finding.

4.3 IGF-1 Receptor Downregulation Induces Remodelling Processes in H292 cells

KD experiments revealed that IR KD strongly caused apoptosis (see chapter 4.1), whereas IGF-1R KD induced morphological changes in the epithelial cells; microscopic observations showed an altered smooth muscle-like cell phenotype of H292, H226 and H460 cells. As representative NSCLC cell line, H292 was analyzed in more detail regarding mRNA expression levels of the EMT markers ET-1, CDH2 and FN1.

ET-1 was enhanced to a comparable extent in IR and IGF-1R KD cells. This indicates that loss of either IR or IGF-1R has the same impact on ET-1 mRNA regulation.

Elevated expression rates of ET-1 were measured in patients suffering from T2DM or insulin resistance (Takahashi et al., 1990). Those patients have a decreased amount of functional IR. Reduced amounts of IR are also achieved by a KD. Therefore, ET-1 expression levels in IR KD cells are in good agreement with findings of Takahashi et al. indicating that *reduced IR levels* might cause *increased ET-1 mRNA expression*. A possible explanation for ET-1 upregulation under these circumstances is presented by Wu-Wong et al.; ET-1 has been shown to stimulate glucose-uptake via ET_A receptors in rat cardiomyocytes (Wu-Wong et al., 2000). It follows that cancer cells most likely initiate upregulation of alternative pathways in absence of IR in order to sustain their metabolic activity. This could also be an explanation for increased ET-1 expression rates in H292 IR KD cells.

This hypothesis appears plausible for IR KD but it does not apply for IGF-1R KD. Since KD of IGF-1R but not IR provoked significantly elevated levels of the two further EMT markers CDH and FN1, it is likely that ET-1 mainly contributes to EMT in IGF-1R KD cells. This assumption is underlined by microscopic observations (see above) and common descriptions of ET-1 as EMT inducer in cancer cells (Rosanò et al., 2005).

As IGF-1R KD seemed to initiate the EMT process, vice versa, the IGF-1R signaling might suppress epithelial cell transformation in H292 cells. This in parts contradicts principles of IGF-1-associated aggressive tumor behavior pattern. Because the IGF-1R is known to trigger metastasis and angiogenesis, it is commonly suggested that these processes are steered by EMT which is a well-accepted basic condition for tumor invasiveness (see Introduction 3.1.1). However, studies in H292 cells clearly evidenced that EMT cannot *generally* be assumed to be

the underlying mechanism. It is more appropriate to consider EMT processes differentiated. While some EMT mediators, e.g. matrix metalloproteinases (MMPs), are proved to promote invasive behavior patterns of tumor cells (Radisky & Radisky, 2010; Walsh & Damjanovski, 2011), others should not be strictly associated with metastasis induction. This apparently concerns the functions of ET-1. Thus, clarification of its precise involvement in EMT and implications in angiogenesis and metastasis represents an interesting issue for further studies.

In search of mechanistic links explaining IGF-1R KD-provoked EMT, two approaches appear plausible and could provide an explanation of above-mentioned observations.
IGF-2 has clearly been observed to induce EMT (Larue & Bellacosa, 2005). Since IGF-1R signaling seems (at least in parts) to counteract EMT in H292 cells, it is assumable that IGF-2 steers EMT via IGF-2R activation; a hypothesis which was already discussed before (see chapter 2.3). After downregulation of IGF-1R, IGF-2R are still available and functional. IGF-1 and IGF-2 will consequently bind IGF-2R due to their high affinity to the receptor. Thus, it becomes increasingly evident that the *IGF-2R* could play a key role in EMT.
A further interesting aspect becomes evident by comparing effects of IGF-1R KD and TGF-β-treatment in H292 cells. Notably, IGF-1 KD and TGF-β-treatment exhibited similar impacts on EMT marker expression. As discussed before (see chapter 2.4), IGF-1 acts as functional antagonist of TGF-β by diminishing effects of the latter on ET-1 and CDH2 mRNA expression. Downregulation of IGF-1R results in reduced IGF-1 effects; in parallel, elevated ET-1, CDH2 and FN1 mRNA expression rates were detected in IGF-1R KD cells.
It therefore can be assumed that IGF-1R signaling counteracts TGF-β action by actively suppressing initiation of EMT.

4.4 Insulin Receptor Takes Mitogenic Features in Absence of IGF-1R in H292 cells

Regarding the cell proliferation rate in H292 cells, IR did not compensate IGF-1R loss under starving conditions. This has also been observed in microscopic (see chapter 4.3) and cell count analysis in all cell lines studied (see chapter 4.1). Thus, autocrine and paracrine

secreted IGF-1 does apparently not activate IR, even when only reduced amounts of IGF-1R are available. This can be explained by the comparable low affinity of IGF-1 for IR-binding (Kurtzhals et al., 2000).

Notably, in H292 IGF-1R KD cells, *insulin-mediated* impacts on [^{3}H]-thymidine incorporation were significantly elevated compared to LV-sh controls. This indicates that IGF-1R-binding is not necessary for mitogenic action of insulin. In contrast to common suggestions, supraphysiological insulin concentrations did obviously not increase cell proliferation exclusively via IGF-1R but also via IR (Soos et al., 1990).

Next to apoptosis prevention by IR, these findings further underline the crucial role of IR in cancer progression, particularly in tumor cell proliferation and survival.

This phenomenon of increased proliferation after insulin exposure can most probably be explained by an amplificated IR downstream signaling. While IGF-1R mRNA is downregulated, it is conceivable that signaling proteins, i.e. IRS docking proteins are liberated and can be used upon IR stimulation. This results in an enhanced IR signaling.

It follows that an IGF-1R antibody therapy in the treatment of cancer might lead to an empowerment of mitogenic features of the IR which impairs the therapeutical success. Indeed, IGF-1R antibody therapies did not reveal the expected success (Vincent et al., 2013). This supports the above-mentioned hypothesis and points out that an exclusive IGF-1R destruction might not be sufficient to eliminate malignancies.

4.5 Mitogenic Signal Transduction Is Interrupted in Insulin Receptor Knockdown Cells

4.5.1 Insulin Induces IGF-1 Receptor Autophosphorylation in the NSCLC Cells

Before analyzing effects of IR downregulation on insulin-mediated IR/IGF-1R phosphorylation, it was necessary to verify *basal amounts of IR and IGF-1R* after IR KD. As expected, IR proteins were hardly detectable on the Western blot membranes in LV-sh-IRa-treated samples compared to LV-sh controls in H292, H226 and H460 cells. This indicates a well-functioning receptor KD. Notably, amounts of IGF-1R proteins were unchanged which

is in line with results of the genome-wide profiling of IR KD cells (see chapter 4.2). A compensatory upregulation of IGF-1R caused by IR KD can therefore be excluded.

Consistent in all cell lines tested, clear pIR/pIGF-1R signals were found in 100 nM insulin-treated IR KD samples. These signals obviously derived from IGF-1R phosphorylation. In comparison to LV-sh controls, no marked differences in their signal intensity were found. It follows that higher nanomolar concentrations of insulin can bind IGF-1R almost as effective as the IR.

Remarkably, H292 cells play an outstanding role. In H226 and H460 LV-sh control cells, 10 nM insulin only caused a slight IR/IGF-1R phosphorylation. However, in H292 LV-sh control cells, 10 nM insulin strongly induced IR/IGF-1R phosphorylation. This reveals different 50% effective concentrations (EC_{50}) of insulin on receptor autophosphorylation within the cell lines tested. Variations in EC_{50} values are widely described in literature (Frasca et al., 1999) and caused by differences in receptor expression levels and in the receptor reserve. Cancer cells are marked by mutations resulting in highly individual expression rates of different growth factor receptors (Hanahan et al., 2000). Indeed, different IR and IGF-1R expression levels have been proved in the NSCLC cells tested (see chapter 1.2.2). Cell line H292 exhibited the most pronounced IR and IGF-1R expression rates which is in accordance to results of basal and insulin-induced IR/IGF-1R autophosphorylation.

In H226 and H460 IR KD cells, no phospho signals could be detected in 10 nM insulin-treated samples. In contrast, in H292 IR KD cells, 10 nM insulin clearly activated IGF-1R phosphorylation. This observation is in good agreement with previous findings. Different perspectives - i.e. [^{3}H]-thymidine incorporation rate analysis (see chapter 1.2.1), MAPK signaling (see chapter 1.3) and insulin's counteracting features on anti-proliferative TGF-β action (see chapter 2.1) - reveal clear mitogenic behavior pattern of the anabolic hormone even in low concentrations, especially in cell line H292. A significantly reduced EC_{50} value of insulin for IGF-1R autophosphorylation serves as possible explanation for these results.

Data of pIR/pIGF-1R Western blotting demonstrate that even 100 nM insulin clearly activated IGF-1R signaling. An IGF-1R activation by insulin in concentrations which are achieved after an inhaled therapy (see chapter 1.1) can therefore be assumed.

4.5.2 AKT Signaling Strongly Depends on Insulin Receptor Expression

Akt signaling was highly activated by insulin in the three NSCLC cell lines; LV-sh control cells revealed a comparable response towards insulin on Akt protein phosphorylation as observed in non-transduced cells (see chapter 1.3). Because Western blot analysis showed that even low pico- and nanomolar concentrations of insulin induced Akt phosphorylation, an involvement of IR and not of IGF-1R appears plausible.

In order to analyze the possible potential of insulin to trigger activation of Akt also via *IGF-1R*, IR KD cells were exposed to 10 nM and 100 nM insulin. A markedly impaired Akt signaling was observed in all IR KD cells tested.

As discussed before (see chapter 4.5.1), in IR KD cells, *IGF-1R autophosphorylation* was clearly induced by 100 nM insulin in H226 and H460 cells and by 10 nM insulin in H292 cells. However, insulin only led to a *slight phosphorylation of downstream Akt proteins* in IR KD cells. Therefore, it is assumable that IGF-1R signal transduction affects Akt activation with a reduced potency compared to IR signal transduction. Akt phospho signals were detected with lower concentrations of insulin (10 nM) which did not cause IGF-1R autophosphorylation, at least in H226 and H460 cells. This finding is in good agreement with previously discussed Western blot results in non-transduced cells (see chapter 1.3).

Analysis of a weak IR KD was performed in parallel in H292 and H226 cells, because both cell lines exhibited prominent pronounced IR levels. In order to examine whether Akt phosphorylation runs in parallel to the extent of IR KD in both cell lines, signaling was analyzed after LV-sh-IRb treatment leading to an approx. 50 % receptor downregulation (see Results 4.1.2). Although a dose-dependent effect was observed, reduced Akt phosphorylation levels were only slightly diminished after LV-sh-IRb treatment. This allows the assumption that *high IR expression levels* are accompanied by a *high receptor reserve*. Vice versa, only a strong receptor downregulation appears to impair Akt signaling significantly.

H460 cells exhibited marked IGF-1R expression levels. In contrast, the IR was expressed to a very low amount. However, downregulation of the latter receptor strongly disturbed mitogenic Akt signaling (see above). Against this background, it was of interest to study IGF-1R involvement and the role of IR in H460 IGF-1R KD cells. Interestingly, IGF-1R KD markedly disturbed *insulin-mediated* Akt phosphorylation. 10 nM insulin did not at all induce

the phosphorylation rate via *IR-binding* in IGF-1R KD cells. Thus, the question arises why insulin clearly induced phosphorylation of Akt proteins in the LV-sh controls that express *IR and IGF-1R*. Since the K_D of insulin towards IR-binding is 10 pM (Kurtzhals et al., 2000), it can generally be suggested that due to low receptor expression levels the EC_{50} is significantly below the K_D in H460 cells. Besides, dependence of insulin-binding to heterodimeric IR/IGF-1R could lead to Akt phosphorylation. IR-A is the predominantly expressed receptor splicing isoform in H460 cells. It appears quite likely that presence of IR-A and IGF-1R is accompanied by presence of HR-A. This general hypothesis of HR involvement in mitogenic processes is also supported by others (Belfiore et al., 2009).

In order to examine whether IGF-1R downregulation also has impacts on Akt signaling in H292 and H226 cells, IGF-1R KD effects were studied in the two latter cell lines. As expected, there were no marked changes in insulin-induced pAkt levels in IGF-1R KD cells compared to controls (data not shown). Consequently, the IGF-1R appears to play a subordinated role in the Akt signaling pathway in H292 and H226 cells which is in accordance to previous findings of this study. This highlights the crucial role of IR in mitogenic signaling, particularly in H292 and H226 cells.

Although a strong IR KD clearly diminished Akt protein phosphorylation, insulin in nanomolar concentrations could in parts activate Akt signaling via IGF-1R activation in all cell lines tested. Nonetheless, especially in H292 and H226 cells, functional IR expression appeared necessary for mitogenic signal transduction. In H460 cells, expression of both, IR and IGF-1R, turned out to be crucial for Akt signaling; by downregulation of either IR or IGF-1R this pathway was markedly impaired.

4.5.3 Mitogenic ERK/MAPK Signaling Is Mediated by Different Mechanisms in the NSCLC Cells Studied

ERK/MAPK phosphorylation revealed large differences of IR involvement within the cell lines tested.

In H292 cells, IR but not IGF-1R appeared to be essential for mitogenic ERK signaling. While IGF-1R KD did not visibly reduce basal and insulin-induced MAPK phosphorylation (data not shown), IR KD had strong impacts on the phosphorylation levels. Basal phospho p44/42 levels were significantly below those of LV-sh controls. In addition, insulin-induced p44/42 protein phosphorylation was significantly less pronounced in cells lacking IR.

It therefore becomes increasingly clear that IGF-1R play a minor role in mitogenic signaling in the MEC cell line H292. In contrast, strong dependence on IR expression could be observed. A weak IR KD also diminished ERK1/2 phosphorylation, albeit to a lesser extent than found in cells with strong IR KD. This finding of a dose-dependent MAPK stimulation after IR downregulation is in line with results of Akt phosphorylation.

In H226 cells, the IGF-1R turned out to be more important for MAPK signal transduction than the IR. Beyond, insulin only had slight impacts on p44/42 protein phosphorylation, as also described and discussed previously (see chapter 1.3). Both findings serve as explanation for a failed (further) induction by insulin in ERK1/2 phosphorylation in IR KD cells. In contrast, in IGF-1R KD cells, basal and insulin-induced phosphorylation levels of p44/42 were markedly reduced.

It hence can be concluded that in H226 cells, presence of IGF-1R is highly necessary for ERK/MAPK signaling.

A further different behavior pattern of IR and IGF-1R involvement in ERK signaling became apparent in H460 cells. Overall, both, IR KD and IGF-1R KD *empowered* MAPK signaling. Since RTK rely on the same downstream mediators in order to transduce signals, e.g. via ERK/MAPK signaling, it possibly could be that other growth factor receptors use the signaling machinery more efficiently in absence of IR or IGF-1R. Particularly EGFR are known to be strongly linked to ERK/MAPK signaling pathways in epithelial cancer cells (Buck et al., 2008). Besides, Buck et al. underline a receptor reciprocity between IGF-1R and EGFR, indicating that MAPK signaling can only be sufficiently downregulated by dual blockade of IGF-1R and EGFR. A further explanatory approach for MAPK findings in H460 cells might be involvement of ETS1-associated protein II (EAPII) in mitogenic signaling pathways. EAPII is largely overexpressed in H460 cells and it has been found to activate ERK/MAPK signaling strongly (Li et al., 2011).

Although ERK/MAPK data strongly differed within the three NSCLC cell lines tested, Western blot analysis could have large impacts on the understanding of IGF-1R and IR involvement in cancer progression. It becomes evident that a generalization of the impact of individual growth factors and receptors in mitogenic signaling in NSCLC can be negated. But however, based on a specific tumor cell analysis, an effective and individual cancer therapy could be established.

VI Summary

1 Background

Since recent years it has been assumed that the anabolic hormone insulin might contribute to tumor cell proliferation as the cognate hormone IGF-1. This hypothesis was supported by epidemiological studies revealing a positive correlation between type 2 diabetes mellitus and cancer. Moreover, several studies report that long-term hyperinsulinemia constitute a potential cause for tumor promotion. It is thus of great importance to detect possible implications of insulin and the insulin receptor (IR) in the development of malignancies.

In the context of steadily increasing rates of type 2 diabetics, it becomes obvious that much research is carried out in the field of diabetes mellitus therapy. One main objective has been the development of a non-invasive route of insulin administration in order to avoid daily subcutaneous hormone injections. Ultimately, in June 2014, a novel inhaled insulin delivery system has been approved in the USA. However, there are safety concerns as supraphysiological concentrations of insulin over a longer period might support mitogenic processes in the lungs. It consequently has to be clarified whether insulin concentrations which can be achieved in the respiratory system after inhalation, trigger tumor cell promotion in human bronchial epithelial cells.

2 Methods

The focus of the present study was on illumination of the roles of insulin and the IR in different non-small cell lung cancer (NSCLC) cell lines (H292, H226 and H460 cells). Effects of insulin - especially in comparison to IGF-1 and TGF-β - were studied by analyzing [^{3}H]-thymidine incorporation, mitogenic signaling and expression of epithelial-mesenchymal transition (EMT)-supporting mediators. Involvement of IR and IGF-1R in tumor cell promoting processes was studied by receptor knockdown (KD) models. Those studies included caspase assays, microarray-based gene expression profiling, [^{3}H]-thymidine incorporation and mitogenic signaling in KD cells.

3 Results

In the three NSCLC cell lines, IR and IGF-1R were present, although with differences in their expression levels. Both receptors were most pronounced in cell line H292. In H226 cells, IR proteins were only slightly (76 %) and IGF-1R proteins were significantly (43 %) less expressed compared to cell line H292. H460 cells revealed the lowest IR protein expression level within the cell lines tested (44 % compared to H292 cells). The IGF-1R protein expression rate was 58 % compared to H292 cells. PCR analysis of IR splicing isoforms exhibited that in H292 cells, IR-A and IR-B were present to a similar amount, whereas in the other two cell lines, one isoform was predominant (H226: IR-B, H460: IR-A). Cell-specific differences were also observed in basal proliferation levels. H460 cells had the highest (25700 dpm) [^{3}H]-thymidine incorporation rate, followed by H226 (5800 dpm) and H292 cells (2400 dpm).

Despite those marked variations, insulin clearly triggered tumor cell proliferation in H292 and H226 cells. 1 μM insulin enhanced the [^{3}H]-thymidine incorporation rate to 280 % and 200 % in H292 and H226 cells, respectively. Notably, those effects were even stronger than effects of physiological concentrations of IGF-1 on [^{3}H]-thymidine incorporation. Anti-proliferative effects of TGF-β (H292: 64 %, H226: 60 %) were cancelled by insulin to control level. Additionally, TGF-β effects on endothelin and N-cadherin expression were also diminished by insulin in H292 and in H226 cells.

Western blot analysis revealed that insulin markedly phosphorylated IR/IGF-1R and downstream Akt proteins in a concentration-dependent manner in the three NSCLC cell lines. However, ERK/MAPK was clearly activated by insulin in cell line H292, exclusively. Receptor studies allowed important insights into the roles of IR and IGF-1R in NSCLC cells. In all three cell lines, even a moderate downregulation of IR but not IGF-1R led to cancer cell death. Accordingly, IR KD enhanced caspase-activity (H292: 550 %, H226: 430 %, H460: 140 %). In search of mechanistic links between IR KD and induction of apoptosis, genome-wide gene profiling was performed. Indeed, several cytokines which are known to activate caspases were among the most prominent upregulated genes. Gene expression of IL24 was increased most strongly in H292 (78-fold), H226 (5-fold) and H460 (160-fold) IR KD cells compared to LV-sh controls. Moreover, IR KD caused elevated gene expression levels of TNFα by 9-, 5- and 3-fold in H292, H226 and H460 cells, respectively. In order to verify the

apoptosis-activating ability of the latter cytokines, caspase 3/7 assays were performed in non-transduced NSCLC cells. TNFα significantly activated caspases (H292: 237 %, H226: 130 %, H460: 231 %). Besides, IL24 led to an increased caspases activity in H292 (127 %) and H226 (116 %).

The important role of the IR for cancer cell promotion became also evident by analyzing mitogenic Akt signaling in IR KD cells. In H292, H226 and H460 IR KD cells, insulin did not lead to an Akt protein phosphorylation via IGF-1R activation. Furthermore, in H292 cells, 1 µM insulin significantly increased the [^{3}H]-thymidine incorporation rate in IGF-1R KD cells to 226 % compared to control cells (without receptor KD).

4 Discussion

Safety concerns about long-term treatment with inhaled insulin remain as insulin was found to be involved in mitogenic processes in the NSCLC cell lines tested. Thus, an inhalable insulin therapy should be strictly prohibited for patients suffering from lung cancer. Moreover, patient groups with an increased prevalence of cancer entities in the respiratory system, e.g. smokers, ex-smokers, people being exposed to air pollution or patients with chronic inflammatory diseases, should be excluded precautionary from an inhaled insulin administration.

Beside insulin's mitogenic effects, it was detected that the anabolic hormone appeared as functional antagonist of TGF-β in H292 and H226 cells. Therefore, it could be interesting to analyze possible links between the insulin and the TGF-β signaling pathways in further studies.

Surprisingly, it turned out that the IR is essential for cancer cell survival in all cell lines tested. IR KD induced apoptosis. Vice versa, the IR could possibly prevent cancer cells from apoptosis. Beyond, KD data revealed that insulin triggers proliferative effects not only via IGF-1R-binding but also via IR-binding which is contrary to common assumptions. Observations of this dimension have not been described in literature yet and provide an interesting approach for cancer therapy.

In addition, receptor KD data might explain why cancer treatment with antibodies directed against the IGF-1R only has not revealed the expected success in NSCLC types. Dual inhibition of IGF-1R and IR most likely represents a more successful approach.

VII Literature References

1. Abdullah, N., Attia, J., Oldmeadow, C., Scott, R. J., & Holliday, E. G. (2014). The architecture of risk for type 2 diabetes: understanding Asia in the context of global findings. *International Journal of Endocrinology*, *2014*, 593982.

2. Agu, R. U., Ugwoke, M. I., Armand, M., Kinget, R., & Verbeke, N. (2001). The lung as a route for systemic delivery of therapeutic proteins and peptides. *Respiratory Research*, *2001*(2), 198–209.

3. American Cancer Society. (2014). Cancer Facts & Figures. Retrieved March 15, 2015, from http://www.cancer.org/acs/groups/content/@research/documents/webcontent/acspc-042151.pdf

4. American Cancer Society. (2015). Lung Cancer. Retrieved May 1, 2015, from http://www.cancer.org/cancer/lungcancer/

5. American Diabetes Association. (2008). Diagnosis and classification of diabetes mellitus. *Diabetes Care*, *31*(Supplement 1), 55–60.

6. Bailyes, E. M., Navé, B. T., Soos, M. A., Orr, S. R., Hayward, A. C., & Siddle, K. (1997). Insulin receptor/IGF-I receptor hybrids are widely distributed in mammalian tissues: quantification of individual receptor species by selective immunoprecipitation and immunoblotting. *The Biochemical Journal*, *1997*(327), 209–215.

7. Bao, C., Yang, X., Xu, W., Luo, H., Xu, Z., Su, C., & Qi, X. (2013). Diabetes mellitus and incidence and mortality of kidney cancer: a meta-analysis. *Journal of Diabetes and Its Complications*, *27*(4), 357–364.

8. Barone, B. B., Snyder, C. F., Peairs, K. S., Stein, K. B., Derr, R. L., Wolff, A. C., & Meri, B. M. A. (2014). Long-term All-Cause Mortality in Cancer Patients With Preexisting Diabetes Mellitus. *The Journal of the American Medical Association*, *300*(23), 2754–2764.

9. Bastaki, S. (2005). Diabetes mellitus and its treatment. *International Journal of Diabetes & Metabolism*, *2015*(13), 111–134.

10. Baxter, R. C. (2014). IGF binding proteins in cancer: mechanistic and clinical insights. *Nature Reviews. Cancer*, *14*(5), 329–341.

11. Baxter, R. C., Bryson, J. M., & Turtle, J. R. (1980). Somatogenic receptors of rat liver: regulation by insulin. *Endocrinology*, *107*(4), 1176–1181.

12. Belfiore, A., Frasca, F., Pandini, G., Sciacca, L., & Vigneri, R. (2009). Insulin receptor isoforms and insulin receptor/insulin-like growth factor receptor hybrids in physiology and disease. *Endocrine Reviews*, *30*(6), 586–623.

13. Benyoucef, S., Surinya, K. H., Hadaschik, D., & Siddle, K. (2007). Characterization of insulin/IGF hybrid receptors: contributions of the insulin receptor L2 and Fn1 domains and the alternatively spliced exon 11 sequence to ligand binding and receptor activation. *The Biochemical Journal*, *403*(3), 603–613.

14. Bhaskar, P. T., & Hay, N. (2007). The Two TORCs and Akt. *Developmental Cell*, *12*(April), 487–502.

15. Bloomgarden, Z. T. (2014). Afrezza: Some questions about a new approach to prandial insulin 关于一种新型餐时胰岛素的一些问题. *Journal of Diabetes*, *6*(July), 489–490.

16. Boyer, B., Roche, S., Denoyelle, M., & Thiery, J. P. (1997). Src and Ras are involved in separate pathways in epithelial cell scattering. *EMBO Journal*, *16*(19), 5904–5913.

17. Buck, E., Eyzaguirre, A., Rosenfeld-Franklin, M., Thomson, S., Mulvihill, M., Barr, S., Ji, Q. S. (2008). Feedback mechanisms promote cooperativity for small molecule inhibitors of epidermal and insulin-like growth factor receptors. *Cancer Research*, *68*(20), 8322–8332.

18. Burgering, B. M., & Coffer, P. J. (1995). Protein kinase B (c-Akt) in phosphatidylinositol-3-OH kinase signal transduction. *Nature*, *376*(6541), 599–602.

19. Calle, E., Rodriguez, C., Walker-Thurmond, K., & Thun, M. J. (2003). Overweight, Obesity, and Mortality from Cancer in a Prospectively Studied Cohort of U.S. Adults — *New England Journal of Medicine*, *2003*(348), 1625–1638.

20. Cappelleri, J. C., Cefalu, W. T., Rosenstock, J., Kourides, I. A., & Gerber, R. A. (2002). Treatment satisfaction in type 2 diabetes: a comparison between an inhaled insulin regimen and a subcutaneous insulin regimen. *Clinical Therapeutics*, *24*(4), 552–564.

21. Cappuzzo, F., Tallini, G., Finocchiaro, G., Wilson, R. S., Ligorio, C., Giordano, L., Santoro, A. (2010). Insulin-like growth factor receptor 1 (IGF1R) expression and survival in surgically resected non-small-cell lung cancer (NSCLC) patients. *Annals of Oncology: Official Journal of the European Society for Medical Oncology*, *21*(September 2009), 562–567.

22. Cargnello, M., & Roux, P. P. (2011). Activation and function of the MAPKs and their substrates, the MAPK-activated protein kinases. *Microbiology and Molecular Biology Reviews*, *75*(1), 50–83.

23. Cefalu, W. T. (2001). Novel routes of insulin delivery for patients with type 1 or type 2 diabetes. *Annals of Medicine*, *33*(9), 579–586.

24. Cefalu W. T. (2004). Concept, strategies, and feasibility of non-invensive insulin delivery. *Diabetes Care*, *27*(1), 239–246.

25. Chancellor, J., Aballéa, S., Lawrence, A., Sheldon, R., Cure, S., Plun-Favreau, J., & Marchant, N. (2008). Preferences of patients with diabetes mellitus for inhaled versus injectable insulin regimens. *PharmacoEconomics*, *26*(3), 217–234.

26. Chandarlapaty, S., Sawai, A., Scaltriti, M., Rodrik-Outmezguine, V., Grbovic-Huezo, O., Serra, V., Rosen, N. (2011). AKT inhibition relieves feedback suppression of receptor tyrosine kinase expression and activity. *Cancer Cell*, *19*(1), 58–71.

27. Chappell, J., Leitner, J. W., Solomon, S., Golovchenko, I., Goalstone, M. L., & Draznin, B. (2001). Effect of insulin on cell cycle progression in MCF-7 breast cancer cells. Direct and potentiating influence. *The Journal of Biological Chemistry*, *276*(41), 38023–38028.

28. Cheema, A., Adeloye, D., Sidhu, S., Sridhar, D., & Chan, K. Y. (2014). Urbanization and prevalence of type 2 diabetes in Southern Asia: A systematic analysis. *Journal of Global Health*, *4*(1), 010404.

29. Chen, C.-R., Kang, Y., Siegel, P. M., & Massagué, J. (2002). E2F4/5 and p107 as Smad cofactors linking the TGFbeta receptor to c-myc repression. *Cell*, *110*(1), 19–32.

30. Chen, G., & Goeddel, D. V. (2002). TNF-R1 signaling: a beautiful pathway. *Science*, *296*(5573), 1634–1635.

31. Chen, Z., Gibson, T. B., Robinson, F., Silvestro, L., Pearson, G., Xu, B., Cobb, M. H. (2001). MAP kinases. *Chemical Reviews*, *101*(8), 2449–2476.

32. Corpet, D. E., Jacquinet, C., Peiffer, G., & Taché, S. (1997). Insulin injections promote the growth of aberrant crypt foci in the colon of rats. *Nutrition and Cancer*, *27*(3), 316–320.

33. Dash, R., Bhoopathi, P., Das, S. K., Sarkar, S., Emdad, L., Dasgupta, S., Fisher, P. B. (2014). Novel mechanism of MDA-7/IL-24 cancer-specific apoptosis through SARI induction. *Cancer Research*, *74*(2), 563–574.

34. Davis, R. J. (2000). Signal transduction by the JNK group of MAP kinases. *Cell*, *103*(2), 239–252.

35. De Luca, A., Maiello, M. R., D'Alessio, A., Pergameno, M., & Normanno, N. (2012). The RAS/RAF/MEK/ERK and the PI3K/AKT signalling pathways: role in cancer pathogenesis and implications for therapeutic approaches. *Expert Opinion on Therapeutic Targets*, *16*(2), 17–27.

36. De Meyts, P., & Whittaker, J. (2002). Structural biology of insulin and IGF1 receptors: implications for drug design. *Nature Reviews. Drug Discovery*, *1*(10), 769–83.

37. DeFronzo, R. A. (1999). Pharmacologic Therapy for Type 2 Diabetes Mellitus. *Annals of Internal Medicine*, *131*(4), 281.

38. Denley, A., Bonython, E. R., Booker, G. W., Cosgrove, L. J., Forbes, B. E., Ward, C. W., & Wallace, J. C. (2004). Structural determinants for high-affinity binding of insulin-like growth factor II to insulin receptor (IR)-A, the exon 11 minus isoform of the IR. *Molecular Endocrinology*, *18*(10), 2502–2512.

39. Dhillon, S., Hagan, S., Rath, O., & Kolch, W. (2007). MAP kinase signalling pathways in cancer. *Oncogene*, *26*(22), 3279–3290.

40. Dong, X.-Y., & Tang, S.-Q. (2010). Insulin-induced gene: a new regulator in lipid metabolism. *Peptides*, *31*(11), 2145–2150.

41. Donnelly, R. P., Sheikh, F., Kotenko, S. V, & Dickensheets, H. (2004). The expanded family of class II cytokines that share the IL-10. *Journal of Leukocyte Biology*, *76*(August), 314–321.

42. Dufourny, B., Alblas, J., van Teeffelen, H. a, van Schaik, F. M., van der Burg, B., Steenbergh, P. H. & Sussenbach, J. S. (1997). Mitogenic signaling of insulin-like growth factor I in MCF-7 human breast cancer cells requires phosphatidylinositol 3-kinase and is independent of mitogen-activated protein kinase. *The Journal of Biological Chemistry*, *272*(49), 31163–31171.

43. Eldridge, L. (2015). Large Cell Carcinoma of the Lungs. Retrieved March 22, 2015, from http://lungcancer.about.com/od/typesoflungcance1/a/Large-Cell-Carcinoma-Of-The-Lungs.htm

44. El-Serag, H. B., Hampel, H., & Javadi, F. (2006). The association between diabetes and hepatocellular carcinoma: a systematic review of epidemiologic evidence. *Clinical Gastroenterology and Hepatology: The Official Clinical Practice Journal of the American Gastroenterological Association*, *4*(3), 369–380.

45. Everhart, J., & Wright, D. (1995). Diabetes mellitus as a risk factor for pancreatic cancer. A meta-analysis. *The Journal of the American Medical Association*, *273*(20), 1605–1609.

46. Fagot-Campagna, A. (2000). Emergence of Type 2 Diabetes Mellitus in Children: Epidemiological Evidence. *Journal of Pediatric Endocrinology and Metabolism*, *13*(Supplement), 1395–1402.

47. FDA. (2014). FDA Briefing Document: Endocrinologic and Metabolic Drugs Advisory Committee Meeting - UCM390864.pdf. Retrieved April 6, 2015, from http://www.fda.gov/downloads/AdvisoryCommittees/CommitteesMeetingMaterials/Drugs/EndocrinologicandMetabolicDrugsAdvisoryCommittee/UCM390864.pdf

48. Fernandez, M. (2004). IGF-I inhibits apoptosis through the activation of the phosphatidylinositol 3-kinase/Akt pathway in pituitary cells. *Journal of Molecular Endocrinology*, *33*(1), 155–163.

49. Ferrell, J. E. (1996). Tripping the switch fantastic: how a protein kinase cascade can convert graded inputs into switch-like outputs. *Trends in Biochemical Sciences*, *21*(12), 460–466.

50. Fountaine, R., Milton, A., Checchio, T., Wei, G., Stolar, M., Teeter, J., Fryburg, D. (2008). Acute passive cigarette smoke exposure and inhaled human insulin (Exubera) pharmacokinetics. *British Journal of Clinical Pharmacology*, *65*(6), 864–870.

51. Frasca, F., Pandini, G., Scalia, P., Sciacca, L., Mineo, R., Goldfine, I. D., Vigneri, R. (1999). Insulin Receptor Isoform A , a Newly Growth Factor II Receptor in Fetal and Cancer Cells Insulin Receptor Isoform A , a Newly Recognized , High-Affinity Insulin-Like Growth Factor II Receptor in Fetal and Cancer Cells. *Molecular and Cellular Biology*.

52. Frasca, F., Pandini, G., Sciacca, L., Pezzino, V., Squatrito, S., Belfiore, A., & Vigneri, R. (2008). The role of insulin receptors and IGF-I receptors in cancer and other diseases. *Archives of Physiology and Biochemistry*, *114*(1), 23–37.

53. Freitag, A., Reimann, A., Wessler, I., & Racké, K. (1996). Effects of bacterial lipopolysaccharides (LPS) and tumour necrosis factor-alpha (TNF alpha) on rat tracheal epithelial cells in culture: morphology, proliferation and induction of nitric oxide (NO) synthase. *Pulmonary Pharmacology*, *9*(3), 149–156.

54. Fresno Vara, J. A., Casado, E., de Castro, J., Cejas, P., Belda-Iniesta, C., & González-Barón, M. (2004). PI3K/Akt signalling pathway and cancer. *Cancer Treatment Reviews*, *30*(2), 193–204.

55. Friberg, E., Orsini, N., Mantzoros, C. S. & Wolk, A. (2007). Diabetes mellitus and risk of endometrial cancer: a meta-analysis. *Diabetologia*, *50*(7), 1365–1374.

56. Fuxe, J., Vincent, T., & De Herreros, A. G. (2010). Transcriptional crosstalk between TGFβ and stem cell pathways in tumor cell invasion: Role of EMT promoting Smad complexes. *Cell Cycle*, *9*(March 2015), 2363–2374.

57. Ghobrial, I. M., Witzig, T. E., & Adjei, A. A. (2005). Targeting Apoptosis Pathways in Cancer Therapy. *A Cancer Journal for Clinicians*, *55*(3), 178–194.

58. Goode, R. K., Auclair, P. L., & Ellis, G. L. (1998). Mucoepidermoid carcinoma of the major salivary glands: Clinical and histopathologic analysis of 234 cases with evaluation of grading criteria. *Cancer*, *82*(7), 1217–1224.

59. Grant, K., Loizidou, M., & Taylor, I. (2003). Endothelin-1: a multifunctional molecule in cancer. *British Journal of Cancer*, *88*(2), 163–166.

60. Grille, S. J., Bellacosa, A., Upson, J., Klein-Szanto, A. J., van Roy, F., Lee-Kwon, W., Larue, L. (2003). The protein kinase Akt induces epithelial mesenchymal transition and promotes enhanced motility and invasiveness of squamous cell carcinoma lines. *Cancer Research*, *63*(9), 2172–2180.

61. Grivennikov, S., & Karin, M. (2008). Autocrine IL-6 Signaling: A Key Event in Tumorigenesis? *Cancer Cell*, *13*(1), 7–9.

62. Guo, P., Luo, Y., Mai, G., Zhang, M., Wang, G., Zhao, M., Zhou, F. (2014). Gene expression profile based classification models of psoriasis. *Genomics*, *103*(1), 48–55.

63. Guo, S. T., Jiang, C. C., Wang, G. P., Li, Y. P., Wang, C. Y., Guo, X. Y., Zhang, X. D. (2013). MicroRNA-497 targets insulin-like growth factor 1 receptor and has a tumour suppressive role in human colorectal cancer. *Oncogene*, *32*(15), 1910–1920.

64. Hanahan, D., Weinberg, R. a, & Francisco, S. (2000). The Hallmarks of Cancer Review University of California at San Francisco. *Cell Press*, *100*, 57–70.

65. Heidegger, I., Ofer, P., Doppler, W., Rotter, V., Klocker, H., & Massoner, P. (2012). Diverse functions of IGF/insulin signaling in malignant and noncancerous prostate cells: proliferation in cancer cells and differentiation in noncancerous cells. *Endocrinology*, *153*(10), 4633–4643.

66. Heinemann, L. (2008). The failure of exubera: are we beating a dead horse? *Journal of Diabetes Science and Technology*, *2*(3), 518–529.

67. Hendler, F., & Ozeanne, B. (1984). Human Squamous Cell Lung Cancers Exress Increased Epidermal Growth Factor Receptors. *Journal of Clinical Investigation*, *74*(August), 647–651.

68. Heuson, J.-C., Legros, N., & Heimann, R. (1972). Influence of Insulin Administration on Growth of the 7,12-Dimethylbenz(a)anthracene-induced Mammary Carcinoma in Intact, Oophorectomized, and Hypophysectomized Rats. *Cancer Res.*, *32*(2), 233–238.

69. Hirano, T., Franzén, B., Kato, H., Ebihara, Y., & Auer, G. (1994). Genesis of squamous cell lung carcinoma. Sequential changes of proliferation, DNA ploidy, and p53 expression. *The American Journal of Pathology*, *144*(2), 296–302.

70. Hirano, T., Ishihara, K., & Hibi, M. (2000). Roles of STAT3 in mediating the cell growth, differentiation and survival signals relayed through the IL-6 family of cytokine receptors. *Oncogene*, *19*(21), 2548–2556.

71. Hombach-Klonisch, S., Bialek, J., Radestock, Y., Truong, A., Agoulnik, A. I., Fiebig, B., Klonisch, T. (2010). INSL3 has tumor-promoting activity in thyroid cancer. *International Journal of Cancer. Journal International Du Cancer*, *127*(3), 521–531.

72. Hombach-Klonisch, S., Hoang-Vu, C., Kehlen, A., Hinze, R., Holzhausen, H.-J., Weber, E., Klonisch, T. (2003). INSL-3 is expressed in human hyperplastic and neoplastic thyrocytes. *International Journal of Oncology*, *22*(5), 993–1001.

73. Hotamisligil, G. S., Murray, D. L., Choy, L. N., & Spiegelman, B. M. (1994). Tumor necrosis factor alpha inhibits signaling from the insulin receptor. *Proceedings of the National Academy of Sciences of the United States of America*, *91*(11), 4854–4858.

74. Hugo, H., Ackland, M. L., Blick, T., Lawrence, M. G., Clements, J. A., Williams, E. D., & Thompson, E. W. (2007). Epithelial--mesenchymal and mesenchymal--epithelial transitions in carcinoma progression. *Journal of Cellular Physiology*, *213*(2), 374–383.

75. Hui, L., Zhang, S., Dong, X., Tian, D., Cui, Z., & Qiu, X. (2013). Prognostic Significance of Twist and N-Cadherin Expression in NSCLC. *PLoS ONE*, *8*(4), 1–10.

76. Hurbin, A., Dubrez, L., Coll, J.-L., & Favrot, M.-C. (2002). Inhibition of apoptosis by amphiregulin via an insulin-like growth factor-1 receptor-dependent pathway in non-small cell lung cancer cell lines. *The Journal of Biological Chemistry*, *277*(51), 49127–49133.

77. Jechlinger, M., Grünert, S., & Beug, H. (2002). Mechanisms in epithelial plasticity and metastasis: insights from 3D cultures and expression profiling. *Journal of Mammary Gland Biology and Neoplasia*, *7*(4), 415–432.

78. Jemal, A., Siegel, R., Xu, J., & Ward, E. (2010). Cancer statistics, 2010. *A Cancer Journal for Clinicians*, *60*(5), 277–300.

79. Jernberg-Wiklund, H., & Nilsson, K. (2007). Control of apoptosis in human multiple myeloma by insulin-like growth factor I (IGF-I). *Advances in Cancer Research*, *97*, 139–65.

80. Johansson, G. S., & Arnqvist, H. J. (2006). Insulin and IGF-I action on insulin receptors , IGF-I receptors , and hybrid insulin / IGF-I receptors in vascular smooth muscle cells. *American Journal of Physiology. Endocrinology and Metabolism*, *291*(5), 1124–1130.

81. Kalluri, R., & Neilson, E. G. (2003). Epithelial-mesenchymal transition and its implications for fibrosis.pdf. *Journal of Clinical Investigation*, *112*(12), 1776–1784.

82. Kalluri, R., & Weinberg, R. (2009). Review series The basics of epithelial-mesenchymal transition. *Journal of Clinical Investigation*, *119*(6), 1420–1428.

83. Khandwala, H. M., McCutcheon, I. E., Flyvbjerg, A., & Friend, K. E. (2000). The Effects of Insulin-Like Growth Factors on Tumorigenesis and Neoplastic Growth. *Endocrine Reviews*, *21*(3), 215–244.

84. Kido, Y., Nakae, J., & Accili, D. (2001). Clinical review 125: The insulin receptor and its cellular targets. *The Journal of Clinical Endocrinology and Metabolism*, *86*(3), 972–929.

85. Kim, A., Khursigara, G., Sun, X., Thomas, F., Chao, M. V, Khursigara, G. U. S., & Franke, T. F. (2001). Akt Phosphorylates and Negatively Regulates Apoptosis Signal-Regulating Akt Phosphorylates and Negatively Regulates Apoptosis Signal-Regulating Kinase 1. *Molecular and Cellular Biology*.

86. Kim, J.-S., Kim, E. S., Liu, D., Lee, J. J., Solis, L., Behrens, C., Lee, H.-Y. (2012). Prognostic impact of insulin receptor expression on survival of patients with nonsmall cell lung cancer. *Cancer*, *118*(9), 2454–2465.

87. Klonisch, T., Müller-Huesmann, H., Riedel, M., Kehlen, A., Bialek, J., Radestock, Y., Hombach-Klonisch, S. (2005). INSL3 in the benign hyperplastic and neoplastic human prostate gland. *International Journal of Oncology*, *27*(2), 307–315.

88. Klonoff, D. C. (2014). Afrezza Inhaled Insulin: The Fastest-Acting FDA-Approved Insulin on the Market Has Favorable Properties. *Journal of Diabetes Science and Technology*, *8*(6), 1071–1073.

89. Koda-Kimble, M. A., Yee Young, L., Alldredge, B. K., Corelli, R. L., Guglielmo, B. J., Kradjan, W. A., & Williams, B. R. (2009). *Applied Therapeutics* (9th ed.). Philadelphia: Wolters Kluwer / Lippincott Williams & Wilkins.

90. Krysan, K., Reckamp, K. L., Dalwadi, H., Sharma, S., Rozengurt, E., Dohadwala, M., & Dubinett, S. M. (2005). Prostaglandin E 2 Activates Mitogen-Activated Protein Kinase / Erk Pathway Signaling and Cell Proliferation in Non − Small Cell Lung Cancer Cells in an Epidermal Growth Factor Receptor-Independent Manner. *Cancer Research*, *65*(14), 6275–6282.

91. Kulik, G., Klippel, a, & Weber, M. J. (1997). Antiapoptotic signalling by the insulin-like growth factor I receptor, phosphatidylinositol 3-kinase, and Akt. *Molecular and Cellular Biology*, *17*(3), 1595–1606.

92. Kuo, W. L., Montag, A. G., & Rosner, M. R. (1993). Insulin-degrading enzyme is differentially expressed and developmentally regulated in various rat tissues. *Endocrinology*, *132*(2), 604–611.

93. Kurtzhals, P., Schäffer, L., Sørensen, A., Kristensen, C., Jonassen, I., Schmid, C., & Trüb, T. (2000). Correlations of receptor binding and metabolic and mitogenic potencies of insulin analogs designed for clinical use. *Diabetes*, *49*(6), 999–1005.

94. Kyriakis, J. M., & Avruch, J.. (2001). Mammalian Mitogen-Activated Protein Kinase Signal Transduction Pathways Activated by Stress and Inflammation. *Physiological Reviews*, *81*(2), 807–859.

95. Labiris, N. R., & Dolovich, M. B. (2003). Pulmonary drug delivery. Part I: Physiological factors affecting therapeutic effectiveness of aerosolized medications. *British Journal of Clinical Pharmacology*, *56*, 588–599.

96. Lamouille, S., Xu, J., & Derynck, R. (2014). Molecular mechanisms of epithelial-mesenchymal transition. *Nature Reviews. Molecular Cell Biology*, *15*(3), 178–196.

97. Larsson, S. C., Orsini, N., Brismar, K., & Wolk, A. (2006). Diabetes mellitus and risk of bladder cancer: a meta-analysis. *Diabetologia*, *49*(12), 2819–2823.

98. Larsson, S., Orsini, N., & Wolk, A. (2005). Diabetes mellitus and risk of colorectal cancer: a meta-analysis. *Journal of the National Cancer Institute*, *97*(22), 1679–1687.

99. Larue, L., & Bellacosa, A. (2005). Epithelial-mesenchymal transition in development and cancer: role of phosphatidylinositol 3′ kinase/AKT pathways. *Oncogene*, *24*, 7443–7454.

100. Lasorella, A., Noseda, M., Beyna, M., Yokota, Y., & Iavarone, A. (2000). Id2 is a retinoblastoma protein target and mediates signalling by Myc oncoproteins. *Nature*, *407*(6804), 592–598.

101. Lawlor, M. A., & Alessi, D. R. (2001). PKB/Akt: a key mediator of cell proliferation, survival and insulin responses? *Journal of Cell Science*, *114*(16), 2903–2910.

102. Lebrun, J.-J. (2012). The Dual Role of TGF β in Human Cancer: From Tumor Suppression to Cancer Metastasis. *ISRN Molecular Biology*, *2012*, 1–28.

103. Lee, T. K., Poon, R. T. P., Yuen, A. P., Ling, M. T., Kwok, W. K., Wang, X. H., Fan, S. T. (2006). Twist overexpression correlates with hepatocellular carcinoma metastasis through induction of epithelial-mesenchymal transition. *Clinical Cancer Research: An Official Journal of the American Association for Cancer Research*, *12*(18), 5369–5376.

104. Li, C., Fan, S., Owonikoko, T. K., Khuri, F. R., Sun, S.-Y., & Li, R. (2011). Oncogenic role of EAPII in lung cancer development and its activation of the MAPK-ERK pathway. *Oncogene*, *30*(September 2010), 3802–3812.

105. Li, C., & Kong, D. (2014). Cancer risks from diabetes therapies: Evaluating the evidence. *Pharmacology & Therapeutics*, 1–11.

106. Lobito, A. a, Ramani, S. R., Tom, I., Bazan, J. F., Luis, E., Fairbrother, W. J., Gonzalez, L. C. (2011). Murine insulin growth factor-like (IGFL) and human IGFL1 proteins are induced in inflammatory skin conditions and bind to a novel tumor necrosis factor receptor family member, IGFLR1. *The Journal of Biological Chemistry*, *286*(21), 18969–18981.

107. Löffler, G., Petrides, P. E., & Heinrich, P. C. (2007). *Biochemie & Pathobiochemie* (8th ed.). Heidelberg: Springer Medizin Verlag.

108. Lowry, O. H., Rosebrough, N. J., Farr, A. L., & Randall, R. J. (1951). Protein measurement with the Folin phenol reagent. *The Journal of Biological Chemistry*, *193*(1), 265–275.

109. Lu, C., Lam, H. N., & Menon, R. K. (2005). New members of the insulin family: regulators of metabolism, growth and now reproduction. *Pediatric Research*, *57*(5), 70R–73R.

110. Ludovini, V., Bellezza, G., Pistola, L., Bianconi, F., Di Carlo, L., Sidoni, A., Crinò, L. (2009). High coexpression of both insulin-like growth factor receptor-1 (IGFR-1) and epidermal growth factor receptor (EGFR) is associated with shorter disease-free survival in resected non-small-cell lung cancer patients. *Annals of Oncology: Official Journal of the European Society for Medical Oncology / ESMO*, *20*(5), 842–849.

111. Lv, T., Yuan, D., Miao, X., Lv, Y., Zhan, P., Shen, X., & Song, Y. (2012). Over-expression of LSD1 promotes proliferation, migration and invasion in non-small cell lung cancer. *PLoS ONE*, *7*(4), 1–8.

112. Magwire, M. L. (2011). Addressing barriers to insulin therapy: the role of insulin pens. *American Journal of Therapeutics*, *18*(5), 392–402.

113. Mandal, T. K. (2005). Inhaled insulin for diabetes mellitus. *American Journal of Health-System Pharmacy*, *62*(13), 1359–1364.

114. Manning, B., & Cantley, L. (2007). AKT/PKB Signalling: Navigating Downstream. *Cell*, *129*(7), 1261–1274.

115. MannKind Corporation. (2014). AFREZZA® (insulin human) Inhalation Powder Prescribing Information. Retrieved May 1, 2015, from http://products.sanofi.us/afrezza/afrezza.html

116. Marek, L., Ware, K. E., Fritzsche, A., Hercule, P., Helton, W. R., Smith, J. E., Heasley, L. E. (2009). Fibroblast Growth Factor (FGF) and FGF Receptor-Mediated Autocrine Signaling in Non – Small-Cell Lung Cancer Cells. *Molecular Pharmacology*, *75*(1), 196–207.

117. Marquis, M., Boulet, S., Mathien, S., Rousseau, J., Thébault, P., Daudelin, J.-F., Labrecque, N. (2014). The non-classical MAP kinase ERK3 controls T cell activation. *PloS One*, *9*(1), e86681.

118. Matthiesen, S., Bahulayan, A., Kempkens, S., Haag, S., Fuhrmann, M., Stichnote, C., Racké, K. (2006). Muscarinic receptors mediate stimulation of human lung fibroblast proliferation. *American Journal of Respiratory Cell and Molecular Biology*, *35*(6), 621–627.

119. Mayer, P., Reitzenstein, U., Warnken, M., Enzmann, H. & Racké, K. (2012). Insulin action on H292 bronchial carcinoma cells as compared to normal bronchial epithelial cells. *Pulmonary Pharmacology & Therapeutics*, *25*(1), 104–114.

120. McArdle, M. a., Finucane, O. M., Connaughton, R. M., McMorrow, A. M. & Roche, H. M. (2013). Mechanisms of obesity-induced inflammation and insulin resistance: Insights into the emerging role of nutritional strategies. *Frontiers in Endocrinology*, *4*(May), 1–23.

121. Mccubrey, J. A., Steelman, L. S., Chappell, W. H., Abrams, S. L., Wong, W. T., Chang, F., Elena, R. (2007). Roles Of The RAS/MEK/ERK pathway in Cell Growth, Malignant Transformation and Drug Resistance. *Biochimica et Biophysica Acta - Molecular Cell Research*, *1773*(8), 1263–1284.

122. Meier, F., Schittek, B., Busch, S., Garbe, C., Smalley, K., Satyamoorthy, K., Herlyn, M. (2005). The RAS/RAF/MEK/ERK and PI3K/AKT signaling pathways present molecular targets for the effective treatment of advanced melanoma.. *Frontiers in Bioscience: A Journal and Virtual Library*, *10*, 2986–3001.

123. Merrick, D. T., Dziadziuszko, R., Szostakiewicz, B., Szymanowska, A., Rzyman, W., Jassem, E., Hirsch, F. R. (2007). High insulin-like growth factor 1 receptor (IGF1R) expression is associated with poor survival in surgically treated non-small cell lung cancer (NSCLC) patients (pts). *ASCO Meeting Abstracts*, *25*(18S), 7550.

124. Miettinen, P. J., Ebner, R., Lopez, a R., & Derynck, R. (1994). TGF-beta induced transdifferentiation of mammary epithelial cells to mesenchymal cells: involvement of type I receptors. *The Journal of Cell Biology*, *127*(6), 2021–2036.

125. Milazzo, G., Giorgino, F., & Damante, G. (1992). Insulin receptor expression and function in human breast cancer cell lines. *Cancer Research*, *52*, 3924–3930.

126. Moodley, Y. P., Misso, N. L. a, Scaffidi, A. K., Fogel-Petrovic, M., McAnulty, R. J., Laurent, G. J., Knight, D. (2003). Inverse effects of interleukin-6 on apoptosis of fibroblasts from pulmonary fibrosis and normal lungs. *American Journal of Respiratory Cell and Molecular Biology*, *29*(4), 490–498.

127. Moustakas, A., & Heldin, C. H. (2007). Signaling networks guiding epithelial-mesenchymal transitions during embryogenesis and cancer progression. *Cancer Science*, *98*(10), 1512–1520.

128. Muraoka-Cook, R. S., Dumont, N., & Arteaga, C. L. (2005). Dual role of transforming growth factor beta in mammary tumorigenesis and metastatic progression. *Clinical Cancer Research*, *11*(13), 937s–943s.

129. Murthy, S. S., Tosolini, A., Taguchi, T., & Testa, J. R. (2000). Mapping of AKT3, encoding a member of the Akt/protein kinase B family, to human and rodent chromosomes by fluorescence in situ hybridization. *Cytogenetics and Cell Genetics*, *88*(1-2), 38–40.

130. Naito, K., Skog, S., Tribukait, B., Andersson, L., & Hisazumi, H. (1987). Cell cycle related [3H]thymidine uptake and its significance for the incorporation into DNA. *Cell and Tissue Kinetics*, *20*(4), 447–457.

131. Nakagawa, M., Uramoto, H., Oka, S., Chikaishi, Y., Iwanami, T., Shimokawa, H., Tanaka, F. (2012). Clinical significance of IGF1R expression in non-small-cell lung cancer. *Clinical Lung Cancer*, *13*(2), 136–42.

132. Nakashima, T., Huang, C., Liu, D., Kameyama, K., Masuya, D., Kobayashi, S., Yokomise, H. (2003). Neural-cadherin expression associated with angiogenesis in non-small-cell lung cancer patients. *British Journal of Cancer*, *88*(11), 1727–1733.

133. Nance, M., Seethala, R. R., Wang, Y., Chiosea, S. I., Myers, E. N., Johnson, J. T., & Lai, S. Y. (2008). Treatment and survival outcomes based on histologic grading in patients with head and neck mucoepidermoid carcinoma. *Cancer*, *113*(August), 2082–2089.

134. National Cancer Institute. (2014, June 30). Non-Small Cell Lung Cancer Treatment (PDQ®). Retrieved March 14, 2015, from http://www.ncbi.nlm.nih.gov/books/PMH0032567/

135. National Diabetes Data Group. (1979). Classification and Diagnosis of Diabetes Mellitus and Other Categories of Glucose Intolerance. *Diabetes*, *28*(12), 1039–1057.

136. Nieman, M. T., Prudoff, R. S., Johnson, K. R., & Wheelock, M. J. (1999). N-Cadherin Promotes Motility in Human Breast Cancer Cells Regardless of their E-Cadherin Expression. *The Journal of Cell Biology*, *147*(3), 631–643.

137. Niven, R. W. (1995). Delivery of biotherapeutics by inhalation aerosol. *Critical Reviews in Therapeutic Drug Carrier Systems*, *12*(2-3), 151–231.

138. Nuffer, W., Trujillo, J. M., & Ellis, S. L. (2014). Technosphere Insulin (Afrezza): A New, Inhaled Prandial Insulin. *Annals of Pharmacotherapy*, *49*(1), 99–106.

139. Olefsky, J. M. (1990). The Insulin Receptor: A Multifunctional Protein. *Diabetes*, *39*(9), 1009–1016.

140. Pandini, G., Frasca, F., Mineo, R., Sciacca, L., Vigneri, R., & Belfiore, A. (2002). Insulin/insulin-like growth factor I hybrid receptors have different biological characteristics depending on the insulin receptor isoform involved. *Journal of Biological Chemistry*, *277*(42), 39684–39695.

141. Peruzzi, F., Prisco, M., Dews, M., Salomoni, P., Grassilli, E., Romano, G., Baserga, R. (1999). Multiple signaling pathways of the insulin-like growth factor 1 receptor in protection from apoptosis, *19*(10), 7203–7215.

142. Pfützner, A., Mann, A. E., & Steiner, S. S. (2002). Technosphere/Insulin--a new approach for effective delivery of human insulin via the pulmonary route. *Diabetes Technology & Therapeutics*, *4*(5), 589–594.

143. Pollak, M.. (2008). Insulin and insulin-like growth factor signalling in neoplasia. *Nature Reviews. Cancer*, *8*(12), 915–928.

144. Pramfalk, C., Lanner, J., Andersson, M., Danielsson, E., Kaiser, C., Renström, I.-M., James, S. R. (2004). Insulin receptor activation and down-regulation by cationic lipid transfection reagents. *BMC Cell Biology*, *5*(7), 1–8.

145. Prisco, M., Romano, G., Peruzzi, F., Valentinis, B., & Baserga, R. (1999). Insulin and IGF-I receptors signaling in protection from apoptosis. *Hormone and Metabolic Research*, *31*(2-3), 80–89.

146. Qi, M., & Elion, E. (2005). MAP kinase pathways. *Journal of Cell Science*, *118*(16), 3569–3572.

147. Quattrin, T., Belanger, A., & Bohannon, N. (2004). Efficacy and Safety of Inhaled Insulin (Exubera) Compared With Subcutaneous Insulin Therapy in Patients With Type 1. *Diabetes*, *27*(11), 2622–2627.

148. Radisky, E. S., & Radisky, D. C. (2010). Matrix metalloproteinase-induced epithelial-mesenchymal transition in breast cancer. *Journal of Mammary Gland Biology and Neoplasia*, *15*(2), 201–212.

149. Rath, P. C., & Aggarwal, B. B. (1999). TNF-induced signaling in apoptosis. *Journal of Clinical Immunology*, *19*(6), 350–364.

150. Rave, K., Bott, S., Heinemann, L., Sha, S., Becker, R. H. a, Willavize, S. a., & Heise, T. (2005). Time-action profile of inhaled insulin in comparison with subcutaneously injected insulin lispro and regular human insulin. *Diabetes Care*, *28*(5), 1077–1082.

151. Rennard, S. I., Basset, G., Lecossier, D., O'Donnell, K. M., Pinkston, P., Martin, P. G., & Crystal, R. G. (1986). Estimation of volume of epithelial lining fluid recovered by lavage using urea as marker of dilution. *Journal of Applied Physiology*, *60*(2), 532–538.

152. Resnicoff, M., Abraham, D., Yutanawiboonchai, W., Rotman, H. L., Kajstura, J., Rubin, R., Baserga, R. (1995). The insulin-like growth factor I receptor protects tumor cells from apoptosis in vivo. *Cancer Research*, *55*(11), 2463–2469.

153. Reuveni, H., Flashner-Abramson, E., Steiner, L., Makedonski, K., Song, R., Shir, A., Levitzki, A. (2013). Therapeutic destruction of insulin receptor substrates for cancer treatment. *Cancer Research*, *73*(14), 4383–4394.

154. Roberts, P. J., & Der, C. J. (2007). Targeting the Raf-MEK-ERK mitogen-activated protein kinase cascade for the treatment of cancer. *Oncogene*, *26*(22), 3291–3310.

155. Robey, R. B., & Hay, N. (2006). Mitochondrial hexokinases, novel mediators of the antiapoptotic effects of growth factors and Akt. *Oncogene*, *25*(34), 4683–4696.

156. Rosanò, L., Spinella, F., Di Castro, V., Decandia, S., Nicotra, M. R., Natali, P. G., & Bagnato, A. (2006). Endothelin-1 is required during epithelial to mesenchymal transition in ovarian cancer progression. *Experimental Biology and Medicine*, *231*(6), 1128–1131.

157. Rosanò, L., Spinella, F., Di Castro, V., Nicotra, M. R., Dedhar, S., Garcia De Herreros, A., Bagnato, A. (2005). Endothelin-1 promotes epithelial-to-mesenchymal transition in human ovarian cancer cells. *Cancer Research*, *65*(24), 11649–11657.

158. Rosenstock, J., Cefalu, W. T., Hollander, P. A., Belanger, A., Eliaschewitz, F. G., Gross, J. L., Duggan, W. T. (2008). Two-year pulmonary safety and efficacy of inhaled human insulin (Exubera) in adult patients with type 2 diabetes. *Diabetes Care*, *31*(9), 1723–1728.

159. Rossato, M., Tavolini, I. M., Calcagno, A., Gardiman, M., Dal Moro, F., & Artibani, W. (2011). The novel hormone INSL3 is expressed in human testicular Leydig cell tumors: a clinical and immunohistochemical study. *Urologic Oncology*, *29*(1), 33–37.

160. Roux, P. P., & Blenis, J. (2004). ERK and p38 MAPK-activated protein kinases: a family of protein kinases with diverse biological functions. *Microbiology and Molecular Biology Reviews*, *68*(2), 320–344.

161. Rui, L., Aguirre, V., Kim, J. K., Shulman, G. I., Lee, A., Corbould, A., White, M. F. (2001). Insulin/IGF-1 and TNF-alpha stimulate phosphorylation of IRS-1 at inhibitory Ser307 via distinct pathways. *The Journal of Clinical Investigation*, *107*(2), 181–189.

162. Santos Cavaiola, T., & Edelman, S. (2014). Inhaled Insulin: A Breath of Fresh Air? A Review of Inhaled Insulin. *Clinical Therapeutics*, *in press*.

163. Sarala, N., Bengalorkar, G., & Bhuvana, K. (2012). Technosphere insulin: A new inhaled insulin. *Practical Diabetes*, *28*(9), 397–398a.

164. Schaeffer, H. J., & Weber, M. J. (1999). Mitogen-activated protein kinases: specific messages from ubiquitous messengers. *Molecular and Cellular Biology*, *19*(4), 2435–2444.

165. Scheuch, G., Kohlhaeufl, M. J., Brand, P., & Siekmeier, R. (2006). Clinical perspectives on pulmonary systemic and macromolecular delivery. *Advanced Drug Delivery Reviews*, *58*(9-10), 996–1008.

166. Schiller, J. H. (2001). Current standards of care in small-cell and non-small-cell lung cancer. *Oncology*, *61*(Suppl. 1), 3–13.

167. Sciacca, L., Vigneri, R., Tumminia, A., Frasca, F., Squatrito, S., Frittitta, L., & Vigneri, P. (2013). Clinical and molecular mechanisms favoring cancer initiation and progression in diabetic patients. *Nutrition, Metabolism, and Cardiovascular Diseases*, *23*(9), 808–815.

168. Sharma, S. D., Meeran, S. M., & Katiyar, S. K. (2010). Proanthocyanidins inhibit in vitro and in vivo growth of human non-small cell lung cancer cells by inhibiting the prostaglandin E(2) and prostaglandin E(2) receptors. *Molecular Cancer Therapeutics*, *9*(3), 569–580.

169. Siddle, K., Urso, B., Niesler, A., Cope, D. L., Molina, L., Surinya, K. H., & Soos, M. A. (2001). Insulin Action. *Biochemical Society*.

170. Siekmeier, R., & Scheuch, G. (2008). Inhaled insulin--does it become reality? *Journal of Physiology and Pharmacology*, *59*(Suppl 6), 81–113.

171. Singh, P., Alex, J. M., & Bast, F. (2014). Insulin receptor (IR) and insulin-like growth factor receptor 1 (IGF-1R) signaling systems: novel treatment strategies for cancer. *Medical Oncology*, *31*(1), 805.

172. Skeen, J. E., Bhaskar, P. T., Chen, C.-C., Chen, W. S., Peng, X., Nogueira, V., Hay, N. (2006). Akt deficiency impairs normal cell proliferation and suppresses oncogenesis in a p53-independent and mTORC1-dependent manner. *Cancer Cell*, *10*(4), 269–280.

173. Soos, M., Whittaker, J., Lammers, R., Ullrich, A., & Siddle, K. (1990). Receptors for insulin and insulin-like growth factor-I can form hybrid dimers. Characterisation of hybrid receptors in transfected cells. *The Biochemical Journal*, *270*(2), 383–390.

174. Steward, B. W., & Wild, C. P. (2014). World Cancer Report 2014 - WHO - OMS -. Retrieved March 1, 2015, from http://apps.who.int/bookorders/anglais/detart1.jsp?codlan=1&codcol=76&codcch=31

175. Surmacz, E. (1995). Overexpression Human Estrogen and Breast of Insulin Cancer Cell for Receptor Line Growth Substrate Induces of in the Requirements Transformation. *Clinical Cancer Research*, *1*(November), 1429–1436.

176. Surmacz, E. (2000). Function of the IGF-I Receptor in Breast Cancer. *Journal of Mammary Gland Biology and Neoplasia*, *5*(1), 95–105.

177. Takahashi, K., Ghatei, M. A., Lam, H. C., O'Halloran, D. J., & Bloom, S. R. (1990). Elevated plasma endothelin in patients with diabetes mellitus. *Diabetologia*, *33*(5), 306–310.

178. Tanaka, S., & Wands, J. R. (1996). Insulin Receptor Substrate 1 Overexpression in Human Hepatocellular Carcinoma Cells Prevents Transforming Growth Factor beta1-induced Apoptosis. *Cancer Research*, *56*, 3391–3395.

179. Taniguchi, C. M., Emanuelli, B., & Kahn, C. R. (2006). Critical nodes in signalling pathways: insights into insulin action. *Nature Reviews. Molecular Cell Biology*, *7*(2), 85–96.

180. Testa, J. R., & Bellacosa, A. (2001). AKT plays a central role in tumorigenesis. *Proceedings of the National Academy of Sciences of the United States of America*, *98*(20), 10983–10985.

181. Thiery, J. P. (2002). Epithelial-mesenchymal transitions in tumour progression. *Nature Reviews. Cancer*, *2*(6), 442–454.

182. Tuomilehto, J., Lindström, J., Eriksson, J. G., Valle, T. T., Hämäläinen, H., Ilanne-Parikka, P., Anne Louheranta, M. S. (2001). Prevention of Type 2 Diabetes Mellitus by Changes in Lifestyle among Subjects with Impaired Glucose Tolerance. *New England Journal of Medicine*, *344*, 1343–1350.

183. Van Greevenbroek, M. M. J., Schalkwijk, C. G., & Stehouwer, C. D. (2013). Obesity-associated low-grade inflammation in type 2 diabetes mellitus: causes and consequences. *The Netherlands Journal of Medicine*, *71*(4), 174–187.

184. Varewijck, A. J., & Janssen, J. A. M. J. L. (2012). Insulin and its analogues and their affinities for the IGF1 receptor. *Endocrine-Related Cancer*, *19*(5), F63–75.

185. Versteyhe, S., Klaproth, B., Borup, R., Palsgaard, J., Jensen, M., Gray, S. G., & De Meyts, P. (2013). IGF-I, IGF-II, and Insulin Stimulate Different Gene Expression Responses through Binding to the IGF-I Receptor. *Frontiers in Endocrinology*, *4*(August), 1–13.

186. Vigneri, P., Frasca, F., Sciacca, L., Pandini, G., & Vigneri, R.. (2009). Diabetes and cancer. *Endocrine-Related Cancer*, *16*(4), 1103–1123.

187. Vincent, E. E., Elder, D. J. E., Curwen, J., Kilgour, E., Hers, I., & Tavaré, J. M. (2013). Targeting non-small cell lung cancer cells by dual inhibition of the insulin receptor and the insulin-like growth factor-1 receptor. *PloS One*, *8*(6), e66963.

188. Wakefield, L. M., Letterio, J. J., Chen, T., Danielpour, D., Allison, R. S., Pai, L. H., O'Shaughnessy, J. (1995). Transforming growth factor-beta1 circulates in normal human plasma and is unchanged in advanced metastatic breast cancer. *Clinical Cancer Research*, *1*(1), 129–136.

189. Walsh, L. a, & Damjanovski, S. (2011). IGF-1 increases invasive potential of MCF 7 breast cancer cells and induces activation of latent TGF-β1 resulting in epithelial to mesenchymal transition. *Cell Communication and Signaling*, *9*(10), 1–11.

190. Wang, Y. Z., & Wong, Y. C. (1998). Sex hormone-induced prostatic carcinogenesis in the noble rat: the role of insulin-like growth factor-I (IGF-I) and vascular endothelial growth factor (VEGF) in the development of prostate cancer. *The Prostate*, *35*(3), 165–177.

191. Warnken, M., Reitzenstein, U., Sommer, A., Fuhrmann, M., Mayer, P., Enzmann, H., Racké, K. (2010). Characterization of proliferative effects of insulin, insulin analogues and insulin-like growth factor-1 (IGF-1) in human lung fibroblasts. *Naunyn-Schmiedeberg's Archives of Pharmacology*, *382*(5-6), 511–524.

192. Watanabe, T., Shinohara, N., Moriya, K., Sazawa, A., Kobayashi, Y., Ogiso, Y., Hashimoto, A. (2000). Signi cance of the Grb2 and Son of Sevenless (Sos) Proteins in Human Bladder Cancer Cell Lines. *International Union of Biochemistry and Molecular Biology*, *49*(4), 317–320.

193. Weinstein, D., Sarfstein, R., Laron, Z., & Werner, H. (2014). Insulin receptor compensates for IGF1R inhibition and directly induces mitogenic activity in prostate cancer cells. *Endocrine Connections*, *3*(1), 24–35.

194. White, J. R., & Campbell, R. K. (2001). Inhaled Insulin: An Overview. *Clinical Diabetes*, *19*(1), 13–16.

195. Wigley, F. W., Londono, J. H., Wood, S. H., Shipp, J. C., & Waldman, R. H. (1971). Insulin across respiratory mucosae by aerosol delivery. *Diabetes*, *20*(8), 552–560.

196. Wild, S., Roglic, G., Green, A., Sicree, R., & King, H. (2004). Global prevalence of diabetes: estimates for the year 2000 and projections for 2030. *Diabetes Care*, *27*(5), 1047–1053.

197. Wolf, I., Sadetzki, S., Catane, R., Karasik, A., & Kaufman, B. (2005). Diabetes mellitus and breast cancer. *The Lancet Oncology*, *6*(2), 103–111.

198. World Health Organisation. (2003). *World Cancer Report*.

199. World Health Organisation. (2012). Leading causes of death in Europe Fact Sheet. Retrieved March 15, 2015, from http://www.euro.who.int/__data/assets/pdf_file/0004/185215/Leading-causes-of-death-in-Europe-Fact-Sheet.pdf

200. World Health Organisation. (2015). Diabetes. Retrieved March 15, 2015, from http://www.who.int/mediacentre/factsheets/fs312/en/

201. Wu-Wong, J. R., Berg, C. E., & Kramer, D. (2000). Endothelin stimulates glucose uptake via activation of endothelin-A receptor in neonatal rat cardiomyocytes. *Journal of Cardiovascular Pharmacology*, *36*(5), S179–S183.

202. Xiao, D., & He, J. (2010). Epithelial mesenchymal transition and lung cancer. *Journal of Thoracic Disease*, *2*, 154–159.

203. Xie, L., Law, B. K., Chytil, A. M., Brown, K. A., Aakre, M. E., & Moses, H. L. (2004). Activation of the Erk pathway is required for TGF-beta1-induced EMT in vitro. *Neoplasia*, *6*(5), 603–610.

204. Xu, J., Lamouille, S., & Derynck, R. (2009). TGF-beta-induced epithelial to mesenchymal transition. *Cell Research*, *19*(2), 156–172.

205. Yamaguchi, Y., Flier, J. S., Benecke, H., Ransil, B. J., & Moller, D. E. (1993). Ligand-binding properties of the two isoforms of the human insulin receptor. *Endocrinology*, *132*(3), 1132–1138.

206. Yarden, Y., & Ullrich, A. (1988). Growth factor receptor tyrosine kinases. *Annual Review of Biochemistry*, *57*, 443–478.

207. Yaturu, S. (2013). Insulin therapies: Current and future trends at dawn. *World Journal of Diabetes*, *4*(1), 1–7.

208. Yoon, S., & Seger, R. (2006). The extracellular signal-regulated kinase: multiple substrates regulate diverse cellular functions. *Growth Factors*, *24*(1), 21–44.

209. Yu, H., & Rohan, T. (2000). Role of the insulin-like growth factor family in cancer development and progression. *Journal of the National Cancer Institute*, *92*(18), 1472–1489.

Dieses Projekt wurde durch Fördermittel des Bundes (Bundesministerium für Gesundheit) finanziert.

VIII Publikationen

Kongressteilnahme

05.-07.03.2013	Deutsche Gesellschaft für Pharmakologie und Toxikologie (DGPT) Jahrestagung 2013 *Insulin increases proliferation, activates MAP kinase and opposes TGFβ-induced epithelial mesenchymal transitory influences in human lung cancer cells*
07.-11.09.2013	European Respiratory Society (ERS) Annual Congress *Role of insulin and IGF-1 receptors in bronchial epithelial cancer cells*
16.-21.05.2014	American Thoriac Society (ATS) 2014 International Conference *Insulin receptor suppresses apoptosis in H292 human bronchial epithelial cancer cells*

Publikation

Titel	Non-Small Cell Lung Cancer Cell Survival Crucially Depends on Functional Insulin Receptors
Autoren	Frisch CM, Zimmermann K, Zilleßen P, Pfeifer A, Racké K, Mayer P
Journal	Endocrine-Related Cancer 22 (4) 609-621 2015

IX Danksagung

An erster Stelle möchte ich mich herzlich bei Herrn Prof. Dr. Racké dafür bedanken, dass er es mir ermöglicht hat, an einem so spannenden und brisanten Thema forschen zu dürfen. Durch die fachlichen Diskussionen und Anregungen habe ich viele Seiten des wissenschaftlichen Arbeitens kennen gelernt und durfte mich stets mit eigenen Ideen in dem Projekt einbringen. Meinen besten Dank für diese Betreuung!

Mein besonderer Dank gilt ebenfalls Herrn PD Dr. Mayer, der mir immer mit Rat und Tat zur Seite stand. Ihm habe ich viele Ideen und Vorschläge zu verdanken, die das Projekt vorangetrieben haben. Die Zusammenarbeit mit ihm und seiner Arbeitsgruppe – allen voran Frau Anja Harst – im BfArM war fachlich sowie zwischenmenschlich eine sehr wertvolle Erfahrung.

Bei Herrn Prof. Dr. Pfeifer bedanke ich mich für die Bereitstellung der Lentiviren, die für das Projekt nötig waren, die Zusammenarbeit an der Veröffentlichung und die wissenschaftlichen Ratschläge; ich habe sein Feedback sehr geschätzt. Neben diesen fachlichen Gründen, möchte ich mich ebenfalls für das nette Miteinander am Institut bedanken!

Herrn Prof. Dr. Jaehde danke ich herzlich für die Übernahme des zweiten Gutachtens und die Möglichkeit, mein Promotionsthema in der Abteilung für Klinische Pharmazie vorzustellen. Hierdurch wurden die pharmakologischen Inhalte unter klinisch-pharmazeutischen Gesichtspunkten beleuchtet und es ergaben sich interessante Diskussionen und Anregungen.

Frau Rita Fuhrmann danke ich vor allem für das harmonische und nette Miteinander im Labor und im Büro! Neben dem Einarbeiten in die Labormethoden zu Beginn meiner Promotionszeit, stand Sie mir stets bei technischen Fragestellungen zur Seite. Dank ihr, Frau Braun und Frau Rossbach habe ich mich in “unserer Arbeitsgruppe” sehr wohl gefühlt!

Allen Kollegen und Freunden am Institut gilt ein ganz besonderer Dank. Es herrschte eine sehr kollegiale und humorvolle Atmosphäre, wie sie sicher selten zu finden ist; insbesondere das “Mensa-Team” werde ich sehr vermissen! Ich bedanke mich bei den Post-Docs, die immer ein offenes Ohr für meine Fragen hatten und die zu meiner wissenschaftlichen Entwicklung einen großen Teil beigetragen haben.

Dennis danke ich dafür, dass er immer an meiner Seite war und mich während meiner Promotion unterstützt und ermuntert hat.

Auch meinem Patenonkel danke ich für seine Unterstützung und dafür, dass er während meiner Promotionszeit mit allen Herausforderungen, die sich mir stellten, stets mitgefiebert hat!

Der größte Dank gilt meinen Eltern, die mich immer mit größtem Engagement unterstützen und mir jederzeit zur Seite stehen. Ohne Euren Rückhalt wäre ich nicht dort, wo ich heute stehe!